Rapid Jewelry Design and Prototype Making

by

Young Yuk Yu

A thesis submitted to
the Hong Kong Polytechnic University
in accordance with the regulations
for the degree of
Master of Philosophy
in the Department of Industrial and Systems Engineering
2002

Thesis Supervisor: Dr. K.M. Yu, Assistant Professor, Department of Industrial and Systems Engineering, The Hong Kong Polytechnic University.
Co-supervisor: Dr. C.K. Kwong, Assistant Professor, Department of Industrial and Systems Engineering, The Hong Kong Polytechnic University.

ABSTRACT

Rapid prototyping (RP) technology has been widely used in making prototypes for quite a long time. However, in-depth study to fabricate jewelry products with RP is not available. This research deals with the production of jewelry by layered manufacturing technology. The work is mainly divided into two parts.

In the first part, the work is focused on slicing process in rapid prototyping of jewelry. A new methodology of direct and adaptive slicing, maximum inscribed slab slicing, is applied to 3D solid jewel ring models to produce maximum inscribed 3D stacked slab models (wax or resin models). Four types of maximum inscribed slicing are introduced: bottom-up vertical slicing, top-down vertical slicing, middle-up vertical slicing and middle-up horizontal slicing. The maximum inscribed slab model will minimize material wastage in post-treatment processes and preserves the symmetric property of the original jewel ring model.

In the second part, a new orientation methodology, the maximum visibility building orientation, is applied to jewel ring models to orient jewel ring models properly for layered manufacturing. Maximum visibility direction will first be obtained. Then, the best-building direction is found. The best-building orientation obtained will build the jewel ring model with high aesthetic quality. The building error is also considered. Extended Gaussian image is applied in extracting the orientation information of jewelry model.

In conclusion, this research demonstrates some feasible methodologies which are specific to improve layered manufacturing based jewelry production.

ACKNOWLEDGEMENTS

I would like to express my sincere and endless gratitude to my supervisor, Dr. K.M. Yu for his constant guidance, encouragement and support through my postgraduate study at the Department of Industrial & Systems Engineering, the Hong Kong Polytechnic University. Discussions with him throughout the past years on various research issues were stimulating and fruitful. Without his help and direction, this work would never be possible.

I would like to thank my research co-supervisor, Dr. C.K. Kwong for his help on this research work.

Finally, the work described in this paper was supported by a grant from the Hong Kong Polytechnic University (Project No.: G-V617).

TABLE OF CONTENTS

GLOSSARY

The notations being used in this thesis are defined as follows:

$\wedge$: and

V_h: half volume of an ellipsoid

S_t: theoretical volume of an ellipsoid

V_a: total volume of an ellipsoid

E: volumetric error (difference between the theoretical volume anf the total volume of an ellipsoid

A_i : planar region obtained from the i^{th} slice

A_{i+1} : planar region obtained from the $i+1^{th}$ slice

A_o: planar region obtained from slicing at z = 0 (center) level of the torus

i, j, k : unit direction vectors corresponding to x, y, z axes

L_{max}: maximum layer thickness achieved by the rapid prototyping system

L_{min}: minimum layer thickness achieved by the rapid prototyping system

$Part_i$: Part of the model between z levels $z = z_i$ and $z = z_{i+1}$

S_i: cross-sectional region obtained from the intersection of planar regions

S_N: cross-sectional region obtained from the intersection of π_N with T

S_o: cross-sectional region obtained from the intersection of π_1 with T

$Slab_{bottom}$: bottom slab

$Slab_{top}$: top slab

$Slab_i$: slab between z levels $z = z_i$ and $z = z_{i+1}$

T: 3D solid torus

z_i : z-coordinate of the i^{th} slice

z_{i+1} : z-coordinate of the $i+1^{th}$ slice

π_i: plane perpendicular to the building direction at level $z = z_i$

π_{i+1}: plane perpendicular to the building direction at level $z = z_{i+1}$

η : Volume efficiency

R: real number $(-\infty, \infty)$

N: natural number (1, 2, 3, ...)

n(u,v): unit normal of parameterized surface patch

E^3: Euclidean space

$\| \|$: norm of vector

$| |$: absolute value of real number

LIST OF FIGURES

LIST OF TABLES

CHAPTER 1

INTRODUCTION

1.1 Background of rapid prototyping

Rapid prototyping technology has been widely used in making prototypes for a long time. The technology mainly involves building prototypes layer by layer using materials such as plastic and wax. Most of the rapid prototyping machines build rapid prototypes in uniform layer thickness. In this research, the focus will be on layer manufacturing of jewel rings. The two main apparatus used is 3D Systems' stereolithography apparatus (Figure 1-1) [3D Systems] and Solidscape's model maker (Figure 1-2) [Solidscape, Inc.]

Figure 1-1. Stereolithography apparatus.

Figure 1-2. Solidscape's model maker.

1.2 Jewelry production and the related problem

1.2.1 Traditional production of jewelry [Kallenberg 2000]

The wax is the heart of jewelry industry. Traditionally, the artist or model maker carves a wax model which is set into a metal container; plaster is poured in until it completely covers the wax model (Figure 1-3). When the plaster has set, the container is placed in a special oven until the wax flows through a channel in the plaster. All that left is imprint of the original. Into this cavity, molten silver is shot, usually by centrifugal force; when the metal sets, the plaster is washed away and the model — now transform into the permanence of metal – remains (Figure 1-4). It is then filed and polished until it is even more perfect than the wax had been, and from this silver pattern, a rubber mold is made (Figures 1-5 and 1-6). The metal original is set aside; molten wax is injected into the cavity of the rubber mold and the entire process is repeated, only now an unlimited number of wax productions can be cast in rubber mold. Then the wax models are taken to casting for the production of precious jewelry (gold, silver and platinum etc.). Final touch up is needed before fine jewelry is produced. The whole traditional process is shown in the flowchart of Figure 1-7.

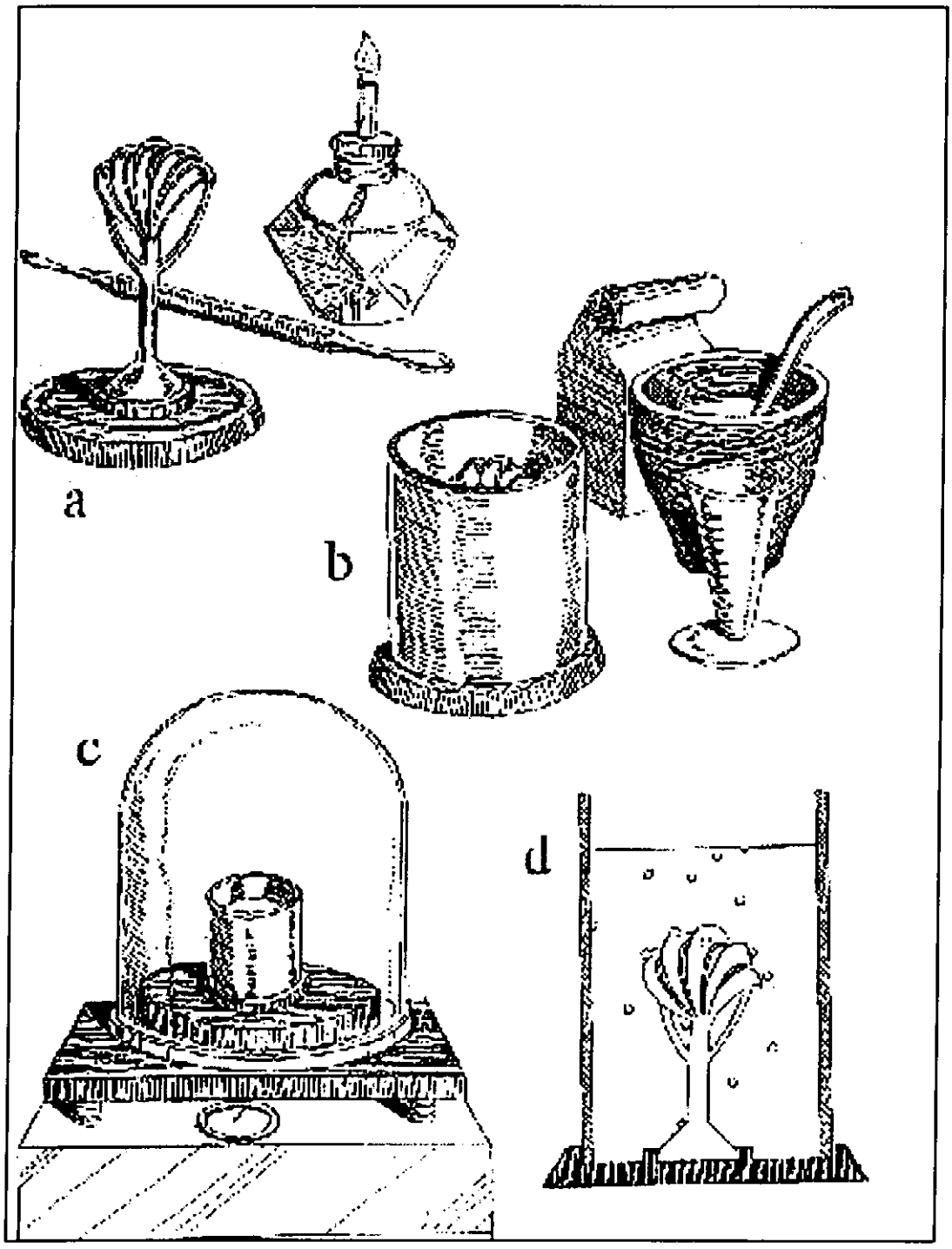

Figure 1-3. Investment casting of the master wax model.
(a) Wax model set in sprue base.
(b) Wax model with flask in position, ready for investing.
(c) Debubblizer.
(d) Cross section of investment flask.

[Kallenberg 2000]

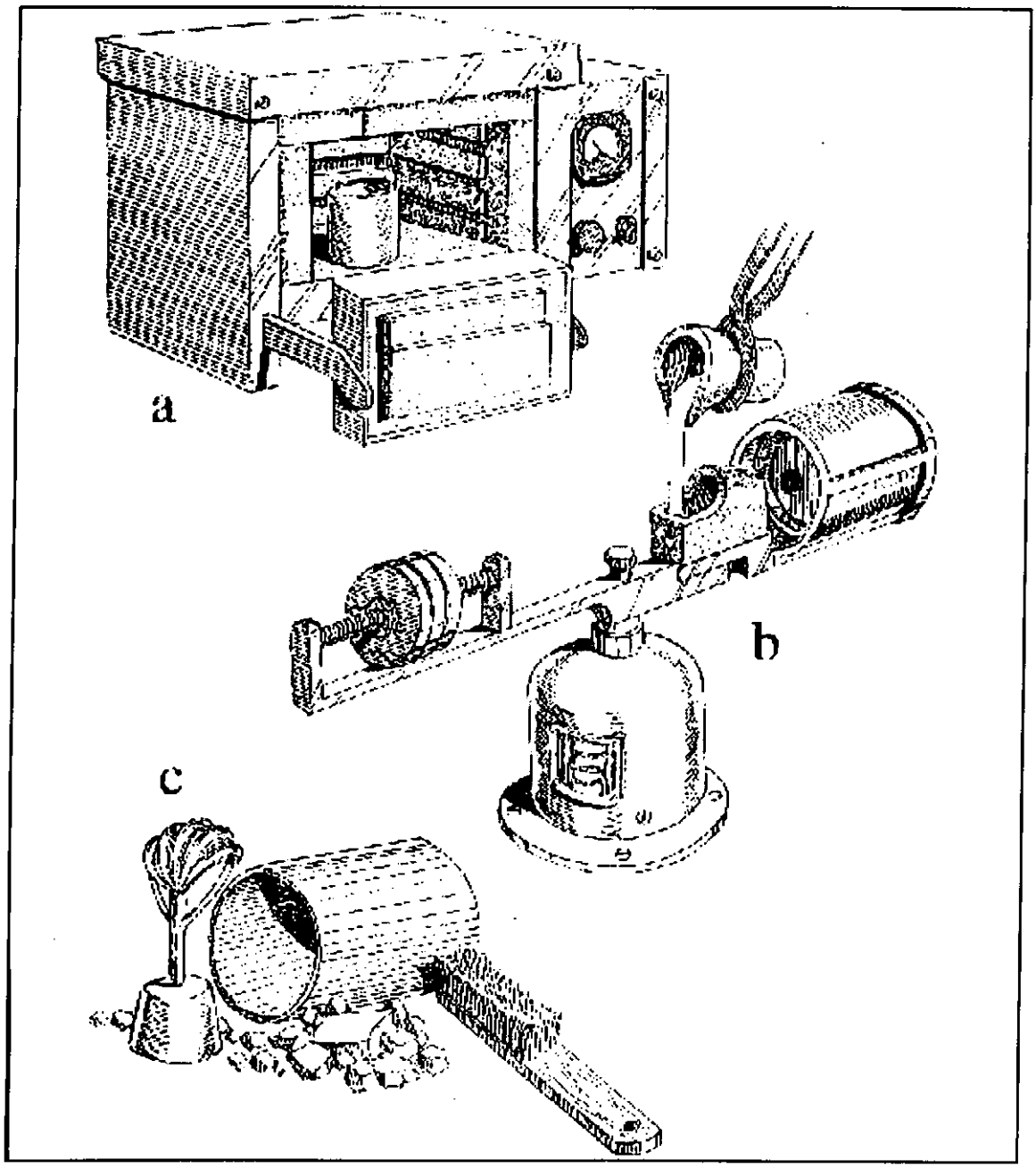

Figure 1-4. Silver pattern production by metal casting.
(a) Burn-out oven.
(b) Centrifugal casting machine.
(c) The cast model.

[Kallenberg 2000]

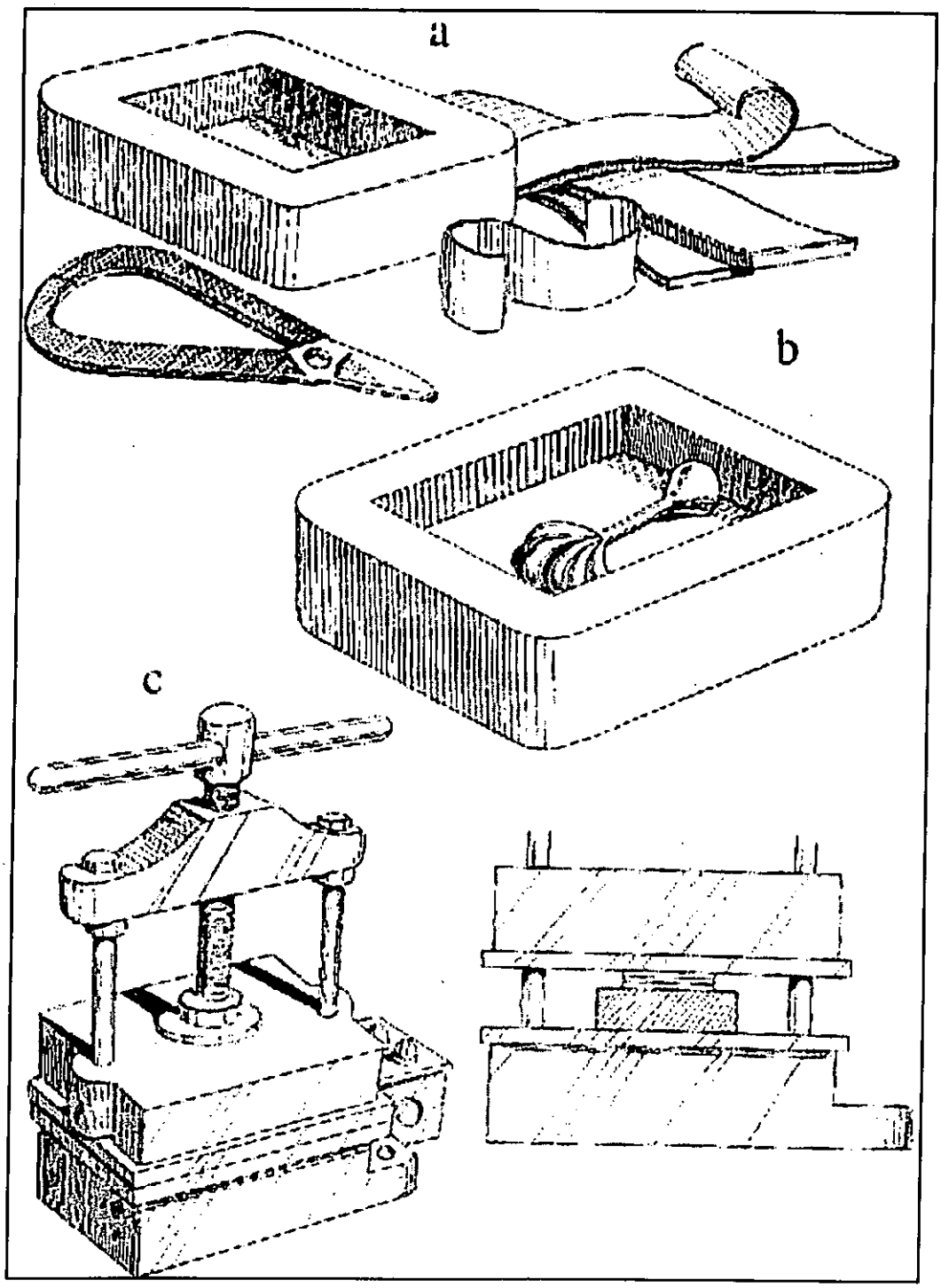

Figure. 1-5. Production of a rubber mold.
(a) Frame for making rubber model.
(b) Metal model placed in frame.
(c) Vulcanizer.

[Kallenberg 2000]

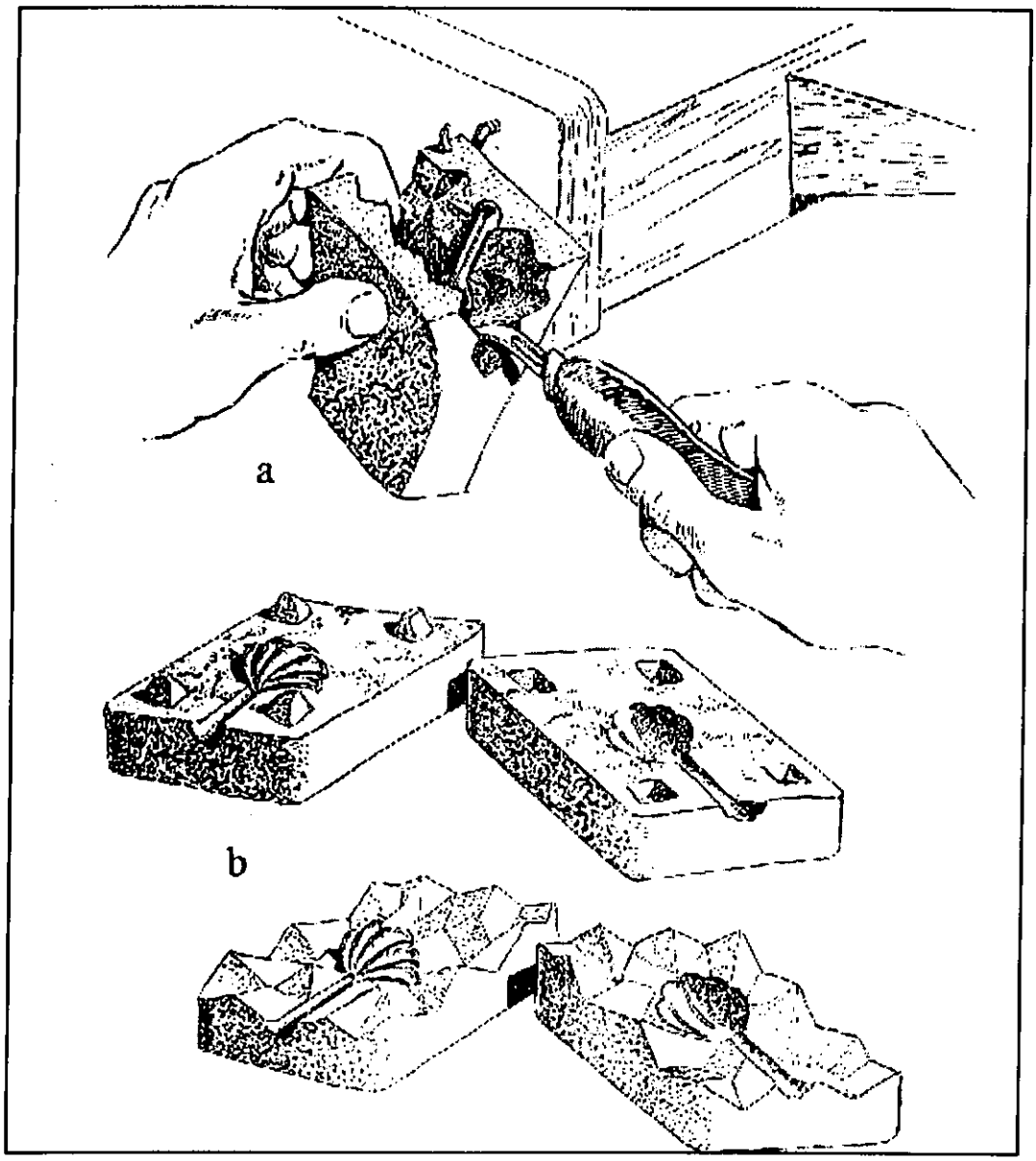

Figure. 1-6. Rubber mold cutting.
(a) Cutting a rubber mold.
(b) Comparison of different cutting techniques.

[Kallenberg 2000]

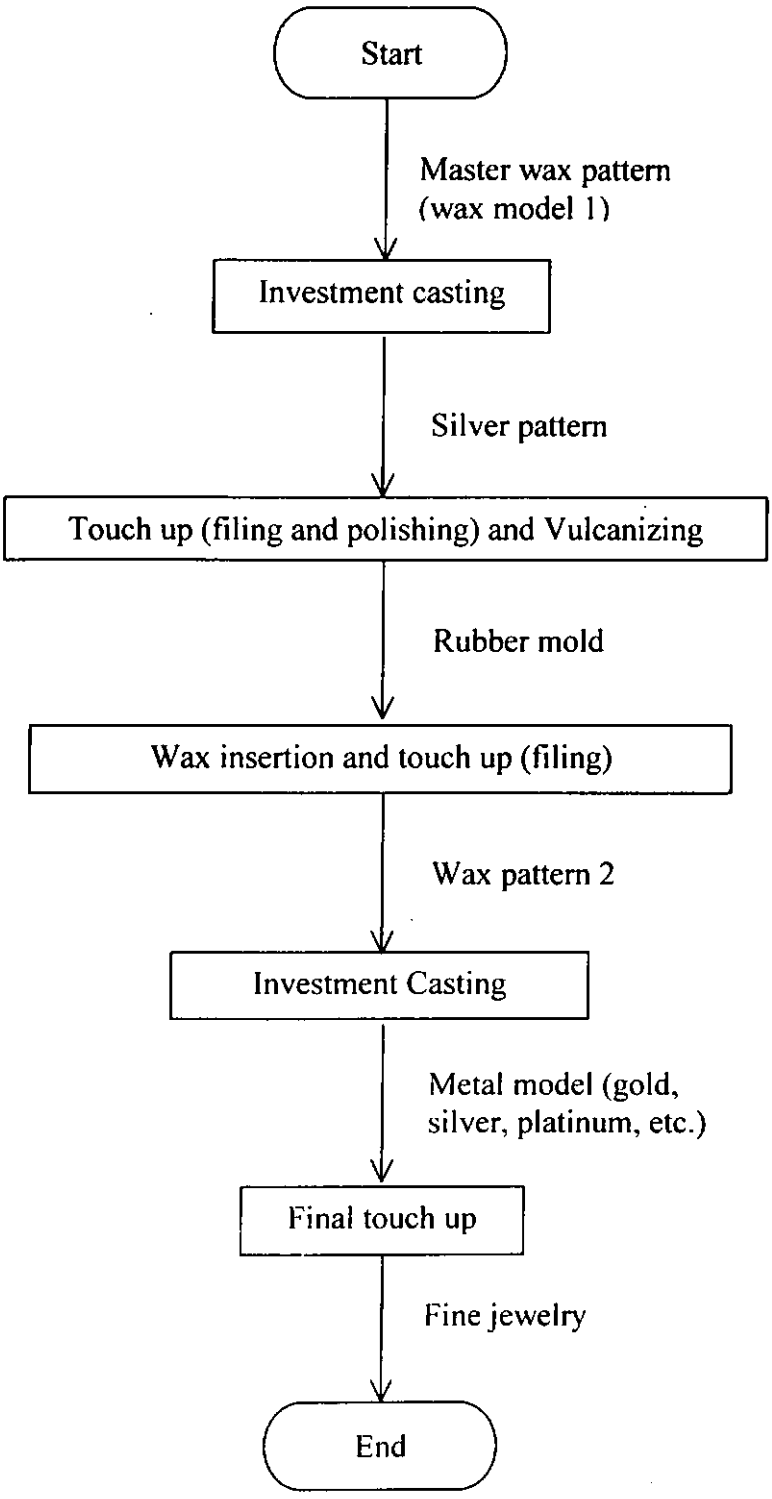

Figure 1-7. Production processes of jewelry.

1.2.2 Contemporary production of jewelry

Nowadays, layered manufacturing has been introduced to jewelry production. Many wax patterns (or resin patterns and other plastics) of the same styles can be produced by rapid prototyping. Thus, the production of silver pattern and rubber mold is not a must. The wax patterns (or the resin patterns and other plastics) can be used to make the jewelry directly by investment casting. If the quality of the rapid prototypes of the jewel ring produced is high, no more touch up is needed before they are used for investment casting. Nowadays, the quality of prototypes produced by layered manufacturing is high, little touch up of the prototypes is needed. Figure 1-8 shows the rapid prototyping (RP) workflow for jewelry product. Figure 1-9 shows the contemporary jewelry production process flow.

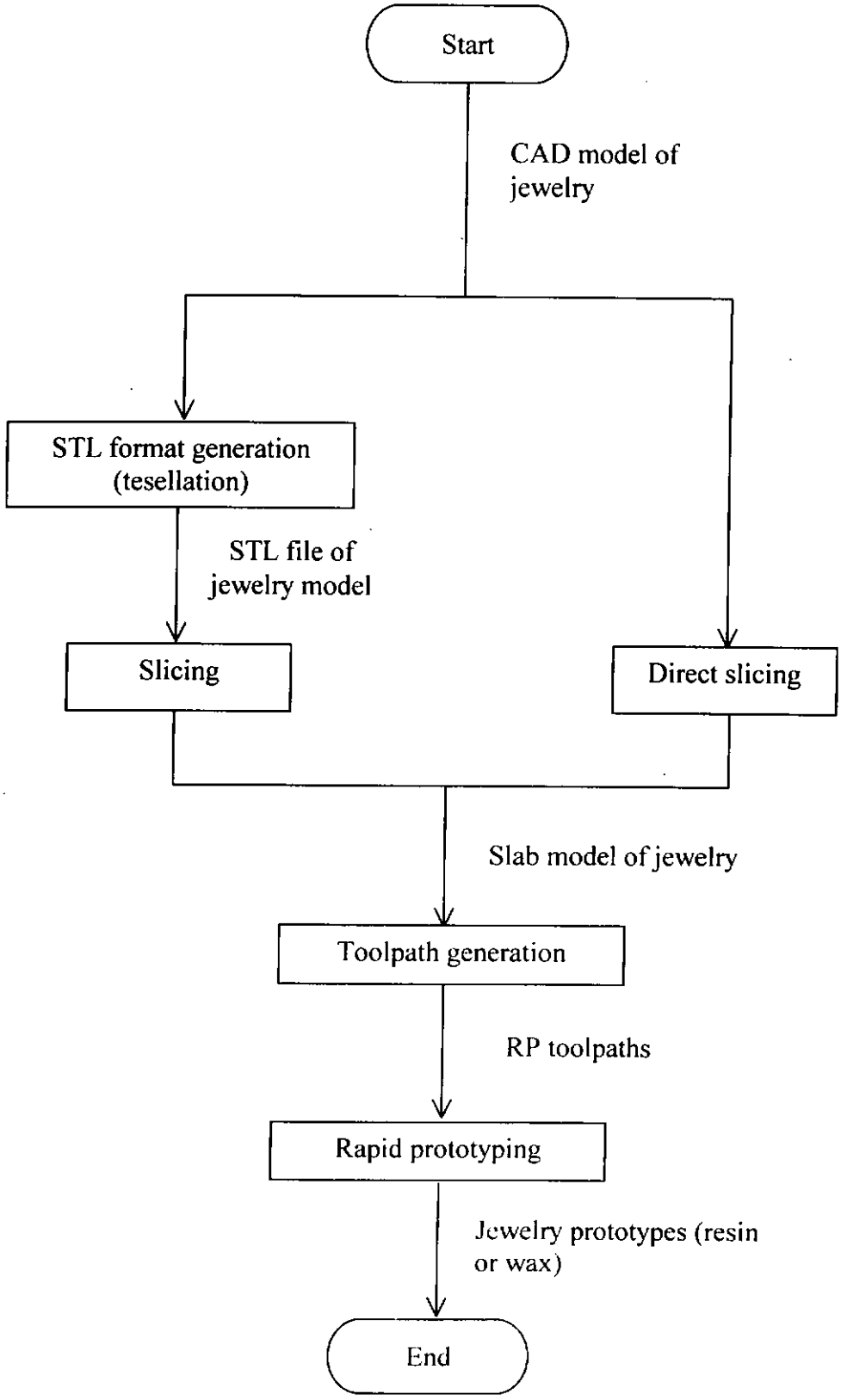

Figure 1-8. Contemporary rapid prototyping workflow for jewelry product.

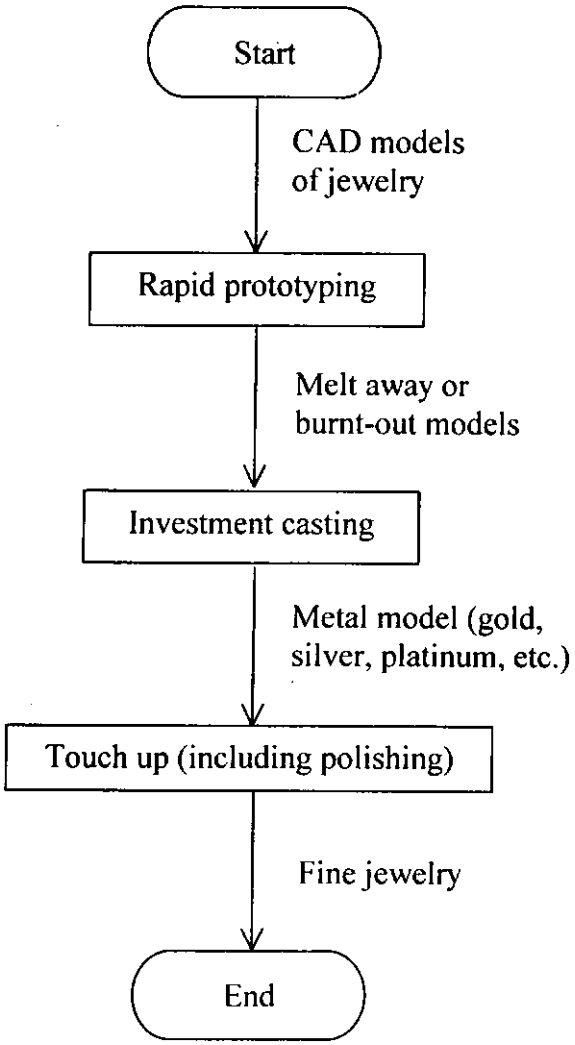

Figure 1-9. Contemporary jewelry production process flow.

1.2.3 The problems

In traditional jewelry production, some problems exist. First, the whole process flow is done manually especially before investing casting, the wax patterns must be reproduced from rubber mold. Therefore, the production efficiency is low. Second, the master wax pattern is made by craftsman. The symmetry, shape and dimension of jewelry may not be made precisely nor repeatable. This will affect the quality reliability of the jewelry products.

In contemporary jewelry production, layered manufacturing is applied to produce rapid jewelry prototypes to enhance the production efficiency, the quality and accuracy of jewelry products. However, some problems still exist. Since the prototypes built are used in the later processes of jewelry production, the process of layered manufacturing will greatly affect the quality and the cost of the final jewelry product. In this research, the quality of jewelry product is defined as the surface finish of the product. Thus, the quality of the rapid prototype of jewelry model will affect the quality of the jewelry product greatly. The quality of rapid prototype is defined by staircase error. The quality of the prototype of the jewelry model, however, may or may not be the best if the staircase error of the prototype is minimum. In addition, the workflow is a generic one and may not be optimal for the jewelry domain. Little research has been done on layered manufacturing of jewelry. They only concern with the building time, support structure and the general process of jewelry production [Frank 1994] [Siu 1997].

Jewelry is divided into several categories like rings, earrings, bangles, necklaces etc. In this research, only jewel rings are considered as they are the simplest type of jewelry.

In jewelry production, three problems are production cost (including material wastage), aesthetic quality of jewelry products and the production efficiency. However, the highest priority problems are minimization of production cost and improvement of aesthetic quality of jewelry products. Therefore, these two problems will be studied in this research.

1.3 Objectives of the research

In the production of functional parts (e.g. engineering parts), dimension accuracy, surface finish and safety are important issues. However, in jewelry production, the concern is different. The first priority problems of jewelry production is concerned with the beautifulness (i.e. aesthetic quality) and production cost minimization (including wastage minimization). Accuracy and tolerance are not the first consideration though they are also important.

Jewelry production has unique characteristics that jewelry is made of precious metal and it is an aesthetic part rather than a functional part. As a result, there are two main objectives in this research. The first is to investigate the theoretical and implementational aspects on minimum precious material wastage in layered manufacturing for jewelry production. The second is to find methodologies that maximally reveal the aesthetic quality of jewelry products.

1.4 Organization of the thesis

The thesis is organized as follows:

Chapter 1: Background of rapid prototyping, production process of jewelry and objectives of the research are described.

Chapter 2: Literature survey about slicing process and building orientation of parts and jewelry in layer manufacturing.

Chapter 3: Methods of slab generation in slicing is described.

Chapter 4: A direct and adaptive slicing method, maximum inscribed slab slicing for building rapid prototypes of jewel rings is explained.

Chapter 5: Gaussian image in building orientation is described.

Chapter 6: A new orientation methodology, maximum visibility building orientation is explained to find the best orientation of jewel rings in layer manufacturing.

Chapter 7: Case studies of the proposed theories: maximum inscribed slab slicing methodology and maximum visibility building orientation are presented.

Chapter 8: Discussion of results and other aspects.

Chapter 9: Future work is described and conclusion is presented.

CHAPTER 2

LITERATURE SURVEY

In this research, slicing and orientation of jewel ring models are concerned. In the following sections, background of these two areas are described.

2.1 Slicing

2.1.1 Slicing process in layered manufacturing

Definition of slicing: slicing is a process that a three dimensional CAD model is converted to series of parallel thin cross sectional layers by intersecting a series of planes with the CAD model or the stereolithography format (STL format) of the CAD model.

In slicing of an object, each two dimensional cross section is a set of closed areas that must be fabricated in a solid material. A solid object is formed by sequentially building and stacking the thin two dimensional layers to form a complete three dimensional object (Figure 2-1) [Johnson 1994a].

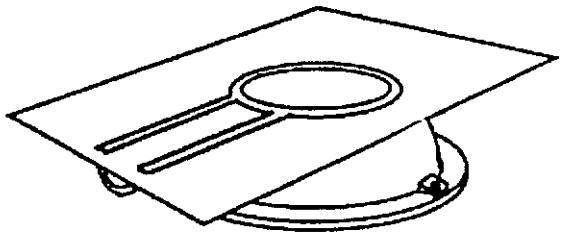

slicing

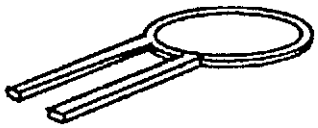

two slices = one layer

Figure 2-1. Slicing of part to form one layer [Johnson 1994a].

Spacing of the slicing planes is matched to the thickness of the solid material layers. Variability of physical layer thickness leads to measurement of the cumulative layer position before performing the next slice calculation. The user can select the layer thickness from consideration of the stair stepping effect (Figure 2-2).

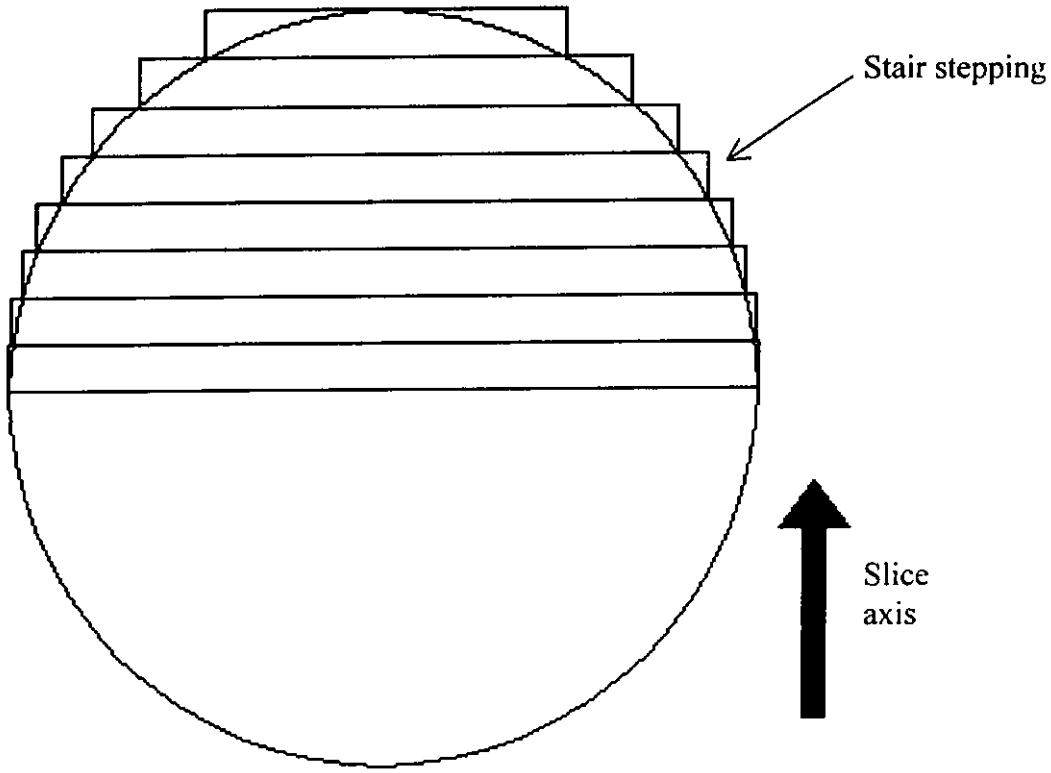

Figure 2-2. Stair stepping of surfaces [Kochan 1993].

2.1.2 Previous related work in slicing process

In 1994, Dolenc and Makela [Dolenc 1994] developed a slicing procedure for the layered manufacturing (LM) process by (i) considering flat and peak areas of the model, (ii) restricting the staircase effect to a user specified tolerance and (iii) offsetting slices for post-treatment operations. In 1994, Suh and Wozny [Suh 1994] described a new adaptive slicing procedure from the exact representation of a part model. The model is divided into sub-regions by considering special features of a part such as vertex peak features (Figure 2-3), edge peak features (Figure 2-4) and face peak features. Each sub-region is sliced adaptively by considering the surface curvature at sampling points. Kulkarni and Dutta [Kulkarni 1995 and Kulkarni 1996] developed an adaptive slicing procedure in 1995 and 1996. A CAD model is first divided into blocks according to the tangency of points and features. Each block is then sliced individually by considering the curvature of the surface in the vertical direction at sampling points of the surface (Figure 2-5). In 1996, Sabourin, Houser and Bohn [Sabourin 1996] used stepwise uniform refinement to slice a model which is firstly divided into thick slabs uniformly. Each slab is sub-divided individually and uniformly according to the specified cusp height. Lee and Yoo [Lee 1997] proposed an idea for direct and adaptive slicing procedure in 1997. The procedure involves the minimization of the stair stepping error by using the mid-planes between the contours as the basis for building layers. A two-sided procedure is used to slice the model in order to improve the accuracy in the z-axis. In 1998, Lee and Choi [Lee 1998] presented a new adaptive slicing algorithm that reduces the computation time for slicing. Optimum sampling points on current sliced contour are searched rapidly by using contour lines. The method involves the comparison of perpendicular distance between two adjacent contours (Figure 2-6). Searching of the optimal sampling points

are sped up by using the characteristic lines (Figure 2-7). In 1998, Zhao and Laperriere [Zhao 1998] proposed another adaptive slicing method for rapid prototyping. The algorithm takes into account the curvature of the surface of the solid model in the vertical direction. A user-specified relative area deviation ratio was introduced in slicing. Lu, Liu and Zhang [Lu 1998] discussed a new adaptive slicing method in which the difference of volume is used as tolerance criterion to deduce the layer thickness. If the current input layer thickness does not satisfy the requirement, layer thickness is reduced until the criterion is satisfied. However, they had not considered the algorithm on how to reduce the layer thickness. They also had not considered the slicing resolution. However, containment problem was discussed by considering the tolerance between the sectional areas of two adjacent slices. In 1999, Mani, Kulkarni and Dutta [Mani 1999] developed a new region-based adaptive slicing method in which a model is divided into different zones. For each zone, the model is further divided into Adaptive Layer Thickness (ALT) region and Common Interface Layer (CIL) for adaptive slicing and uniform slicing respectively.

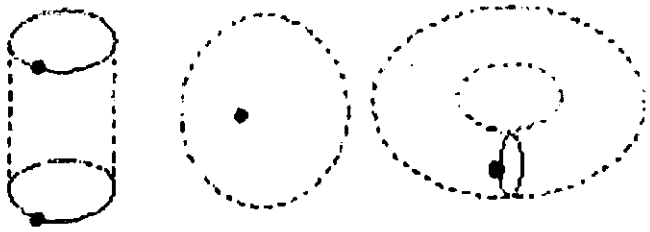

(a) Topology vertices.

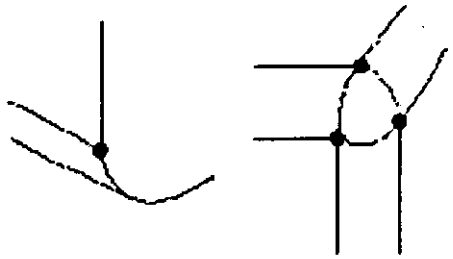

(b) Smooth vertices.

Figure 2-3. Vertex peak features.

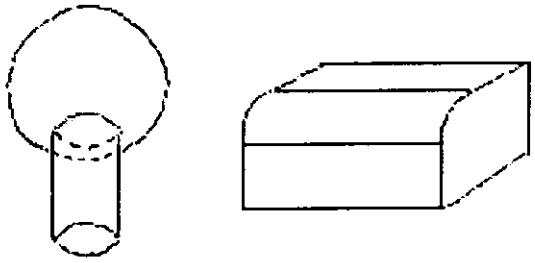

(a) Horizontal edges.

(b) Extreme points.

Figure 2-4. Edge peak features [Suh 1994].

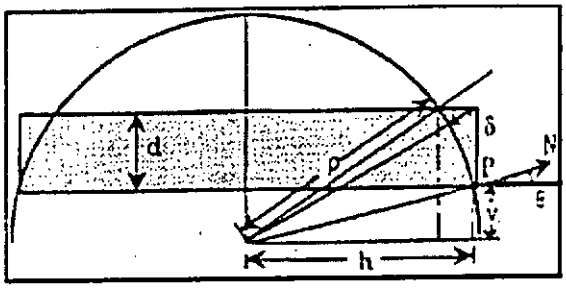

(a) Point P lies in the upper semicircle.

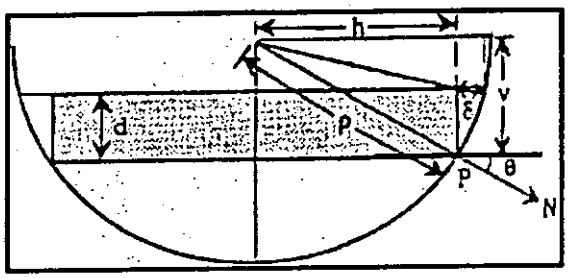

(b) Point P lies in the lower semicircle.

Remark:

P: sampling point at which the surface is maximum curvature in the vertical direction.

d: thickness of the layer

N: surface normal at point P

θ: the angle that the surface normal makes to the horizontal

δ: the allowed cusp height

Figure 2-5. Curvature of sampling point P is used to calculate the layer thickness d [Kulkarni 1995].

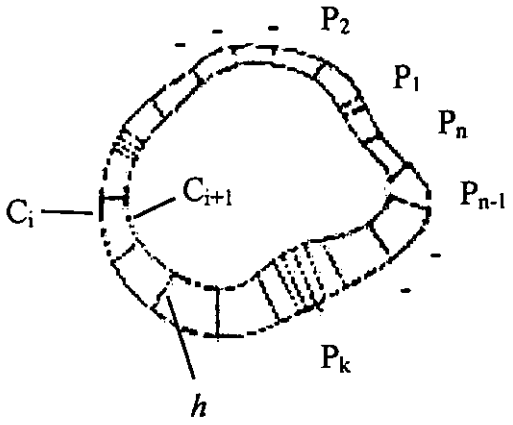

(a) Perpendicular distance between slices.

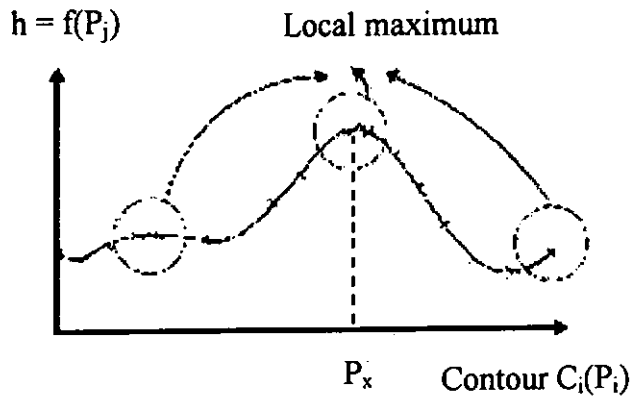

(b) Determination of the optimum point.

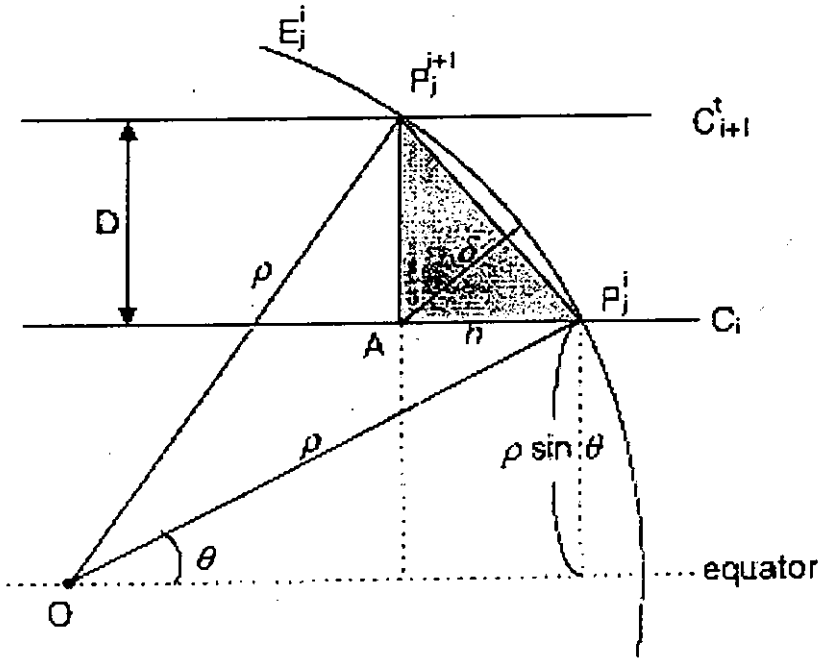

(c) Relationship between h and δ.

Remark:

h: perpendicular distance between slices

C: slicing contour

P: sampling point(s)

δ: cusp height

Figure 2-6. Searching of optimum sampling points on current sliced contour rapidly by using contour lines and the comparison of perpendicular distance between two adjacent contours [Lee 1998].

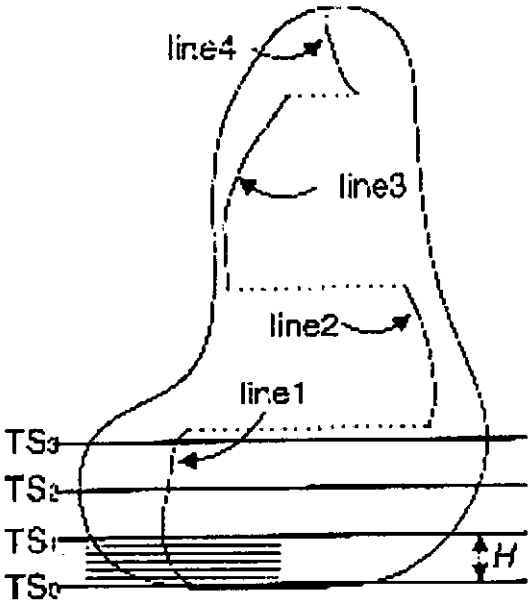

Figure 2-7. Illustration of character lines [Lee 1998].

2.1.3 Brief summary of previous slicing methods

In summary, the previous research mainly used surface curvature to deduce the layer thickness. However, this would be quite complicated and time consuming. Besides, slicing criteria is different for different consumer goods. Therefore, slicing methodology should be considered for particular industry like jewelry production.

2.2 Building orientation

2.2.1 Orientation of built part in layered manufacturing process

Building orientation is a process that CAD models (or STL format of the model) are put on a suitable position on the building platform such that the parts are stabilized and have high quality during layer fabrication process (i.e. part building).

2.2.2 Previous related work in building orientation

There are a number of researches being done in the past about part orientation in rapid prototyping or layered manufacturing. In 1994, Frank and Fadel [Frank 1994] proposed an expert system tool for determining the preferred part building orientation for stereolithography processes. An expert system was used to interact with the user to assess the most critical issues for deciding the optimal part building position. Three aspects were concerned in the expert system: surface finish, build time and support structure. Surface finish is considered as the most important, then the build time and finally, the support structures. The research defines specific geometric features such as a hole or a plane. Characteristic feature axis is defined and orientation of specific geometric features is described. In 1994, Allen, Dutta and Arbor [Allen 1994] determined the best direction to build an object by layered manufacturing processes. The object was constructed with minimal support structures and was stable, and rested on a planar base. Ray-structure computation was used for each orientation in analyzing the support structure. The object intersects with rays will produce intersection points. The intersection points are then classified by the direction of normals. For face with normal pointing upwards, the corresponding point on the object does not need support, otherwise, the boundary points on the object may need support. For the latter, they will be further classified as supported or unsupported. If

the angle between the face normal and the negative z-axis (building direction) is smaller than the user specified angle, support will be added. Otherwise, the points are unsupported.

In 1995, Cheng, et al. [Cheng 1995] developed a multiple objective-function as a formulation to derive the optimal orientation for stereolithography process. Two objective functions are defined. The primary objective function considers the part accuracy. The influence by the types of surfaces on the accuracy will be represented by a weight. The secondary objective function deals with the build time. The build time of the orientation obtained from primary objective function is checked.

In 1997, Ng and Tan [Ng 1997] optimized the part orientation in rapid prototyping processes by using feature-based functions. Three factors were used to determine the optimal orientations: part accuracy, build time and support structures. Two functions: feature weight and feature objective value were used to analyze the part accuracy and to determine the potential candidates for optimal part orientation. Optimal orientation was then chosen from the potential candidates based on minimal building time using minimum number of layers. In 1997, Xu, et al. [Xu 1997] sliced a CAD model directly by introducing an adaptive variable thickness slicer implemented on a solid CAD modeller and obtain an optimal building orientation by considering building time, part accuracy and part stability in SLA. The building time is measured in terms of the number of layers to be built. In building parts using SLA, part accuracy can be improved by minimizing the overhang area. Overhang area is calculated by using a function. If the projection of the mass center falls within the convex hull of the base geometry, the part is assumed to be in a stable building direction. If not, the part is unstable in that building direction. In 1997, Xu, et al. implemented an adaptive variable slicer on a solid CAD modeler [Xu 1997]. The

slicer employs a genetic algorithm to find the minimal layer thickness allowed at certain referenced height for a given cusp height tolerance. They concerned the optimal orientation with adaptive slicing for part building in stereolithography system. Part building time, building accuracy and part stability are also concerned.

In 1998, Loh, et al. analysed the selection of different optimal orientations of parts in different RP processes [Loh 1998]. In 1998, Maswood, et al. described a methodology to compute the volumetric error developed in selected primitives for any orientations of parts [Maswood 1998]. Primitives like cylinders, cubes, spheres, cones and pyramids were used for experiments. Orientations of primitives range from 0 to 90 degrees. Volumetric error was calculated for layers for each primitives and the best orientation in each case is found. FDM is used in the experiments. In 1998, Campbell developed a new algorithm to optimize the build orientation by considering different surface roughness of different features in the RP model [Campbell 1998]. The aim of the optimization is to ensure that specific surface roughness requirements are met while also keeping the overall average surface roughness to a minimum. The required surface roughness values are embedded into a featured-based product model by the designer. An application module then uses empirical surface roughness data to calculate the actual values which will be achieved for each feature. This process is repeated for orientation intervals of five degrees on the x and y axes. Once the optimum orientation has been calculated, a sensitivity analysis can be performed to see what effect changes in orientation and /or surface roughness specification will have. In 1998, Alexander, et al. proposed methods for calculating cost and orientation of parts in layered manufacturing [Alexander 1998]. Part orientation is analyzed from a generic point of view and the solution is not specific to any process and material. A general cost model is discussed to apply to different layered manufacturing processes.

Cost for multiple orientations can be calculated to find the cheapest. Hur and Lee determined the optimal orientation of part in stereolithography process in 1998 [Hur 1998]. An algorithm is developed to calculate the staircase area, quantifying the process errors and calculating optimal layer thickness. The optimal orientation can be determined by considering these criteria.

Xu, et al. discussed the selection of building direction for four RP processes in 1999: stereolithography (SL), selective laser sintering (SLS), fusion deposition modeling (FDM) and laminated object manufacturing (LOM) [Xu 1999]. The influence of the process characteristics on the selection of appropriate orientation with different RP processes is illustrated in the example. In 1999, Pham, et al. produced a decision-support tool to help RP users to orient the prototype correctly in RP machine to obtain the best trade-off between time, cost, and accuracy [Pham 1999]. The decision support tool is aimed at stereolithography. The tool is a feature based system produced using an object-oriented programming language and a solid modeling CAD environment. Cost, time, problematic features, optimally oriented features, overhanging area, and support volume are considered when recommending a build direction to the user.

2.2.3 Brief summary of previous orientation methodologies

In general, the previous researches concern mainly with part accuracy, build time, support structure and part stability of the prototype to be built in the RP machine. However in jewelry production, aesthetic quality is the main concern. In layered manufacturing of jewelry, the building orientation will definitely affect the

quality of the prototype. Thus, a new methodology is introduced in this research to give the best-built orientation for jewelry production.

2.3 Previous solution for the problem

For academic research, slicing and building orientation of jewel ring prototypes are concerned. In the former part, a new slicing methodology is proposed to minimize the production cost (including wastage minimization) of jewel rings. Only symmetrical jewel rings are considered. In the second part, building orientation is concerned in order to improve the beautifulness (i.e. aesthetic quality) of jewel rings.

In previous research, Chua, et al. demonstrated the use of three dimensional graphics and computer numerical control (CNC) technologies in jewelry design in 1989 [Chua 1989]. The effective integration of these technologies made it possible to rapidly produce accurate and complex objects which were previously crafted by highly skilled pattern makers. In 1991, Chua and Gay discussed the effectiveness of integrating CNC, metrology and three-dimensional computer-aided design and manufacturing systems (CAD/CAM) in the design and manufacture of rings [Chua 1991a]. The integration of such systems provides a powerful means of capturing geometrical data of complex solid objects for which no drawing exists. The captured geometry can then be modified, analysed and submitted for machining as desired. In 1991, Chua, et al. also reported on how the traditional process can be shortened through the use of computer-based tools and rapid prototyping technology [Chua 1991b]. The research work studied the Singapore jewelry manufacturing practices in an attempt to upgrade the quality and quantity of production with the use of a comprehensive CAD/CAM systems and Stereolithography Apparatus (SLA). In 1995, Ipplito, et al. demonstrated the integration of reverse engineering, rapid prototyping and investment casting in the jewelry's craft [Ipplito 1995]. The complex shape of most items of jewelry restricts the use of CAD techniques in their manufacture. The

usual practice is to regard a new jewel as a new modification of previous piece. Reverse engineering is then employed to reduce the CAD modelling time. The paper illustrates how this can be done by combining a 3D scanner laser with a rapid prototyping and investment casting. In 1997, Siu attempted to identify the loss of quality of craftsmanship-intensive products [Siu 1997]. The concept of "integrated craftsmanship" was constructed and developed to assist the integration of traditional goldsmith's and jewelry designers' techniques in jewelry designing and making and to modify or change attitudes to quality control in mass production system. In 1998, Leong, et al. investigated the effect of microblasting process on the surface finish of jewelry models built using SLA [Leong 1998]. In 1999, Wong, et al. described the development of a management information system with a specially designed decision support system to meet the specific requirements of Hong Kong's jewelry industry [Wong 1999].

In the previous research, they mainly studied the application of different existing technologies like CAD/CAM and rapid prototyping systems in jewelry production process in order to improve the production efficiency or enhance the production quality. However, they integrated existing technologies instead of creating new methodologies to solve the problem. Besides, they have not considered the improvement of the production cost (including material wastage). nor the aesthetic quality of jewelry products in details.

2.4 Industrial practice

In this research, the aim is focused on slicing and building orientation of jewel ring prototypes to minimize the production cost (including wastage minimization) of jewel rings (only symmetrical jewel rings are considered) and improve the beautifulness (i.e. aesthetic quality) of jewel rings respectively. Thus, the part of CAD model construction process is not taken into consideration. However, some descriptions of modern industrial practice is introduced.

In general, commercial practices being applied in the jewelry industry are based on reverse engineering methods. They can be grouped into three categories:

(i) A physical model of jewelry exists and its dimensions can be obtained by direct measurement (e.g. by vernier caliper). Finally, three-dimensional CAD model is drawn and prototypes are made.

(ii) Multiple, orthogonal hand-drawing of a jewel exists and its dimensions are obtained by direct measurement (e.g. by using ruler) from the drawings. Eventually, three-dimensional model is drawn and prototypes are made.

(iii) Images files/photos (top view, front view are included) of a jewel exist(s) and NURBS curves of the jewel can be traced out directly from images files or photos. Finally, three-dimensional model is drawn and prototypes are made.

Methods (i) and (ii) are not too reliable. The reason is that the dimensions of jewelry is just measured from a finished product made by craftsman and hand-drawing respectively. Errors may occur in measurement. Therefore, the CAD model drawn may have errors. In method (iii), the dimensions and shape of jewelry is traced from the image file or photos of the jewelry. Errors may occur in trace of curves and measurement.

CHAPTER 3

SLAB GENERATION IN SLICING

In Chapter 1, the initial input of jewelry production process is the master wax models. In this chapter, the master wax models (or master resin models) will be produced by layered manufacturing process. To simplify the problem, these will be used in jewel ring production and shrinkage is also ignored.

3.1 Slab generation

Slicing is an essential step in layered manufacturing. In direct slicing, the input is a closed surface model or a solid model. The output is a stacked slab model which is an approximation of the original one (Figure 3-1). In indirect slicing with tessellation, curved objects will have one more approximation

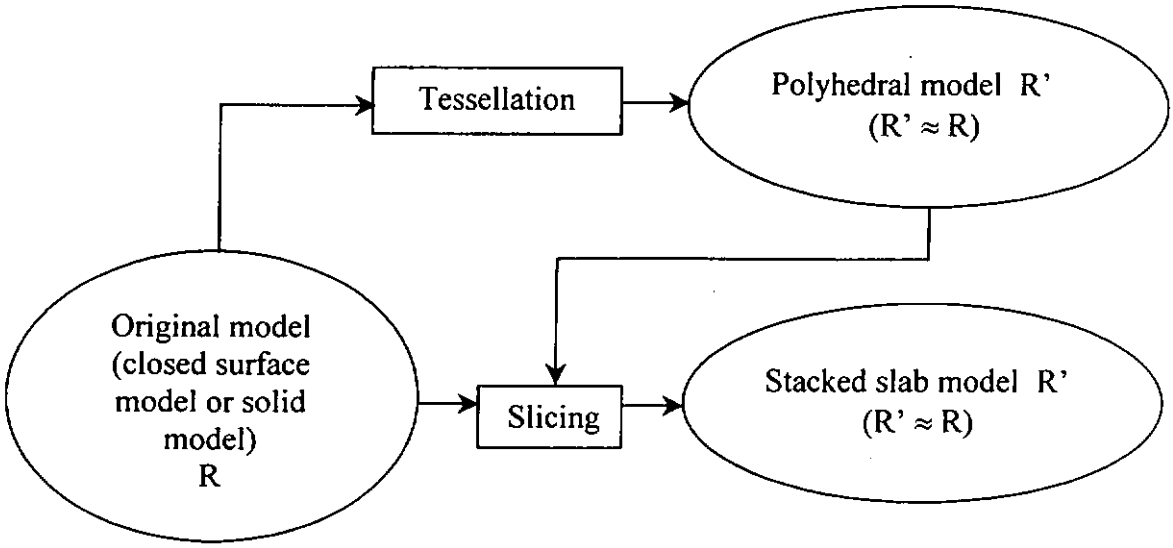

Figure 3-1. Input and output of slicing.

In traditional slab generation, the object is sliced uniformly by section planes (Figure 3-2). Slabs are then generated by extruding the intersection result. There are four ways of extrusion. In the first case, the intersection points are extruded upwards to form the slabs (Figure 3-3a). As the bottommost slice is extruded upwards, the bottom part of the object cannot be built. For downward extrusion in the second case, the uppermost part of the object is not built (Figure 3-3b).

In the third case, the slab model extruded will enclose the object. For instance in Figure 3-3c, the intersection points on the upper half of the object are extruded upwards while the intersection points on the lower half of the object are extruded downwards.

In the fourth case, the slab model extruded will be enclosed by the object. For instance in Figure 3-3d, the intersection points on the upper half of the object are extruded downwards while the intersection points on the lower half of the object are extruded upwards. As the bottommost slice is extruded upwards and the uppermost slice is extruded downwards, the lowest part and the topmost part of the object cannot be built respectively.

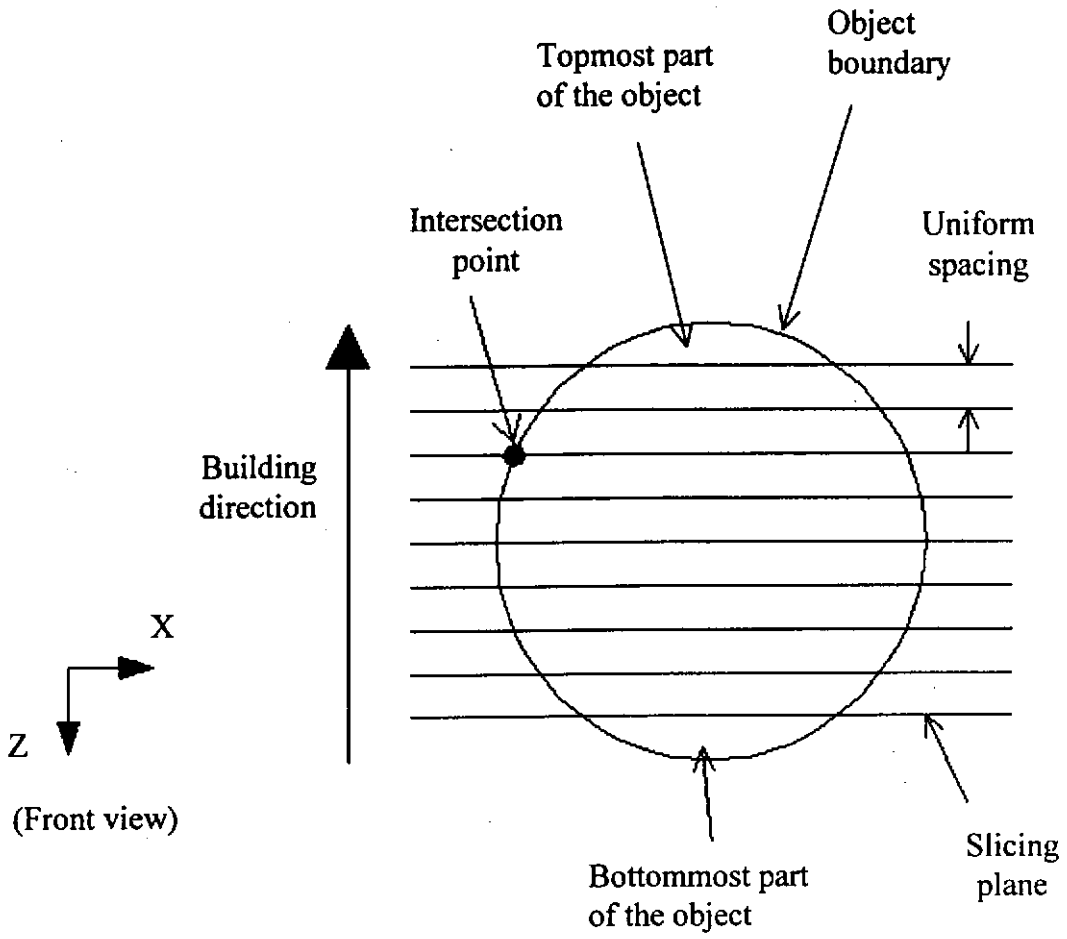

Figure 3-2. Slicing planes intersect with the object.

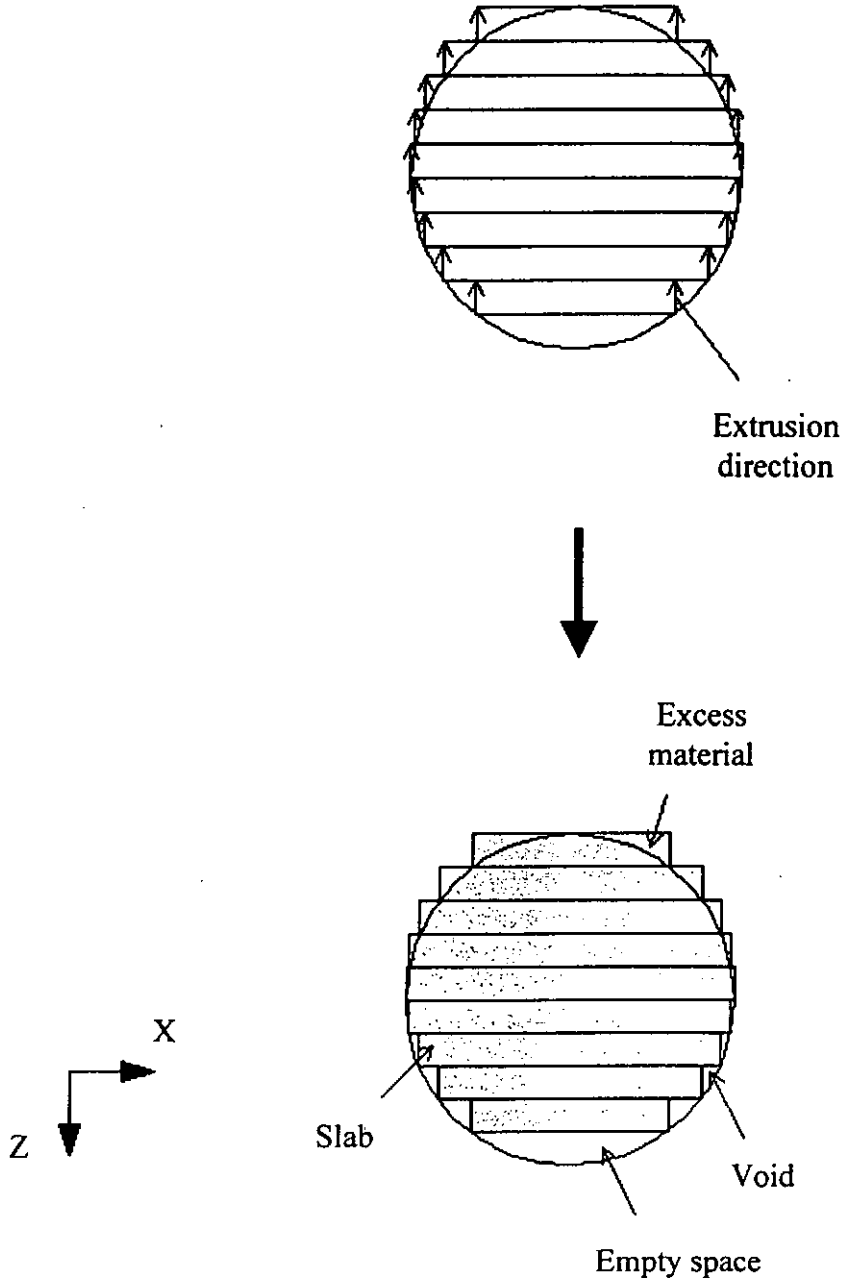

(a) Upward extrusion slab generation.

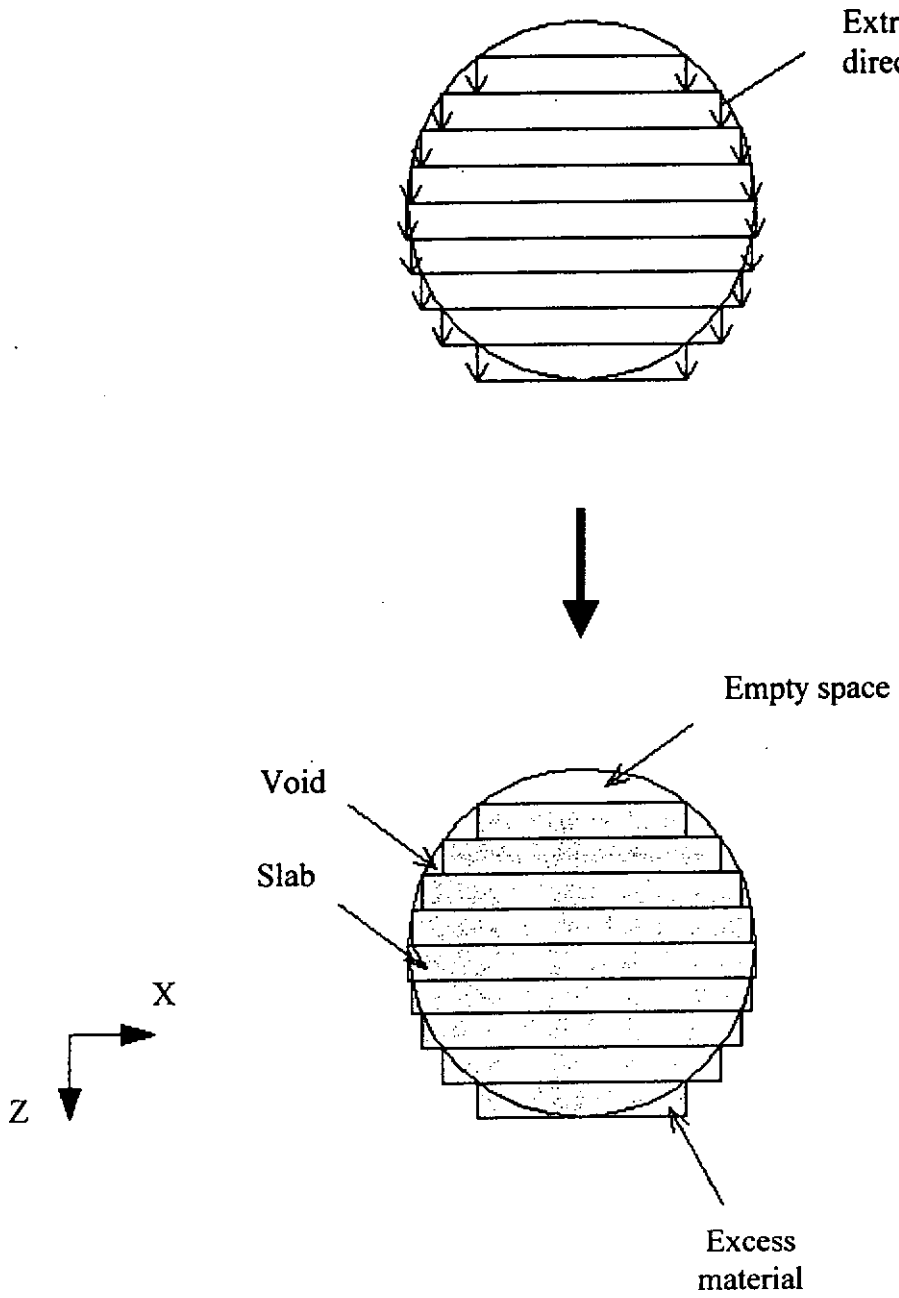

(b) Downward extrusion slab generation.

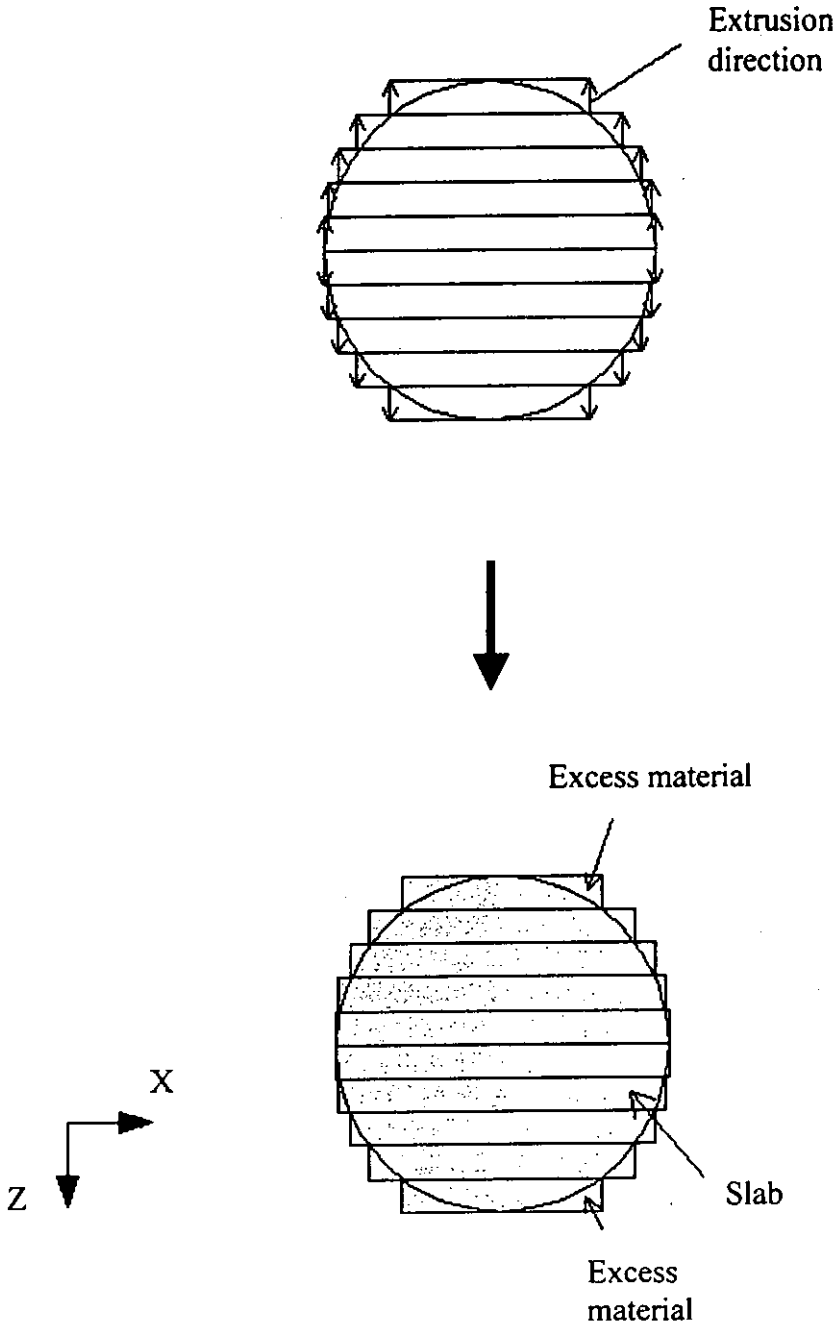

(c) Circumscribing slab generation.

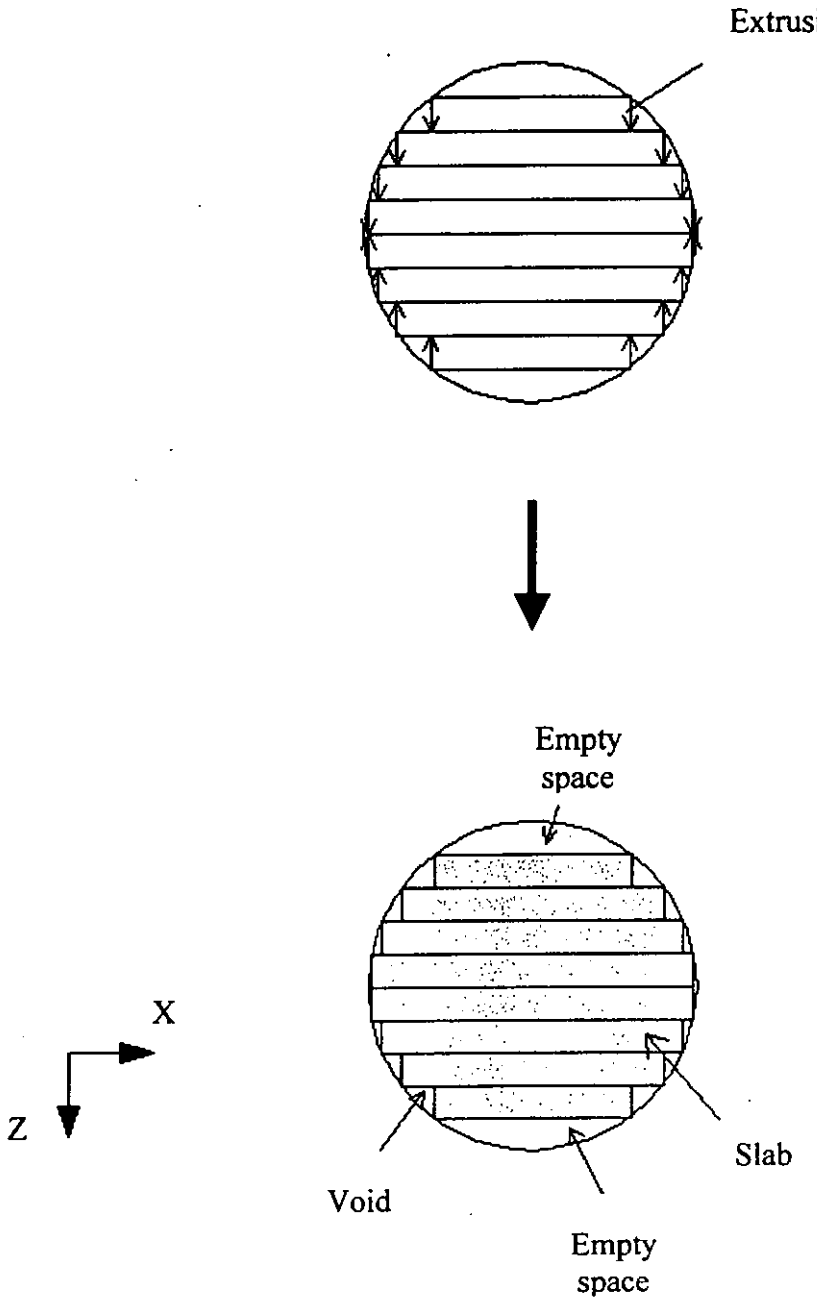

(d) Inscribing slab generation.

Figure 3-3. Possible slab generation.

3.2 Slab approximation

From the various extrusion methods, there are three ways in which the stacked slab model R' can approximate the original object R [Johnson 1994b]. In the first case, R and R' (Figure 3-4a) intersect with each other but do not enclose one another. Mathematically, $R \cap^* R' \neq R \wedge R \cap^* R' \neq R' \wedge R \cap^* R' \neq \varnothing$. In this case, material needs to be removed from and added to the physical prototype. In practice, it is difficult to locate which part of the physical prototype needs material addition and which part needs material removal in order to maintain the size and shape of the original model. In the second case (Figure 3-4b), R' encloses R. Mathematically, $R \subset R'$. In this case, excess material needs to be removed from the physical prototype in order to maintain the size and shape of the original model. The material to be removed is treated as waste. In the third case (Figure 3-4c), R encloses R'. Mathematically, $R' \subset R$. In this case, material needs to be added to the physical prototype in order to maintain the size and shape of the original model.

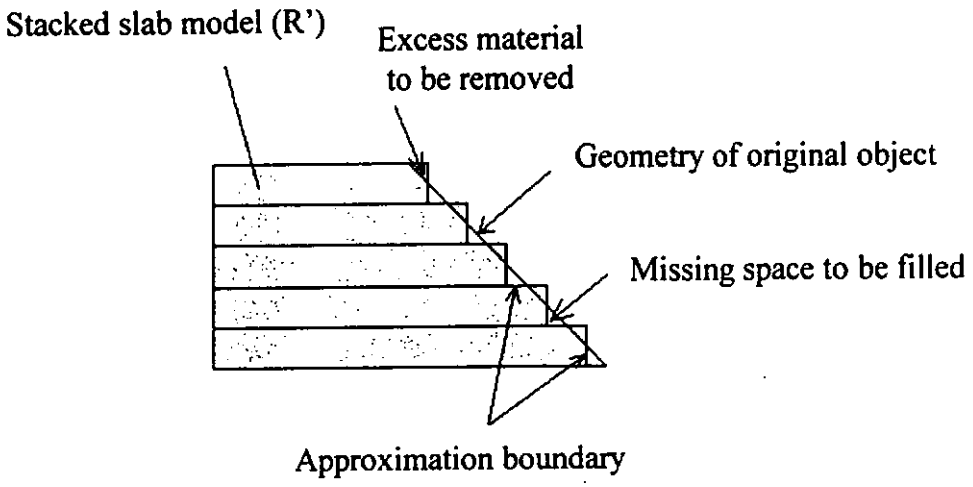

(a) Intersection approximation.

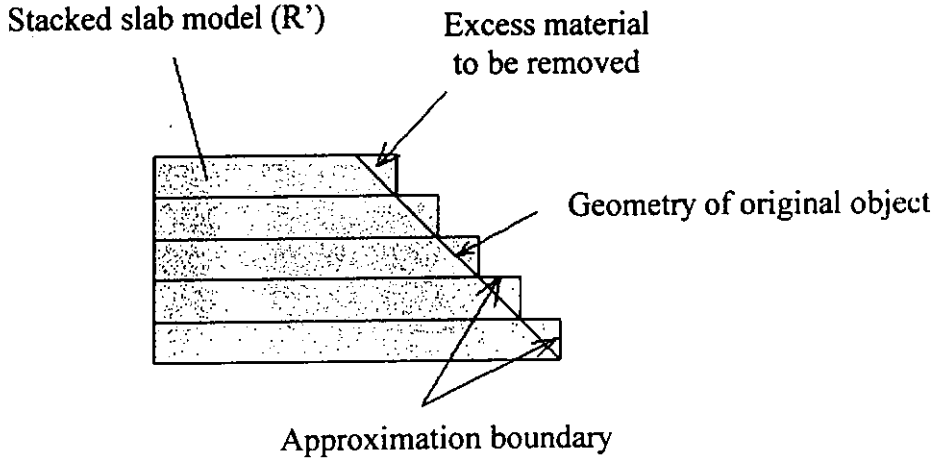

(b) Circumscribing approximation.

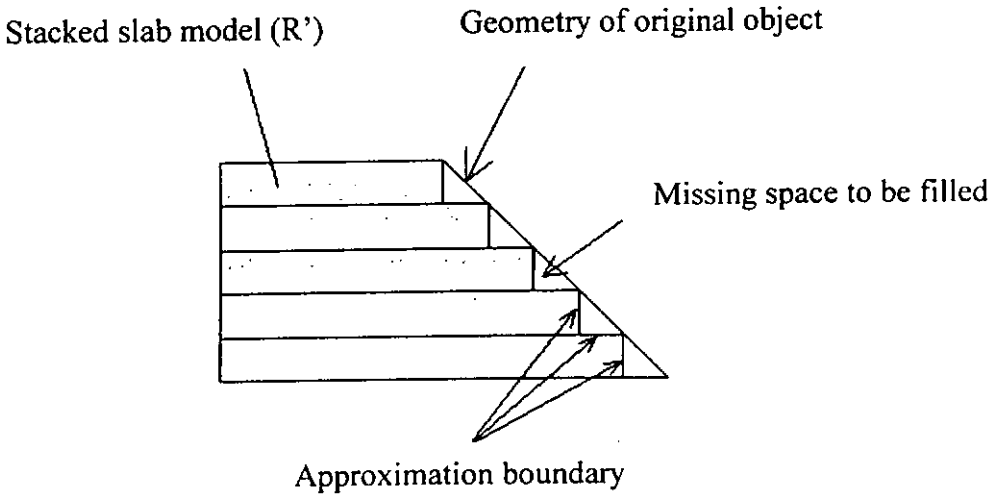

(c) Inscribing approximation.

Figure 3-4. Slab approximation.

3.2.1 Error of slab model

In slicing, the stacked slab model approximates the original object by generating slabs. Therefore, the volume of slab model is different from the original one. In the following section, an ellipsoid is used as an example to illustrate the volumetric error in the approximation.

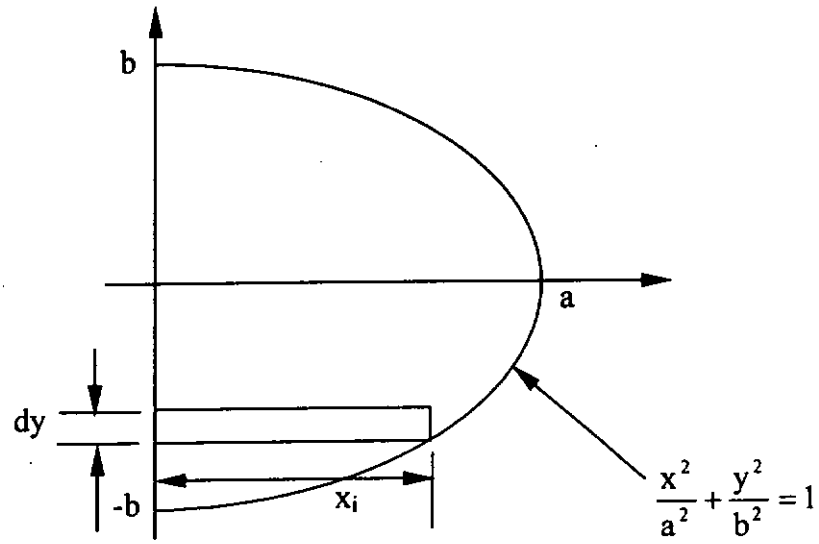

(a) Ellipsoid generated by rotating half of an ellipse curve.

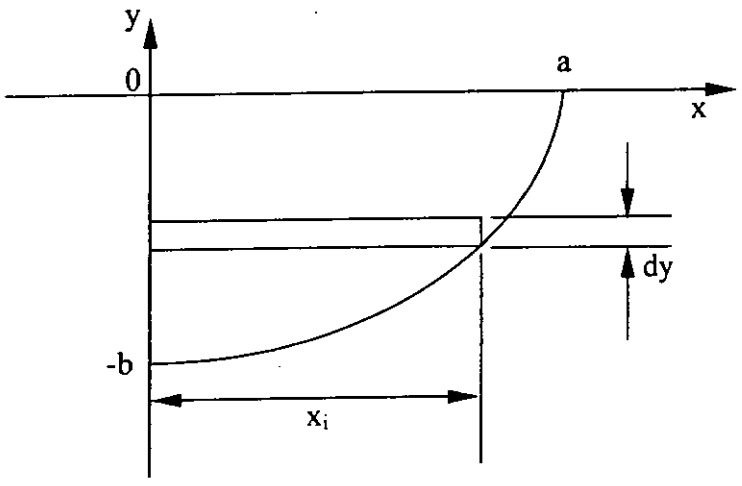

(b) Slicing of ellipsoid at i^{th} interval.

Figure 3-5. Error in slab model generation of an ellipsoid.

The volume of ellipsoid can be calculated from the volume generated by the rotation of the half of the ellipse curve (Figure 3-5a).

Theoretical volume of ellipsoid (S_t):

$$\int_{-b}^{b} \pi x^2 dy = \int_{-b}^{b} \pi \left[a^2 \left(1 - \frac{y^2}{b^2} \right) \right] dy$$

$$= \left[a^2 \pi y \right]_{-b}^{b} - \left[\frac{\pi a^2 y^3}{3b^2} \right]_{-b}^{b}$$

$$= \frac{4}{3} \pi a^2 b$$

Assume the region are sliced into n intervals (Figure 3-5b).

Then at i^{th} interval:

$$V_i = \pi x_i^2 dy$$

$$= \pi \left[a^2 (1 - \frac{y_i^2}{b^2}) \right] dy$$

where $dy = \frac{b-0}{n} = \frac{b}{n}$

Thus half volume of ellipsoid V_h

$$= \pi \left\{ a^2 \left(1 - \frac{\left(\frac{b}{n}\right)^2}{b^2} \right) \right\} \frac{b}{n} + \ldots\ldots + \pi \left\{ a^2 \left(1 - \frac{\left(\frac{ib}{n}\right)^2}{b^2} \right) \right\} \frac{b}{n} + \ldots\ldots \pi \left\{ a^2 \left(1 - \frac{\left((n-1)\frac{b}{n}\right)^2}{b^2} \right) \right\} \frac{b}{n}$$

$$= \sum_{i=0}^{n-1} \pi \left\{ a^2 \left(1 - \frac{\left(\frac{ib}{n}\right)^2}{b^2} \right) \right\} \frac{b}{n}$$

Then total volume $V_a = 2\ V_h$

Volumetric error equals to:

$E = S_t - V_a$

$$= \frac{4}{3}\pi a^2 b - 2\left[\sum_{i=0}^{n-1}\pi\left\{a^2\left[1-\frac{\left(\frac{ib}{n}\right)^2}{b^2}\right]\right\}\frac{b}{n}\right]$$

3.3 Jewel ring specific requirement

In the production of functional parts (e.g. engineering parts), dimension accuracy, surface finish and safety are important issues. However, jewelry is aesthetic product. Accuracy and tolerance are not the first consideration in jewelry production. Instead, jewelry production is concerned with the beautifulness and wastage of precious metal like gold, platinum, silver, etc.

There are many types of jewelry: jewel rings, earrings, bangles, necklaces, etc. In this research, only rings are considered as rings are the most common and popular item among all types of jewelry. There are many types and styles of jewel rings. Some have diamonds, ruby or other gemstones. Some are symmetrical but some are not and some are irregular in shape. A new slicing methodology is investigated in this research which emphasizes on how to build a symmetrical jewel ring symmetrically and minimize the wastage of precious metal.

3.3.1 Wastage minimization

As mentioned in Chapter 1 (Figure 1-5), if the master RP pattern is an inscribed model (Figure 3-6), the metal model before final touch up is also an inscribed model. That is, material addition is needed for this metal model. Since jewel rings are made of precious metals such as silver, gold and platinum. Thus, in rapid prototype building, material addition is more preferred than material removal in the post-treatment processes in order to minimize production cost and wastage. As a result, the slab model in Figure 3-4c (R encloses R') is chosen as a potential representation for jewel ring rapid prototype. However, the bottom part and the top part in Figure 3-3d cannot be built. To circumvent this, slabs with minimum possible

slicing thickness (L_{min}) are used to the produce the top and bottom slabs (Figure 3-7). This will minimize the precious material to be removed.

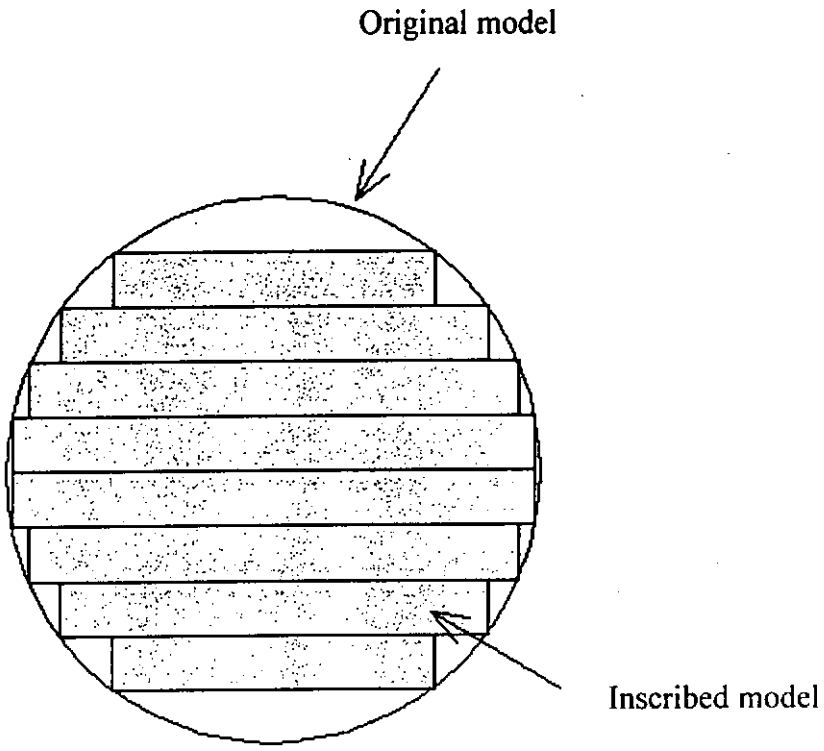

Figure 3-6. Original model and inscribed model in inscribed slab slicing.

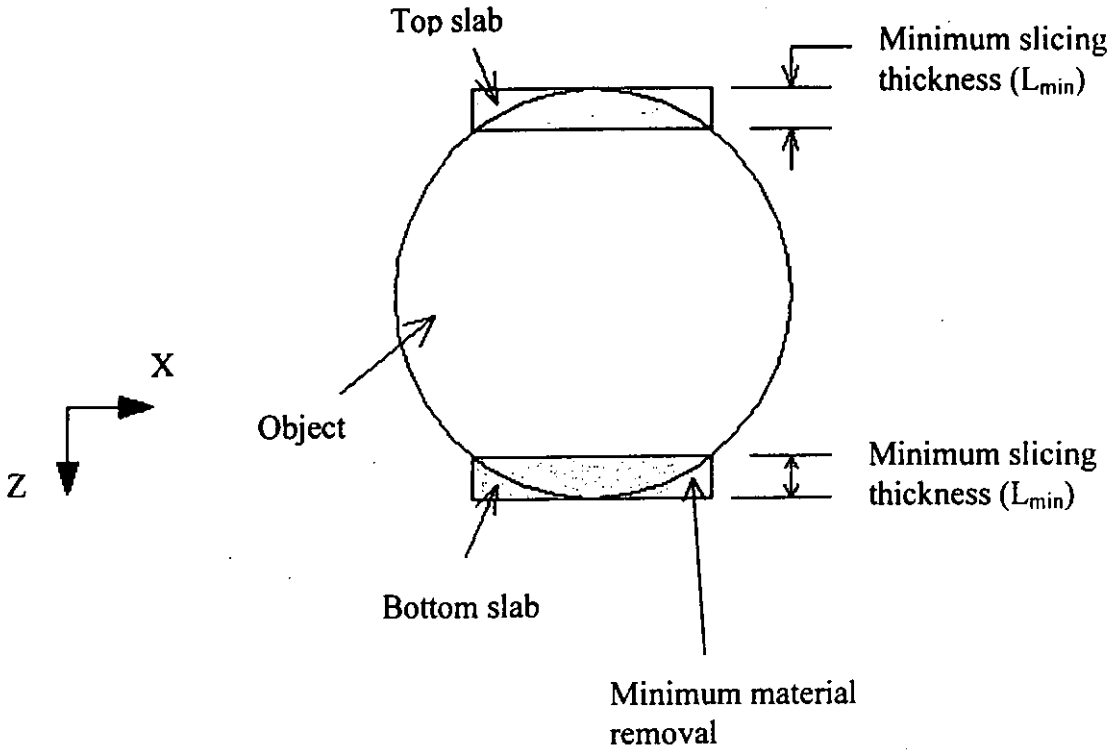

Figure 3-7. Minimum slicing thickness of the top and bottom slabs.

3.3.2 Symmetry preservation

If a jewel ring possesses certain symmetrical property, the stacked slab model should maintain the same symmetrical property. Otherwise, the quality of the jewel rings will be affected. For instance, some jewel rings are symmetrical (Figures 3-8a to 3-8d) but some are not. In addition, each jewel ring has its unique centroid and unique principal axes (or unique principal planes) [Meriam 1997]. These are intrinsic properties of the jewel rings and are independent of the reference coordinate system.

Without loss of generality, the coordinate system of the rapid prototyping hardwares (or softwares) is aligned with the principal axes of the jewel rings, i.e. where the products of inertia I_{xy}, I_{xz}, I_{yx}, I_{yz}, I_{zx} *and* I_{zy} vanish. This will maximize the maintenance of the symmetric property.

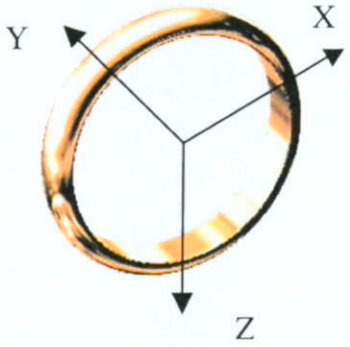

(a) Jewel rings symmetrical about principal planes XY, YZ and ZX.

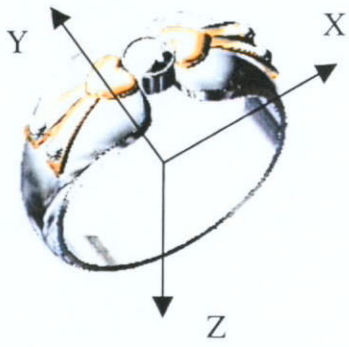

(b) Jewel rings symmetrical about principal planes YZ and ZX.

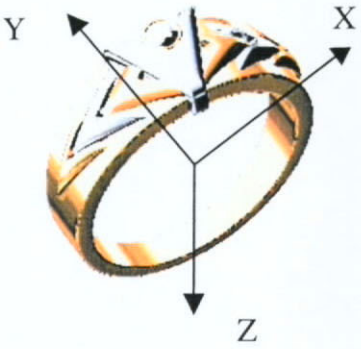

(c) Jewel ring symmetrical about principal plane YZ.

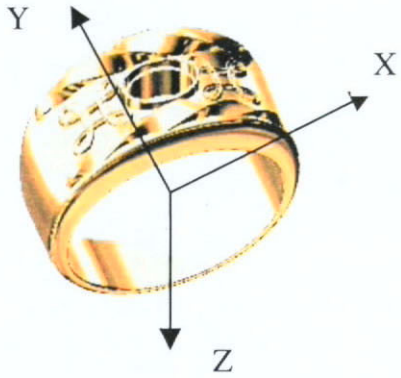

(d) Jewel ring symmetrical about principal plane ZX.

Figure 3-8. Symmetric jewel rings.

CHAPTER 4

MAXIMUM INSCRIBED SLAB SLICING

Four types of maximum inscribed slab slicing will be investigated in this research. They include bottom-up vertical slicing, top-down vertical slicing, middle-up vertical slicing and middle-up horizontal slicing. These four methodologies sliced CAD model of the jewel ring in different ways and the jewel ring model will also build in different orientations. A 3D solid torus (Figure 4-1) is used as a simplified representation of jewel ring models to illustrate the methodologies.

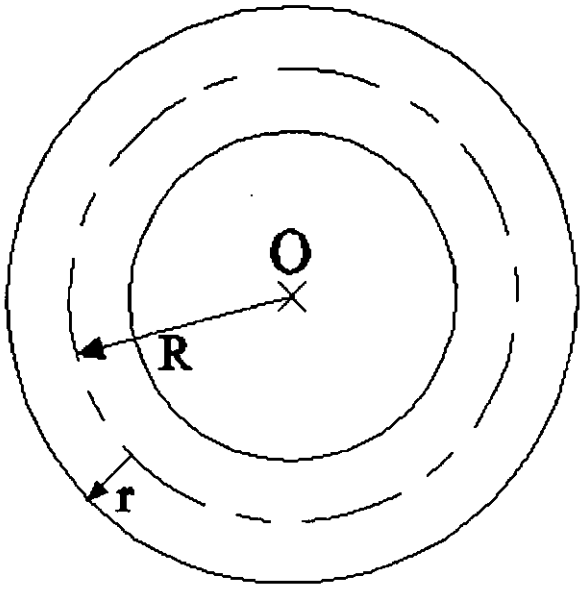

Figure 4-1. Torus used for illustration of slicing (left hand coordinate system).

4.1 Bottom-up vertical slicing

This type of slicing is applicable to the four types of jewel ring models (Figures 3-8a to 3-8d). The torus is sliced in the vertical direction from bottom to top (Figure 4-2). The slicing algorithm of the solid torus can be divided into three steps to produce the bottom slab, the middle slabs and the top slab. Before the slicing process starts, users need to input the volume efficiency, minimum and maximum layer thickness. Volume efficiency η ($0.85 \leq \eta \leq 1$) is defined as the ratio of the volume of slab between two slices to the volume of the exact model being sliced between these two slices (Figure 4-3). The minimum and maximum layer thicknesses achievable by the rapid prototyping systems are denoted by L_{min} and L_{max} respectively where $L_{max} = \lambda * L_{min}$ and $\lambda \in N$.

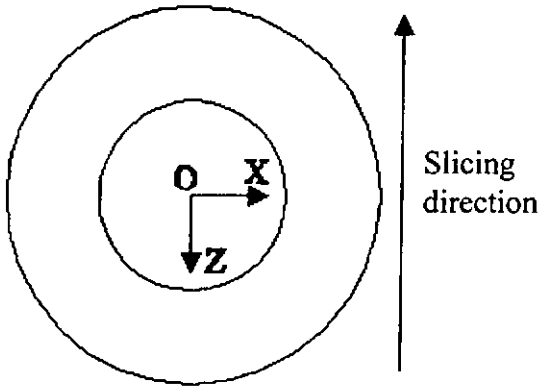

Figure 4-2. Position and orientation of torus in bottom up vertical slicing.

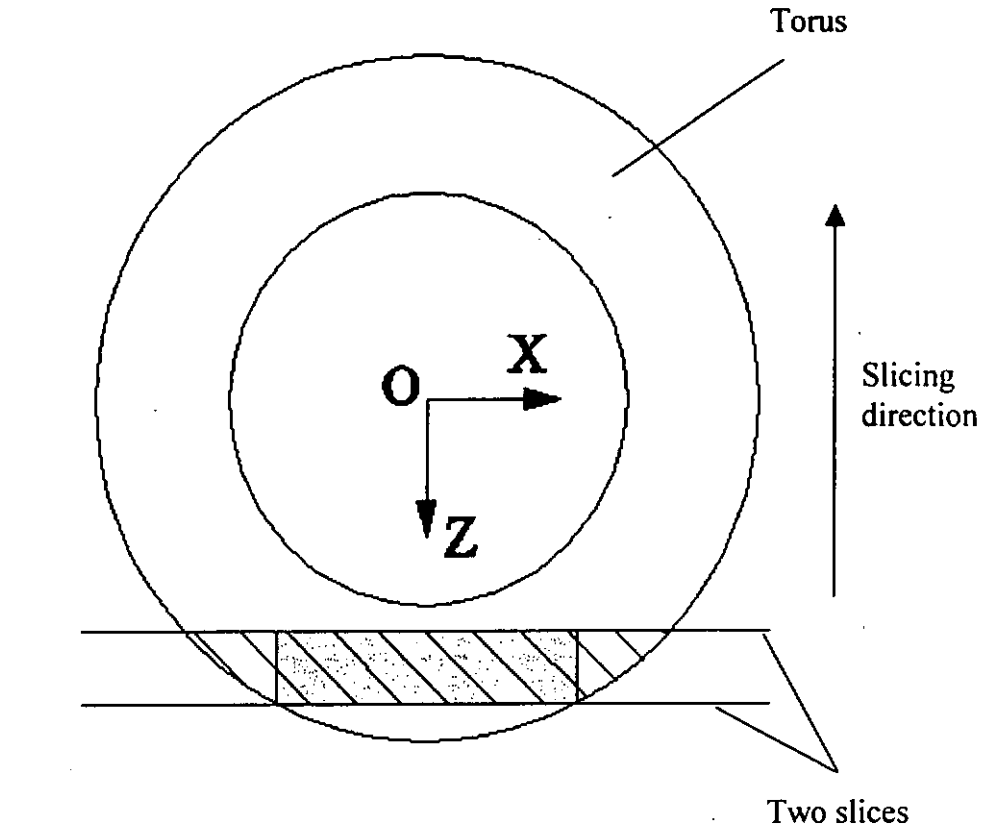

Figure 4-3. Slab and part between two slices.

4.1.1 Bottom slab production

In traditional layered manufacturing process, the bottom contact point of the torus cannot be built (Figure 4-4), no matter how small the height of the first slice is. To produce the bottom point, the planar region A_1 from the first slice is extruded downwards to the level of the bottom point to form a slab, $Slab_0$ (Figure 4-6). In maximum inscribed slab slicing, $Slab_i \subset Part_i$. However in the current case, if $Slab_0 \subset Part_0$ ($Part_0$: part of torus between Z level of the bottom point and Z level of the first slice), the bottom point cannot be built. As a result, the bottom point is built with $Slab_0 \not\subset Part_0$. The shaded region in Figure 4-6 is the excess material to be removed from the physical prototype of the torus. As L_{min} is the minimum layer thickness, the first slab, $Slab_0$ has the minimum excess material. Similar case occurs in the top slab production.

Therefore in this step, only one slice is involved. The planar region A_1 is obtained by intersecting the torus with the plane π_1 (Equation 4-1). The intersection is regularized as the objects other than the torus may have dangling intersection result. Then, A_1 is set to be S_0 (Equation 4-2). S_0 is extruded downwards to form the bottom slab, $Slab_0$ (or $Slab_{bottom}$) (Equation 4-3) as shown in Figure 4-5. The extrusion height is L_{min} and the direction is $\boldsymbol{k}$. The path of extrusion is L_0 (Equation 4-4).

Mathematically,

Slicing :

$$T \cap^{\bullet} \pi_i \rightarrow A_i \qquad (4-1)$$

$$A_i \rightarrow S_o \qquad (4-2)$$

Extrusion :

By Minkowski operation [Guo 1998]

$$Slab_o = S_o \oplus L_o$$

$$= \{\mathbf{d} \in \mathbf{R}^3 : \mathbf{d} = \mathbf{a} + \mathbf{b}, \mathbf{a} \in S_o, \mathbf{b} \in L_o\} \qquad (4-3)$$

where L_o is a straight line segment such that

$X = 0$,

$Y = 0$ and

$$Z = t\,R + (1-t)(R - L_{min}) \qquad t \in [0,1] \qquad (4-4)$$

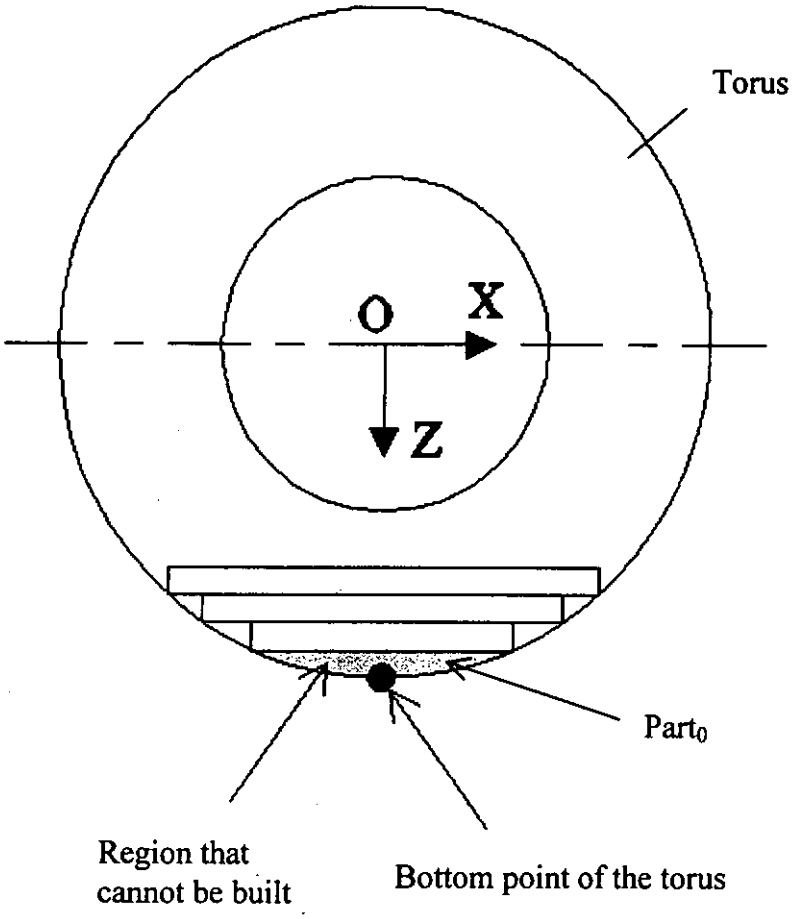

Figure 4-4. Bottom point of the torus that cannot be built in traditional slicing.

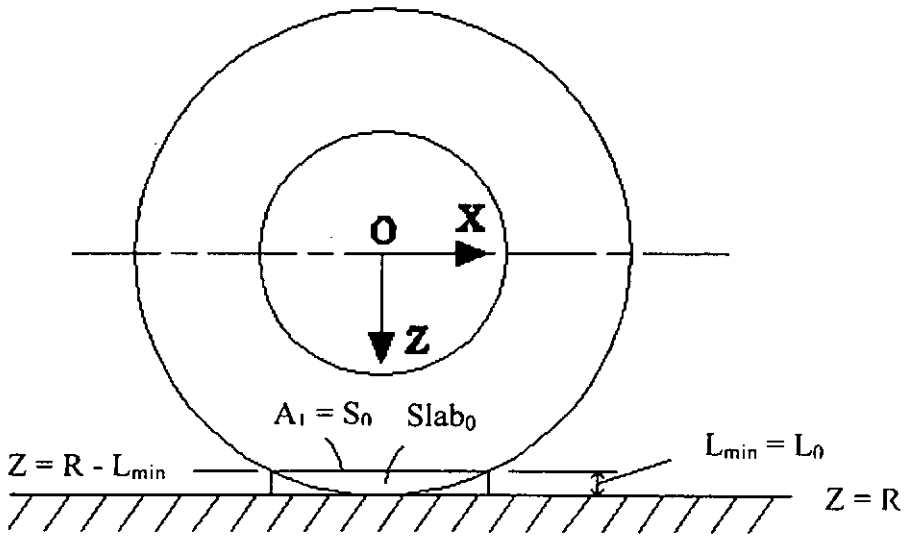

Figure 4-5. Production of bottom slab.

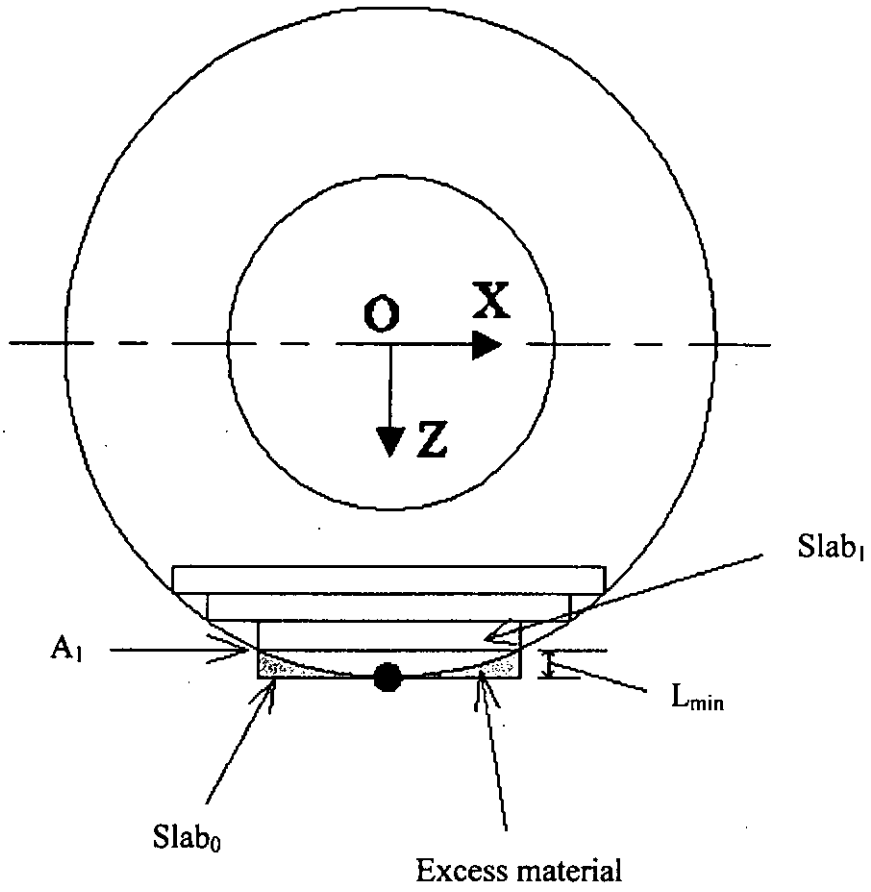

Figure 4-6. Bottom point building in maximum inscribed slab slicing.

4.1.2 Middle slabs production

The essential steps of producting middle slab are as follows:

1. The torus is sliced at the levels $Z = Z_i$ and $Z = Z_{i+1}$.
2. Cross-sectional slices A_i and A_{i+1} are obtained.
3. Critical point between the two slicing levels $Z = Z_i$ and $Z = Z_{i+1}$ is detected.
4. Slab thickness (i.e. layer thickness) is optimized.

The torus is first sliced at $Z = Z_i$ to produce planar region A_i where i ranges from 1 to N – 1 for middle slabs production (Equation 4-5). In fact, A_1 is already obtained in the production of bottom slab. Next, the condition, $Z_i + R \leq L_{min}$, is checked to decide whether the top slab or other middle slabs is produced in the following step. After that, the torus is sliced at $Z = Z_{i+1} = Z_i - n * L_{min}$ to produce planar region A_{i+1} (Equation 4-6), where $1 \leq n \leq \lambda$ and $n \in N$. A_i is shown in Figure 4-7. λ is inputted by the users. Figure 4-6 illustrates the positions of A_i and A_{i+1}. After A_{i+1} is produced, A_{i+1} is translated from $Z = Z_{i+1}$ to $Z = Z_i$ in the direction of **k** to produce the planar region A_{i+1}' (Equation 4-7). Then, critical points are detected to ensure the inscribing criterion.

Mathematically,

Slicing at π_i :

$$T \cap^{*} \pi_i \rightarrow A_i$$

$$A_i = \{ \mathbf{P} \mid \mathbf{P} \in T \wedge \mathbf{P} \in \pi_i \} \qquad (4-5)$$

Slicing at π_{i+1}:

$$T \cap^{*} \pi_{i+1} \rightarrow A_{i+1}$$

$$A_{i+1} = \{ \mathbf{P} \mid \mathbf{P} \in T \wedge \mathbf{P} \in \pi_{i+1} \} \qquad (4-6)$$

Translation :

$$A_{i+1}' = \{ \mathbf{P} \mid \mathbf{P} = \mathbf{Q} + |Z_{i+1} - Z_i| \mathbf{k}, \mathbf{Q} \in A_{i+1} \} \qquad (4-7)$$

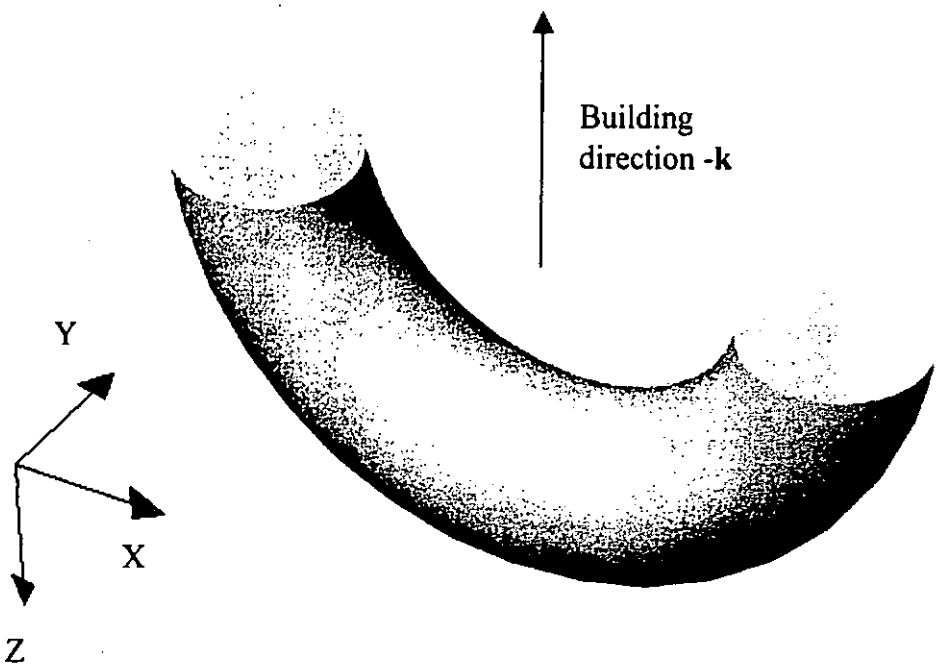

Figure 4-7. Isometric view of planar region A_i.

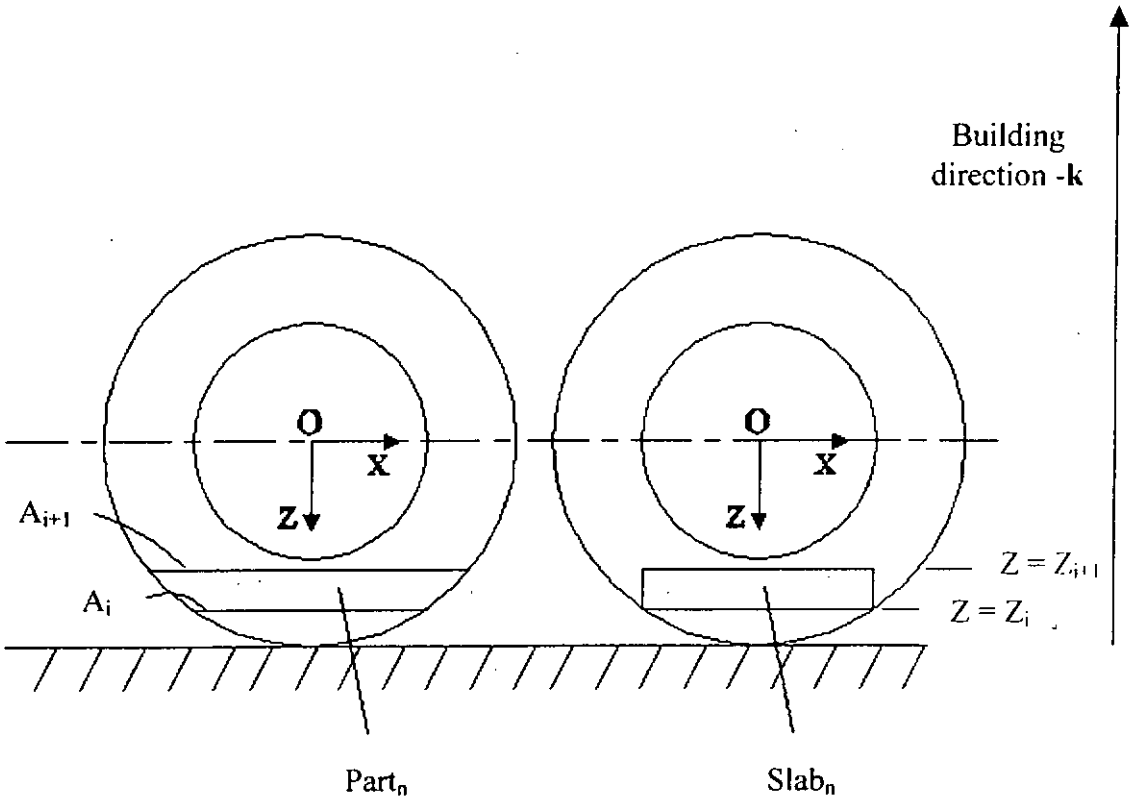

Figure 4-8. Positions of $Slab_n$ and $Part_n$.

4.1.2.1 Detection of critical point

After obtaining planar regions A_i and A_{i+1}, they need to be compared to find a resultant cross-sectional planar region S_i for the production of $Slab_n$ ($n \in N$ and $1 \leq n \leq \lambda$).

This is necessary because if A_{i+1} is above the equator Z = 0 and A_i is below Z = 0 (Figure 4-8), there exists a problem in which $Slab_n \not\subset Part_n$. To avoid the violation of the inscribing criterion, the problematic area in the torus will be characterized by critical points. Critical points are points in which

1. their tangent planes are parallel to the building direction **-k** and

2. concave with respect to the building direction (Figures 4-9a to 4-9c).

In bottom up vertical slicing, points A and B are critical points which satisfy the two conditions stated above (Figure 4-10). The equator is a plane which passes through the center of the torus and is perpendicular to the building direction **–k**.

If $Z_{i+1} < 0$ and $Z_i > 0$, Z_i is below the equator and Z_{i+1} is above the equator. Planar region A_0 is formed by slicing at Z = 0 (Equation 4-8). A_0 is then translated from Z = 0 to $Z = Z_i$ to form A_0' (Equation 4-9). After that, A_i, A_{i+1}' and A_0' are intersected to form planar region S_i (Equation 4-10a). S_i is then extruded by a height of $Z_i - Z_{i+1}$ in the direction of **-k** to produce $Slab_n$ (Equation 4-11). The path of extrusion L_i is given in Equation 4-12.

Mathematically,

Slicing :

$$T \cap^{*} \pi_o \rightarrow A_o$$

$$A_o = \{ \mathbf{P} \mid \mathbf{P} \in T \wedge \mathbf{P} \in \pi_o \} \qquad (4\text{-}8)$$

Translation :

$$A_o' = \{ \mathbf{P} \mid \mathbf{P} = \mathbf{Q} + |Z_o - Z_i|\mathbf{k}, \mathbf{Q} \in A_o \} \qquad (4\text{-}9)$$

Intersection of planar regions :

$$S_i = A_i \cap^{*} A_{i+1}' \cap^{*} A_o' \qquad (4\text{-}10a)$$

Extrusion :

$$Slab_n = S_i \oplus L_i$$

$$= \{\mathbf{d} \in \mathbf{R}^3 \mid \mathbf{d} = \mathbf{a} + \mathbf{b}, \mathbf{a} \in S_i, \mathbf{b} \in L_i\} \qquad (4\text{-}11)$$

where L_i is a straight line such that

$X = 0$,

$Y = 0$ and

$$Z = t\,(Z_i - n * L_{min}) + (1 - t)\,Z_i \qquad t \in [0,1], n \in \mathbf{N} \qquad (4\text{-}12)$$

If Z_{i+1} and $Z_i > 0$ are on the same side of the equator (Figure 4-8), S_i is just formed by $A_i \cap^{*} A_{i+1}'$ (Equation 4-10b).

$$S_i = A_i \cap^{*} A_{i+1}' \qquad (4\text{-}10b)$$

In order to maximize the computational efficiency in slicing and to minimize material addition to the prototype in post-processing, the slab should be as thick as possible (i.e. between L_{min} and L_{max}). However, if the slab is too thick, the staircase effect becomes prominent and the quality of the slab model will be affected. Thus, the thickness of slab should be optimized in order to produce an optimal slab, $Slab_i$ ($i \in N$ and $i = 1, 2, 3, \ldots\ldots, N-1$).

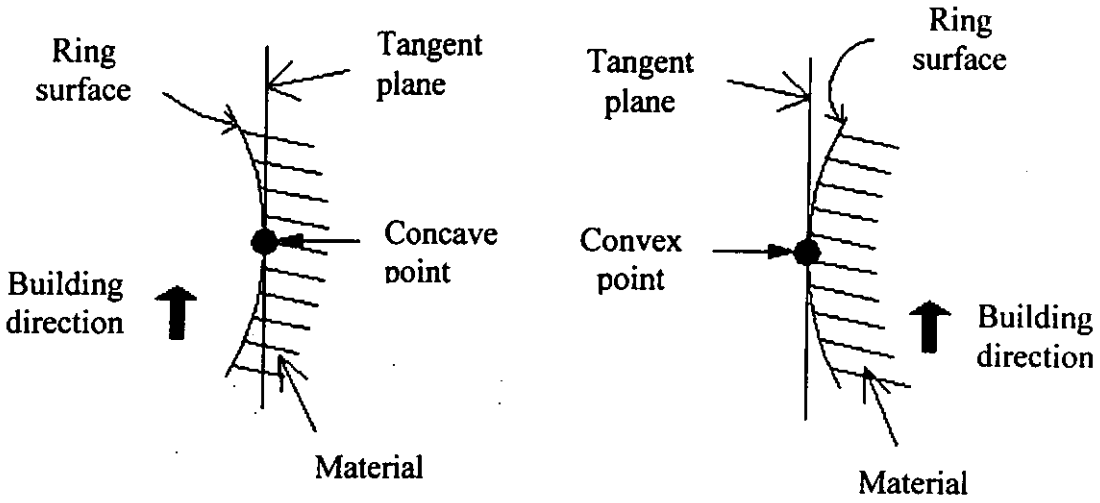

(a) Concave critical point.

(b) Convex critical point.

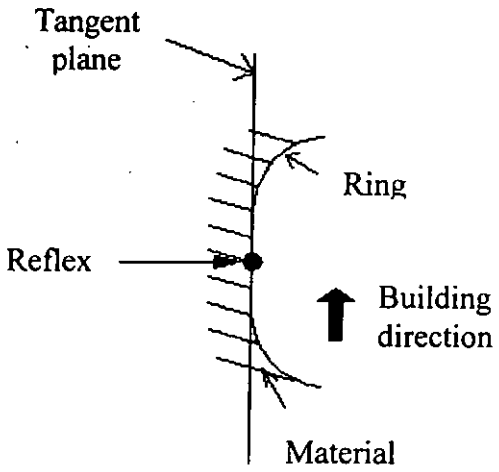

(c) Reflex point.

Figure 4-9. Critical point analysis.

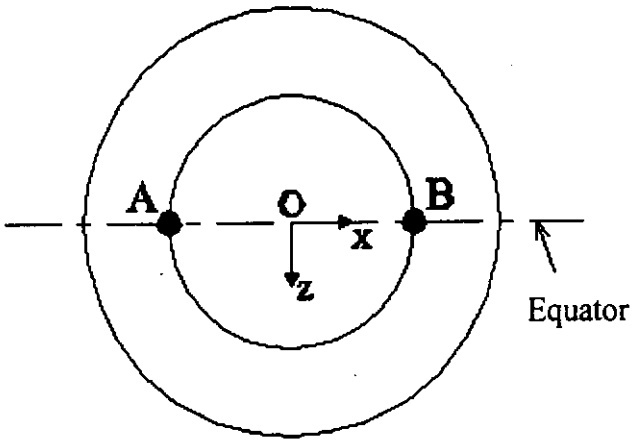

Figure 4-10. Position of critical points.

4.1.2.2 Optimization of slab thickness

In the optimization process, the value of volume efficiency, η, is inputted by the user. The condition $Z_{i+1} > -R$ needs to be satisfied to ensure that the next slice does not equal to or beyond the maximum height of the torus. The volume efficiency of the current slab, $Slab_n$, is denoted by η_n and is defined to be the ratio of volume of $Slab_n$ to volume of $Part_n$ (Figure 4-7), i.e. $\eta_n = \frac{\text{volume of Slab}_n}{\text{volume of Part}_n}$. If $\eta_n \geq \eta$, the current slab is accepted and $Slab_i$ is set equal to $Slab_n$.

If $\eta_n < \eta$, n is decremented by 1. A new $Slab_n$ is produced and η_n is checked again with η. The procedure is repeated until $\eta_n \geq \eta$ or λ slabs have been tested.

After optimizing $Slab_i$, the procedure is repeated by increasing i by 1. The process of producing middle slabs is repeated until $Z_i + R \leq L_{min}$. If $Z_i + R \leq L_{min}$, the last slab (topmost slab) is produced.

4.1.3 Top slab production

The last slice forms the planar region A_N (Equation 4-14) which is set equal to S_N (Equation 4-15). S_N is then extruded by a height of L_{min} and in direction **-k** to form the top slab, $Slab_N$ (or $Slab_{top}$) (Equation 4-16). The path of extrusion is L_i (Equation 4-17). The processes are shown in Figure 4-11.

Mathematically,

Slicing :

$$T \cap^{\bullet} \pi_N \rightarrow A_N$$

$$A_N = \{ \mathbf{P} \mid \mathbf{P} \in T \wedge \mathbf{P} \in \pi_N \} \qquad (4\text{-}14)$$

$$A_N \rightarrow S_N \qquad (4\text{-}15)$$

Extrusion :

$$Slab_N = S_N \oplus L_N$$

$$= \{ \mathbf{d} \in \mathbf{R}^3 \mid \mathbf{d} = \mathbf{a} + \mathbf{b}, \mathbf{a} \in S_N, \mathbf{b} \in L_N \} \qquad (4\text{-}16)$$

where L_N is a straight line such that

$$X = 0,$$

$$Y = 0 \text{ and}$$

$$Z = t\,(Z_N - L_{min}) + (1 - t)\,Z_N \qquad t \in [0,1] \qquad (4\text{-}17)$$

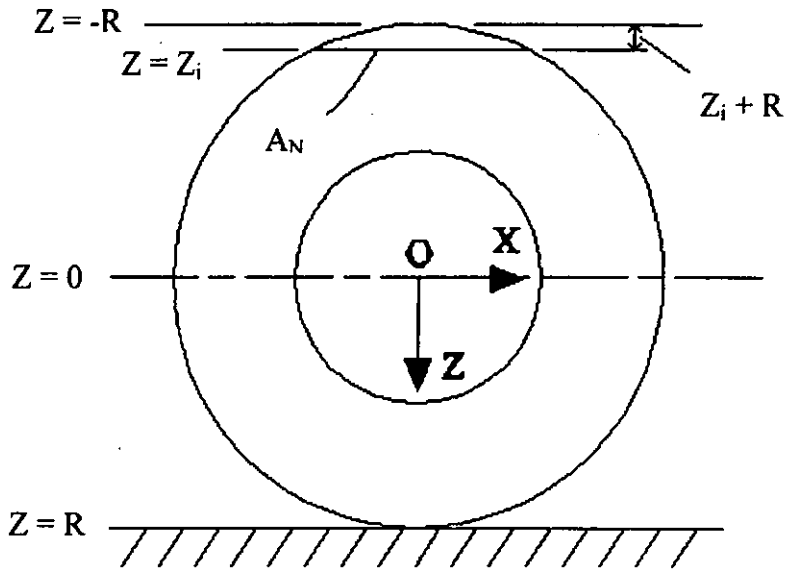

(a) Production of last sliced planar region A_N.

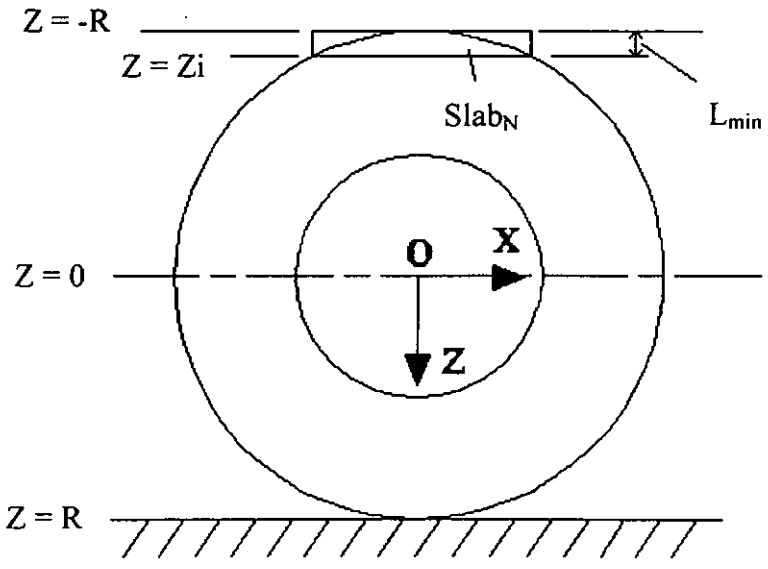

(b) Production of top slab for $Z_i + R = L_{min}$.

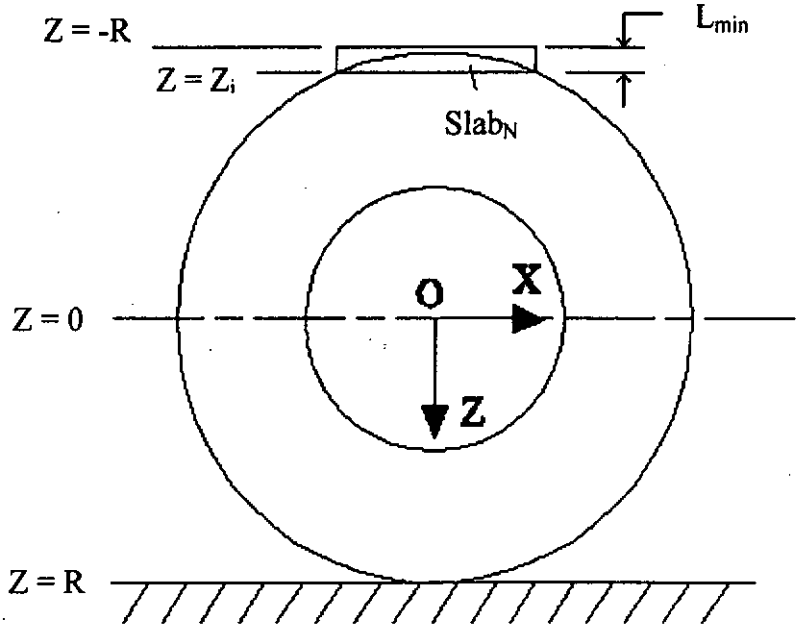

(c) Production of top slab for $Z_i + R < L_{min}$.

Figure 4-11. Production of top slab.

4.1.4 Slab model generation

After all slabs are produced, they are stacked and unioned together to form a maximum inscribed slab model of the torus (Equation 4-18).

$$R \approx R' = \bigcup_{\forall i}^{*} Slab_i \qquad i = 0, 1, 2, ..., N \qquad (4-18)$$

Only a very small amount of excess material needs to be removed from the bottom and the top of the stacked slab model. In addition, other part of the slab model only needs minimum material addition.

In the maximum inscribed slab slicing, the thickness of slab is equal to n * L_{min} where $1 \le n \le \lambda$ and $n \le N$ in the middle slab production. Obviously, slab thickness varies as n varies. Therefore, the slicing approach is adaptive.

4.2 Top-down vertical slicing

This type of slicing is applicable to the four types of jewel ring models (Figures 3-8a to 3-8d). In this case, the torus is sliced in the vertical direction from top to bottom. The slicing algorithm of the solid torus can also be divided into three main steps to produce the top slab (first slab), the middle slabs, and the bottom slab (last slab). Top slab is produced first and then the middle slabs. Finally, the bottom slab is produced. All slabs are then unioned to form the maximum inscribed slab model. The algorithm is similar to those for bottom up vertical slicing but the signs and directions are reversed.

4.3 Middle-up vertical slicing

This type of slicing is applicable to jewel ring models which are symmetrical about the principal plane YZ (Figures 3-8a to 3-8c). The jewel ring is placed in a position such that the symmetrical plane is perpendicular to the building direction **–k**. The jewel ring is then sliced in the vertical direction from the symmetrical plane to the top (Figure 4-12). The slabs produced are then mirrored with respect to the symmetrical plane of the jewel ring to form a maximum inscribed slab model. The slicing algorithm of the solid torus is divided into three main steps to produce the middle slabs first and then the top slab, and finally mirror copying the upper half slabs with respect to the equator.

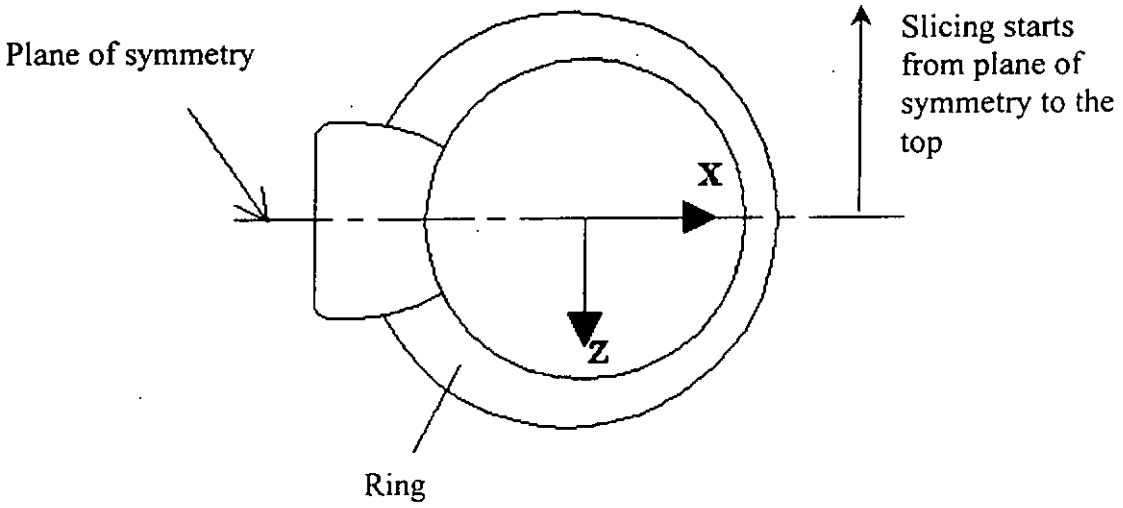

Figure 4-12. Jewel ring model is sliced from symmetrical plane to top in middle-up vertical slicing.

4.4 Middle-up horizontal slicing

This type of slicing is applicable to jewel ring models which are symmetrical about the principal plane ZX (Figures 3-8a, 3-8b and 3-8d). The jewel ring is placed in a position such that the plane of symmetry is perpendicular to the building direction **–k**. The jewel ring is then sliced in the vertical direction from the plane of symmetry to the top (Figure 4-13). The process is similar to those in middle-up vertical slicing.

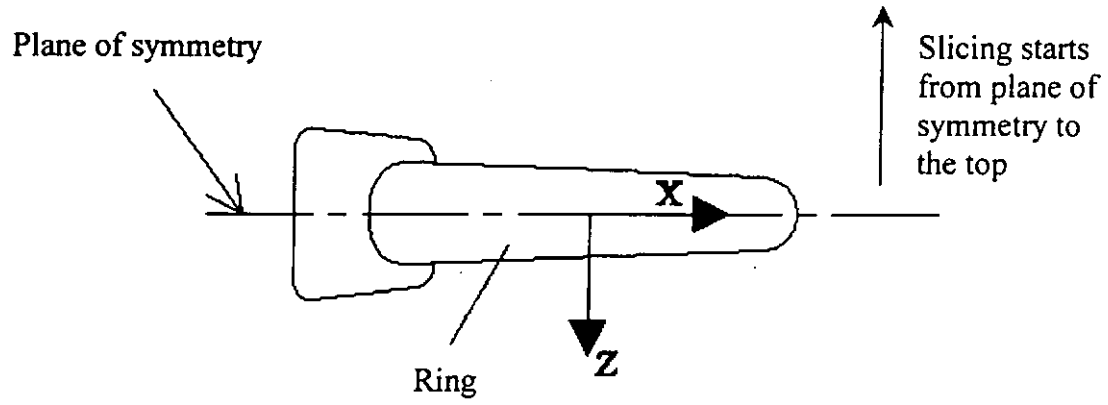

Figure 4-13. Jewel ring model is sliced from symmetrical plane to top in middle-up horizontal slicing.

CHAPTER 5

GAUSSIAN IMAGE IN OBJECT ORIENTATION

5.1 Introduction

Inherently, layered manufacturing is a slab approximation process even though direct slicing and adaptive slicing is used (Figure 5-1). The prototype quality depends on building orientation. In industrial practice, building orientation is mainly decided by the experience of the operator. No systematic analysis is applied in deciding the building orientation.

In previous research works, building orientation is computed with regard to part accuracy, building time, support structure and part stability. As jewel ring is an aesthetic part rather than a functional part, aesthetic quality is the main concern in jewelry production. That is, the jewel ring must be visually beautiful. Besides, the staircase approximation error is better minimized from the perspective of the observer. In layered manufacturing of jewelry, the best build orientation is defined in this research as the direction with least error visible instead of build time, accuracy, or minimization of support.

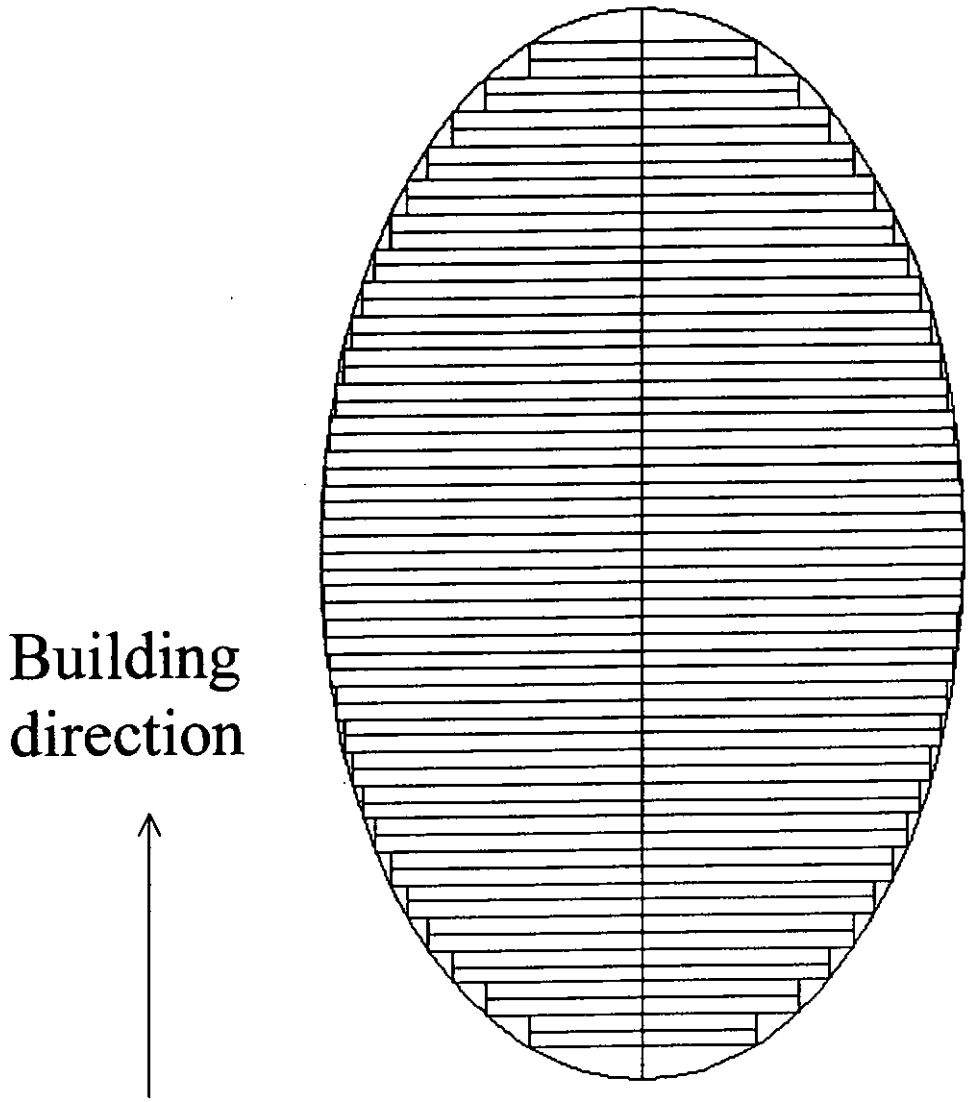

Figure 5-1. Slab approximation in layered manufacturing for a particular orientation of part.

5.2 The problem

In this research, a new methodology, **maximum visibility building orientation** is introduced to find the best-built orientation of jewel ring in layered manufacturing.

The methodology is to find the direction in which maximal observed boundary information has the best quality. For any three-dimensional object, different viewing directions will give different boundary information to the viewer. Except for highly symmetrical objects, some viewing directions will provide the maximum information. That is, the direction in which maximum projection area can be observed. This direction is called the maximum visibility direction.

Steps To Obtain Best-built Orientation

In this research, a three steps algorithm is proposed to obtain the best-built orientation. First, the orientation information is extracted from the CAD model. Second, the maximum visibility direction is determined. Finally, the best quality building direction is determined.

To obtain the maximum visibility building orientation, two steps are needed. First, the orientation information is extracted from the CAD model. The aim is to find the distribution of directions of the facets after tessellation of the CAD model. Second, the maximum visibility direction is determined using the projection area criterion. For step one, the Gaussian image is used to represent the orientation information of the CAD model. For the second step, the Gaussian image is extended to include the local area associated with a particular viewing direction. Figure 5-2 shows the flowchart of the whole process to find the maximum visibility direction.

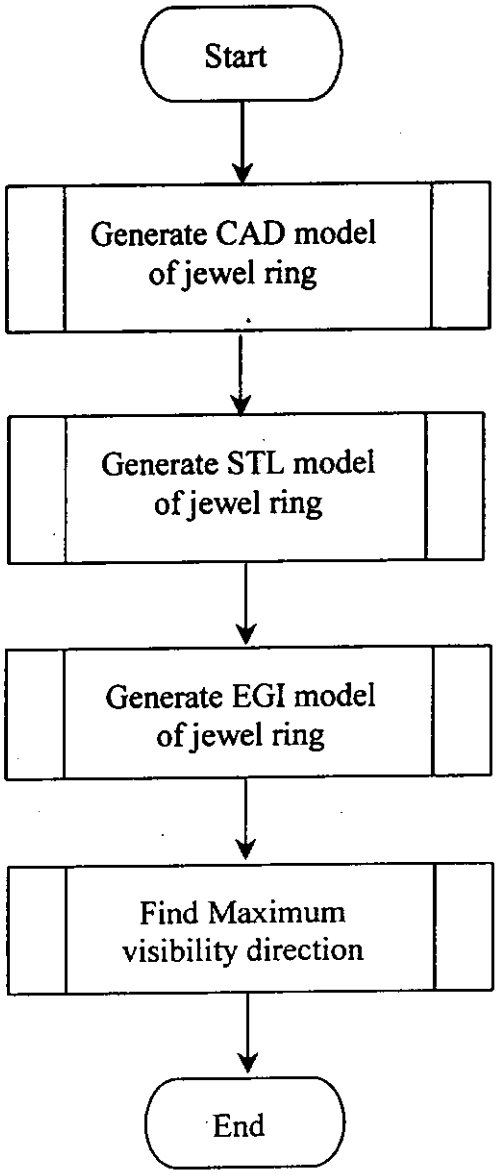

Figure 5-2. Work flow to determine maximum visibility direction.

5.3 Gaussian image

The Gaussian image (GI) of an object is obtained by associating with each point on its boundary surface a point on the Gaussian sphere which has the same surface orientation as shown in Figure 5-3. For convex object with positive Gaussian curvature everywhere, no two points have the same surface normal. Thus, the mapping from the object to the Gaussian sphere is invertible. However, if the convex surface has patches with zero Gaussian curvature, curves or even areas on it may correspond to a single point on the Gaussian sphere [Horn 1984]. The general many-to-one mapping for arbitrary object encapsulates only the orientation information, Figure 5-3. Other geometric information, like size, surface type, is not considered.

In general, an object can be non-convex and multi-connected. The Gaussian image of an object is simply a collection of directions. Besides, the Gaussian image is a many-to-one map and all elements have unit length. Moreover, it is independent of other geometric properties, like position in the boundary surfaces, size, surface type, etc.

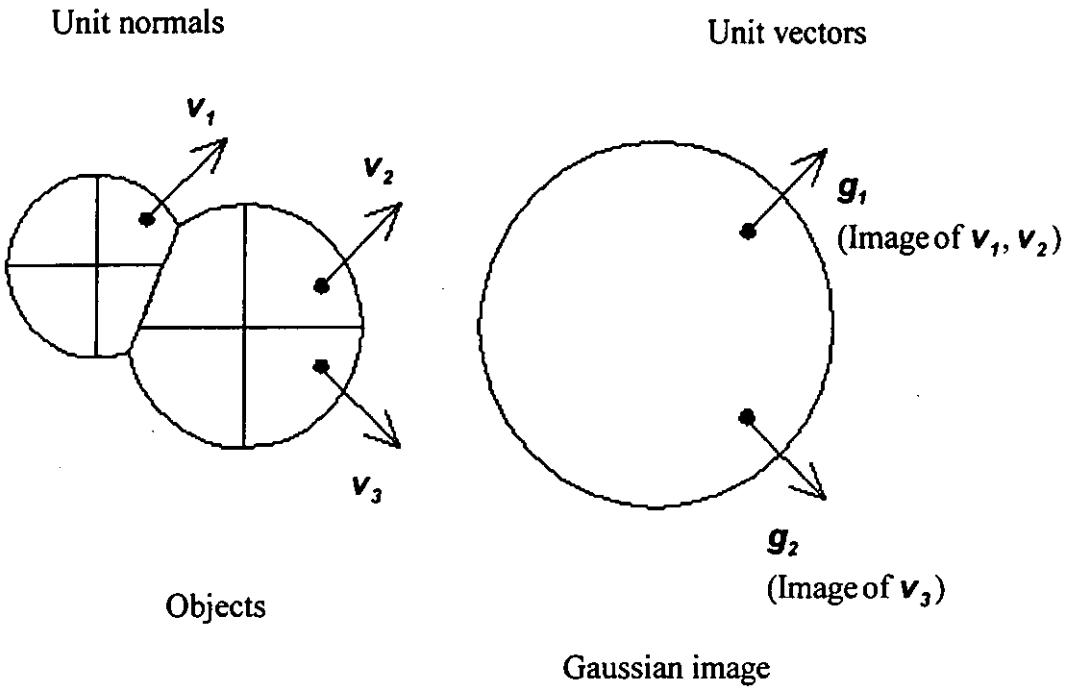

Figure 5-3. Gaussian image of an object.

5.3.1 Gaussian Image Mathematics

$\mathbf{n}(u,v) : \partial S \backslash \{\text{singular points}\} \rightarrow S^2$

$\mathbf{n}$ = unit normal of parameterized surface patch,

$$\mathbf{n} = \mathbf{P}_u \times \mathbf{P}_v / \| \mathbf{P}_u \times \mathbf{P}_v \|$$

$\mathbf{P}(u, v)$ = position vector

$\partial S \backslash \{\text{singular points}\}$

= boundary points of solid S except non-smooth singularities (i.e. edges & vertices)

S^2 = unit sphere in E^3

5.3.2 Gaussian Image Limitation

Although Gaussian image is a useful representation of an object, elements in the Gaussian image cannot be compared as they simply represent directions (scalars like angle measures can be compared but not direction vectors). Besides, maximum visibility direction cannot be determined by using the Gaussian image of an object. The reason can be seen in Figure 5-4. In Figure 5-4, two objects are shown in two dimension. They have the same Gaussian image but their maximum visibility direction (i.e. direction observing largest area) is different. This is because the elements of the Gaussian image have same unit magnitude.

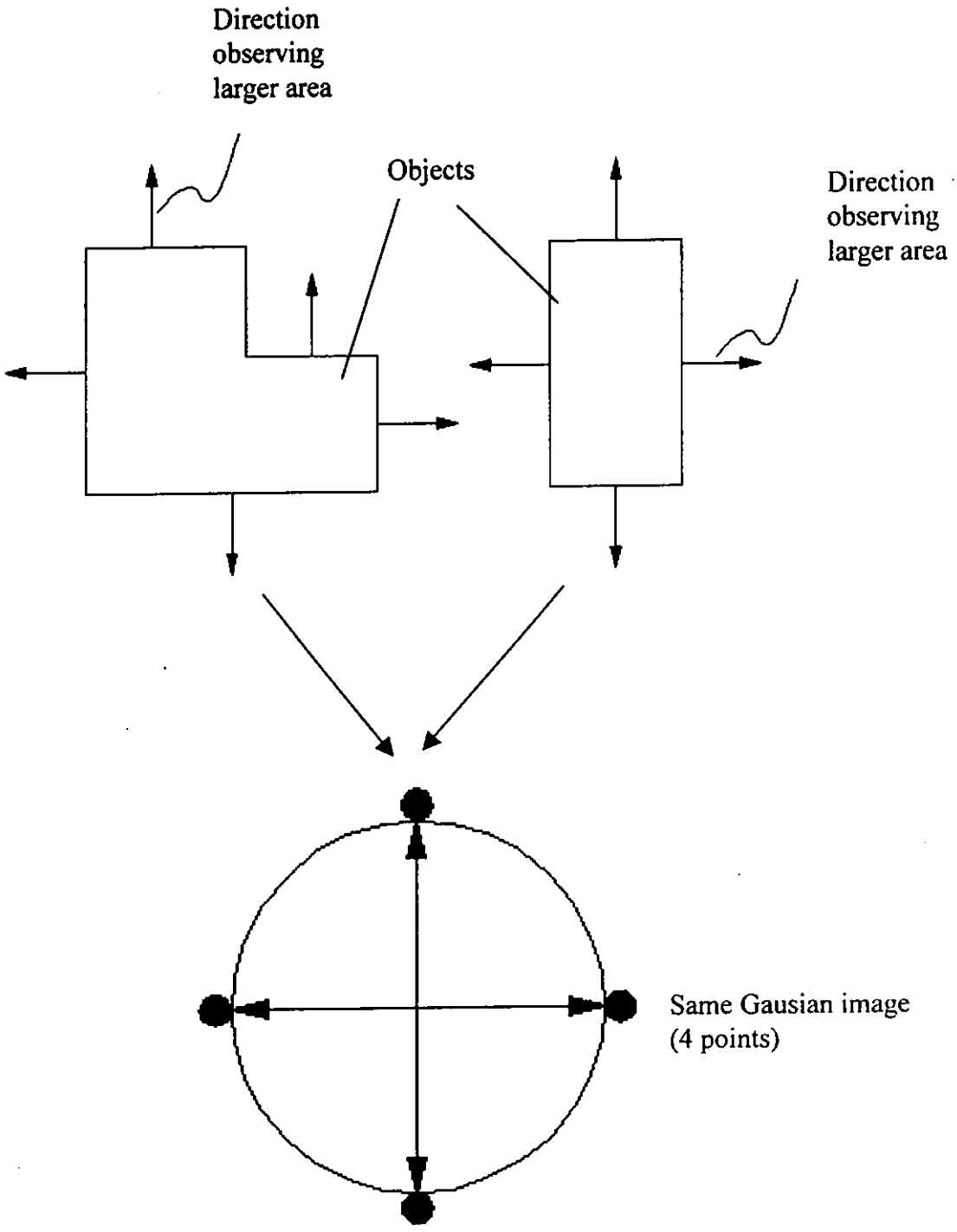

Figure 5-4. Two objects have the same GI but they have different maximum visibility direction.

5.4 Extended Gaussian Image (EGI)

The Gaussian image will only give a collection of directions and many free normals with same direction cosines will map to the same image point on S^2. Therefore, direction from larger area cannot be differentiated from those with smaller area. To extend the Gaussian image for rapid jewelry production, regions of the jewelry product visible in the same direction should be approximately weighted. In the research, the EGI for rapid jewelry production use will have elements of Gaussian image weighted by area. In other words, elements in EGI may have different lengths. This allows comparison of directions with different projection areas. If a lot of boundary points in the object have the same outward normal, the corresponding image in EGI will be longer. The EGI of an object is independent of the position of surface boundary point and it represents the frequency distribution of the surface normals (Figure 5-5_. In this case the EGI of an object is represented by a 2D histogram.

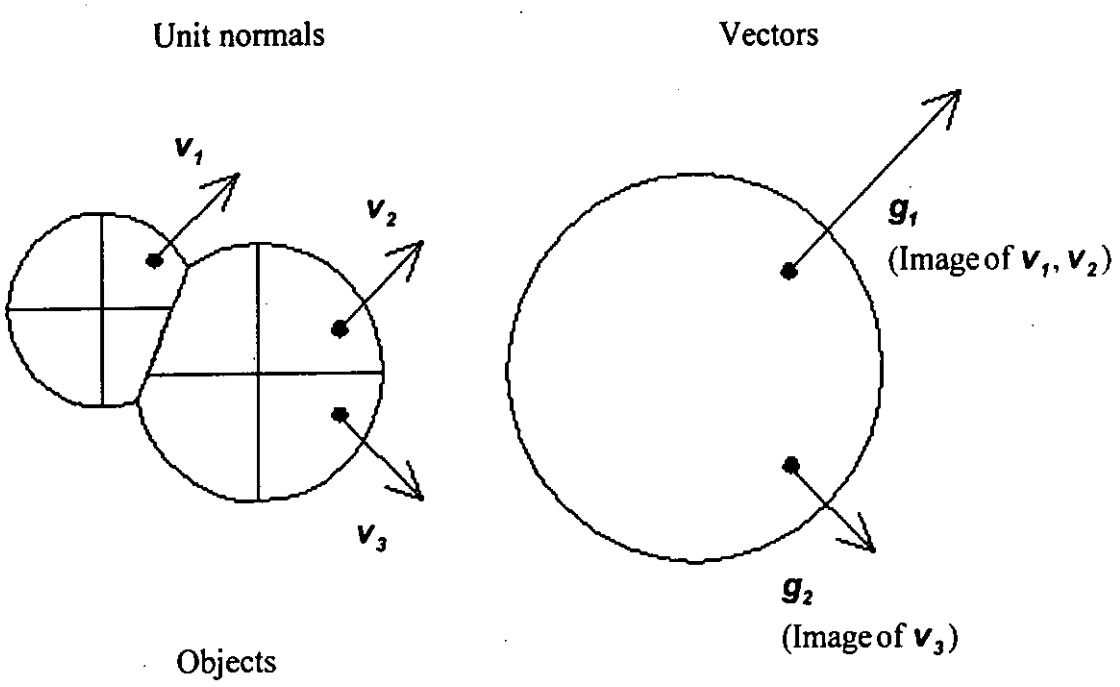

Figure 5-5. Extended Gaussian image of an object.

5.5 Discretized extended Gaussian image

In general, it is difficult if not computationally expensive to find the EGI of smooth (curved) non-convex object. A polygonal approximation is therefore used. In particular, triangular facetted approximation in STL file format is employed to obtain the EGI.

Without loss of generality, an ellipsoid is used to explain how to obtain the discretized EGI model of an object. Each vector in Figure 5-6a represents a surface normal direction. As ellipsoid has smooth curved surface, its EGI has infinite normal direction. Figure 5-6b shows a discretized ellipsoid. The polygonal approximated model (e.g. STL) has finite number of normal direction. Figure 5-6c shows the EGI of the ellipsoid. The length of vector equals to the total projection area in the same viewing direction. Tails of all vectors are pointed from the sphere centre.

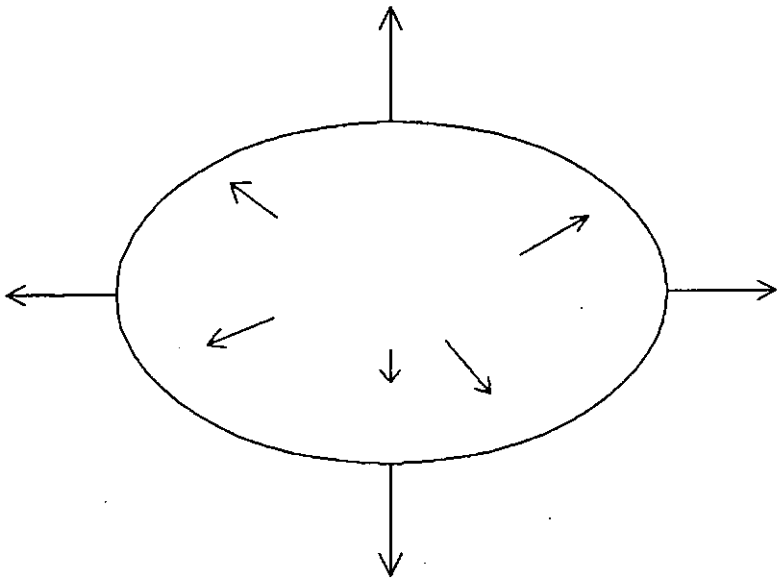

(a) Ellipsoid with some of its surface normals.

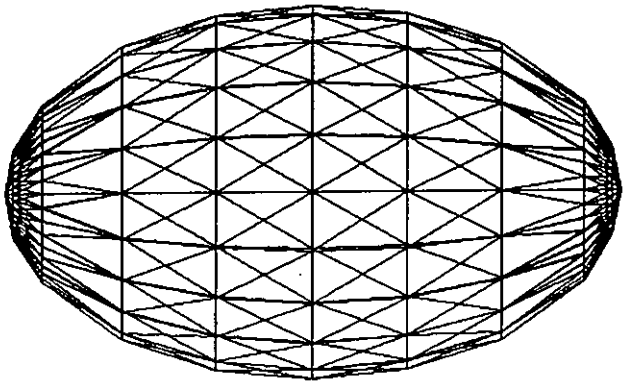

(b) Facet approximated model of the ellipsoid.

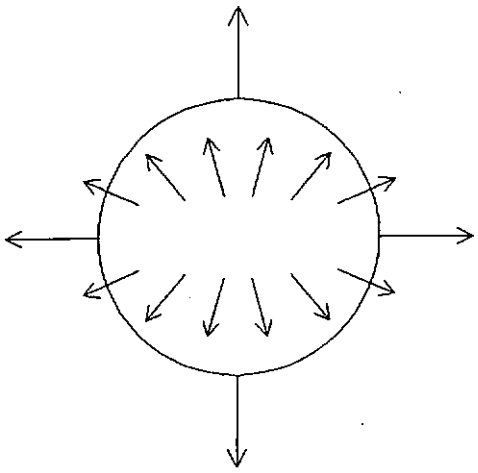

(c) EGI model of the ellipsoid.

Figure 5-6. Steps for obtaining EGI of an ellipsoid.

CHAPTER 6

MAXIMUM VISIBILITY BUILDING ORIENTATION

Maximum visibility building orientation is a process in which a building direction of a jewel ring is generated. The projection area of the jewel ring model along this direction may not be maximum but the prototype built should have minimum error (best surface quality) in the maximal visible direction.

6.1 Area of a STL Facet

STL file format has become the *de facto* standard of the rapid prototyping and manufacturing field [Jacobs 1996]. The object is tessellated, in STL format. The STL file basically consists of X, Y and Z coordinates of the three vertices of each surface triangle, as well as an index that describes the orientation of the surface normal. For each triangular facet of the STL model, there is a unit surface normal vector $\mathbf{n}_i$. Each triangular facet has three vertices and they are (X_{1i}, Y_{1i}, Z_{1i}), (X_{2i}, Y_{2i}, Z_{2i}) and (X_{3i}, Y_{3i}, Z_{3i}).

The area for the i[th] facet is A_i. A_i can be expressed as follows:

vector product form (Figure 6 - 1):

$$A_i = \frac{1}{2} \| P_1P_2 \| \times \| P_1P_3 \| \sin\theta$$

$$= \frac{1}{2} \| P_1P_2 \| \times \| P_1P_3 \|$$

$$= \frac{1}{2} \| P_2 - P_1 \| \times \| P_3 - P_1 \|$$

$$= \frac{1}{2} \begin{Vmatrix} \mathbf{i} & \mathbf{j} & \mathbf{k} \\ x_2 - x_1 & y_2 - y_1 & z_2 - z_1 \\ x_3 - x_1 & y_3 - y_1 & z_3 - z_1 \end{Vmatrix}$$

or

$$A_i = \sqrt{A_{1i}^2 + A_{2i}^2 + A_{3i}^2}$$

$$\text{whereas } A_{1i} = \frac{1}{2} \begin{vmatrix} Y_{1i} & Z_{1i} & 1 \\ Y_{2i} & Z_{2i} & 1 \\ Y_{3i} & Z_{3i} & 1 \end{vmatrix}$$

$$A_{2i} = \frac{1}{2} \begin{vmatrix} Z_{1i} & X_{1i} & 1 \\ Z_{2i} & X_{2i} & 1 \\ Z_{3i} & X_{3i} & 1 \end{vmatrix}$$

$$A_{3i} = \frac{1}{2} \begin{vmatrix} X_{1i} & Y_{1i} & 1 \\ X_{2i} & Y_{2i} & 1 \\ X_{3i} & Y_{3i} & 1 \end{vmatrix}$$

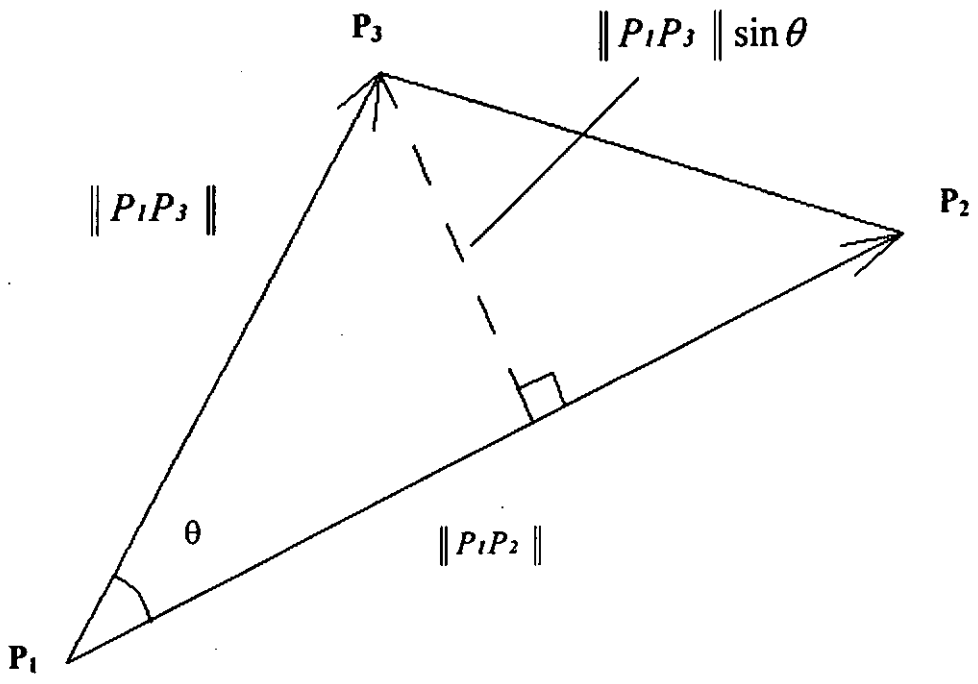

Figure 6-1. Three points of a triangle in vector form.

6.2 EGI Element

Each facet of the STL model has a unit surface normal $\mathbf{n}_i$ and a magnitude of area A_i. The vector representation of the weighted facet orientation is thus $A_i\mathbf{n}_i$. Each element in the EGI model has direction $\mathbf{n}_i$ and magnitude $\Sigma_j A_{ji}$, j is the number of facets having the same unit surface normal $\mathbf{n}_i$. Therefore, the vector representation of an element in the EGI is $\Sigma_j A_{ji}\mathbf{n}_i$. Each element in the EGI is the sum of all facet areas in the same viewing direction (Figure 6-2).

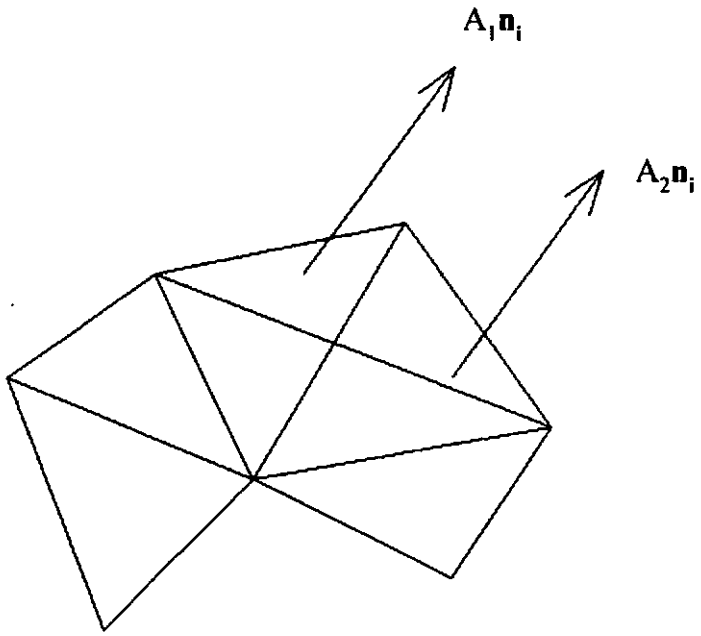

(a) STL facets of an object.

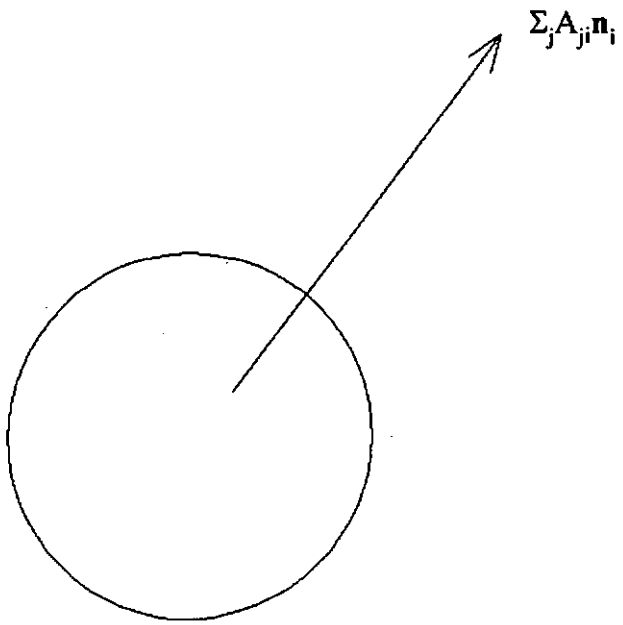

(b) EGI of an object.

Figure 6-2. Element in EGI of an object by summing all facet area in the same viewing direction.

In summary, EGI for jewelry is a projection area weighted needle map or orientation histogram. It is a unit sphere with needles of different lengths at different positions. However, it has not told us where is the maximum visibility direction.

6.3 Maximum Area Combination

In previous sections, the visibility direction vector is obtained by summing all vectors having different weightings in area of their corresponding facets. In this section, it will prove that the resultant vector after summation is maximal in magnitude. If the resultant vector is maximal in magnitude, that means the resultant vector is the maximum visibility direction.

Case 1: Facets with the same orientation

In Figure 6-3a, a planar polygon with area A is shown. After the surface is tessellated (Figure 6-3b), m ($m \in N$) triangles of different sizes are formed. As the surface is planar, all triangles have the same unit normal $\mathbf{n}_i$. If all the normals with their corresponding weight are summed, the magnitude of the resultant vector will be equal to the area of the original polygon.

In mathematical representation,

$$A_1\boldsymbol{n}_i + A_2\boldsymbol{n}_i + A_3\boldsymbol{n}_i + \ldots + A_m\boldsymbol{n}_i = \boldsymbol{n}_i\,(A_1 + A_2 + A_3 + \ldots + A_m) \qquad m \in Z^+$$
$$= \boldsymbol{n}_i A$$

As the area of the planar polygon is A, thus, the resultant vector is maximum in magnitude after summation and the resultant vector is the maximum visibility direction of the planar surface. Without loss of generality, the same conclusion can be drawn for disconnected case (Figure 6-4).

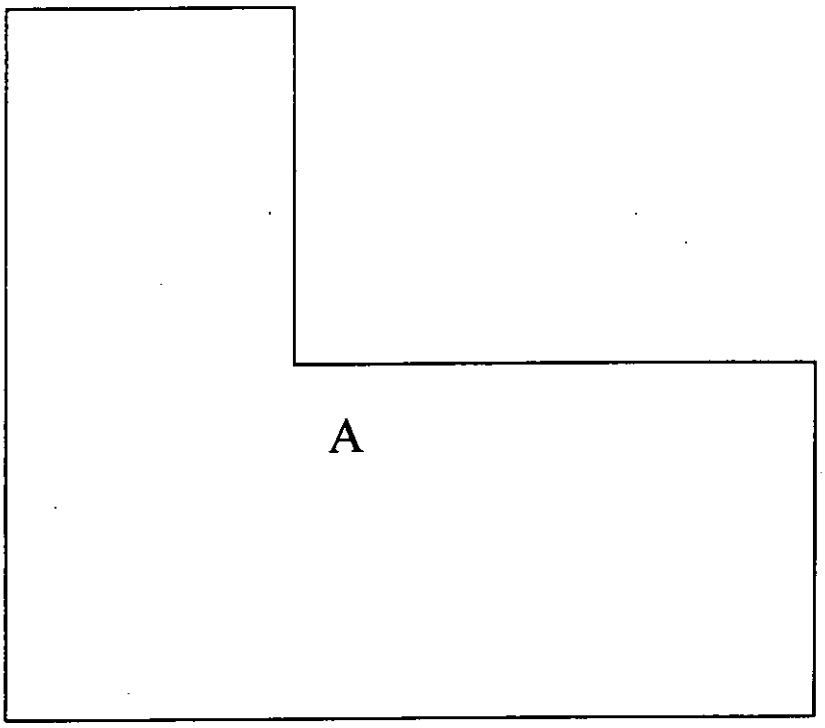

(a) A planar surface with area A.

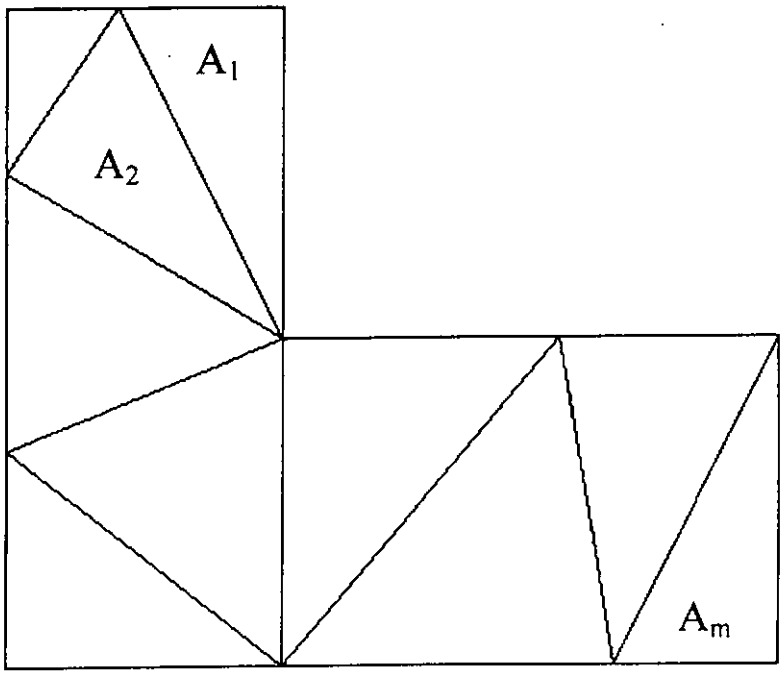

(b) A planar surface with area A is tessellated into m triangles with different areas.

Figure 6-3. Tessellated representation of a planar surface.

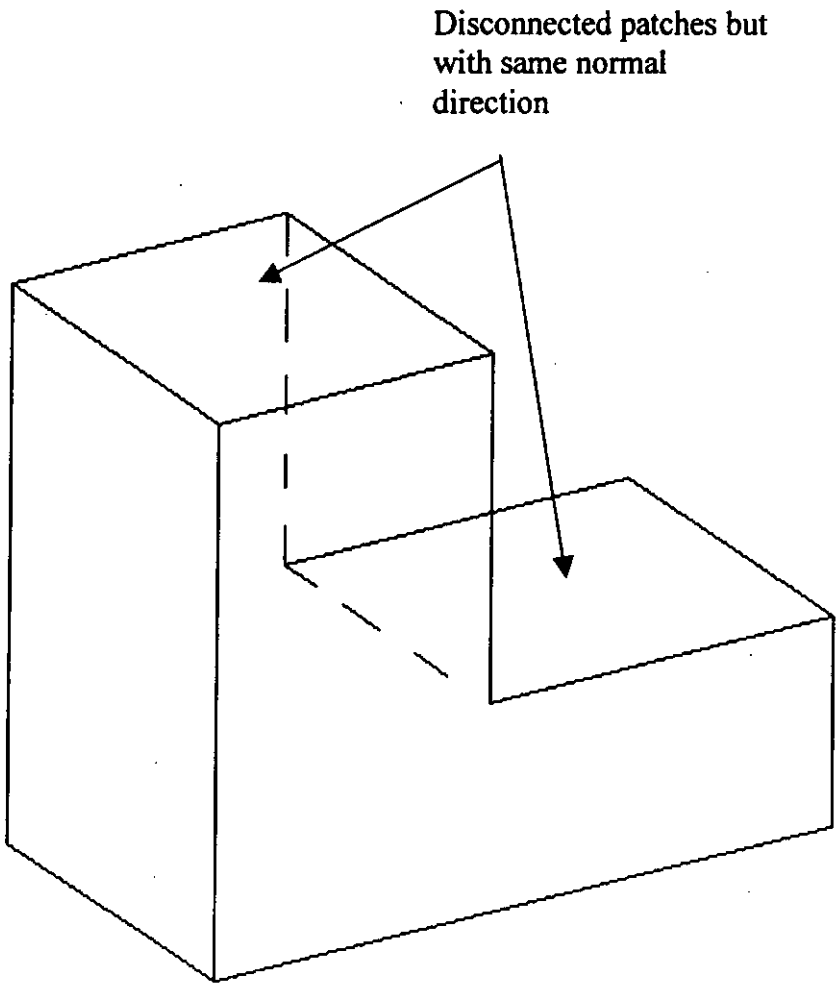

Figure 6-4. Disconnected patches with same normal direction in an object.

Case 2: Facets with different orientations

In Figure 6-5, A_1 and A_2 are two directed areas of two different facets with different normal directions and areas of magnitude A_1 and A_2 respectively. Mathematically, $A_1 = A_1 n_1$ and $A_2 = A_2 n_2$. A_{12} is the resultant vector obtained by combining (need not be summation) the two vectors.

The following will prove that the orientation of A_{12} will give maximum projection areas from A_1 and A_2.

In Figure 6-5, if we use arbitrary orientation θ to observe A_1 and A_2, the projection area is given by $\|A_{12}\| = \|A_1\| \cos\theta + \|A_2\| \cos(\theta_{12} - \theta)$

In order to find the maximum projection area, $\|A_{12}\|$ is differentiated twice with respect to variable orientation .

$$\frac{d\|A_{12}\|}{d\theta} = -\|A_1\| \sin\theta + \|A_2\| \sin(\theta_{12} - \theta)$$

$$\frac{d^2\|A_{12}\|}{d\theta^2} = -\|A_1\| \cos\theta - \|A_2\| \cos(\theta_{12} - \theta)$$

Setting first derivative to zero and second derivative to less than zero will thus give maximum $\|A_{12}\|$, i.e.

$$\frac{d\|A_{12}\|}{d\theta} = 0$$

$$\Rightarrow \|A_1\| \sin\theta = \|A_2\| \sin(\theta_{12} - \theta)$$

Now substituting θ into second derivative,

$$-\|A_1\|\cos\theta - \|A_2\|\cos(\theta_{12}-\theta) < 0,$$

$$\frac{d^2\|A_{12}\|}{d\theta^2} < 0$$

$$\Rightarrow A_{12} = A_1 + A_2 \text{ gives maximum} \|A_{12}\|$$

If there exist more than two normal vectors (i.e. more than two facets), the resultant vector after summation of all normal vectors with different area weighting is also maximal in magnitude. This can be proved by mathematical induction.

Let m be the total number of facets and assume

$A_{1m} = \sum_{i=1}^{m-1} A_i + A_m$ for maximum $\|A_{1m}\|$ is true for any m where $m \in Z^+$ and $m \geq 2$.

To prove: $A_{1m+1} = \sum_{i=1}^{m} A_i + A_{m+1}$ for maximum $\|A_{1m+1}\|$ is true.

By mathematical induction,

$$A_{1\,m+1} = A_{1\,m} + A_{m+1}$$
$$= A_1 + A_2 + \ldots + A_m + A_{m+1}$$

$\because A_{1\,m} = A_1 + A_2 + \ldots + A_m$ is true for maximum $\|A_{1m}\|$

$\therefore A_{1\,m} + A_{m+1} = A_1 + A_2 + \ldots + A_m + A_{m+1}$ is true for maximum $\|A_{1\,m} + A_{m+1}\|$

$\Rightarrow A_{1\,m+1} = A_1 + A_2 + \ldots + A_m + A_{m+1}$ is true for maximum $\|A_{1\,m+1}\|$

Therefore, vector sum will give maximal combination of directed areas.

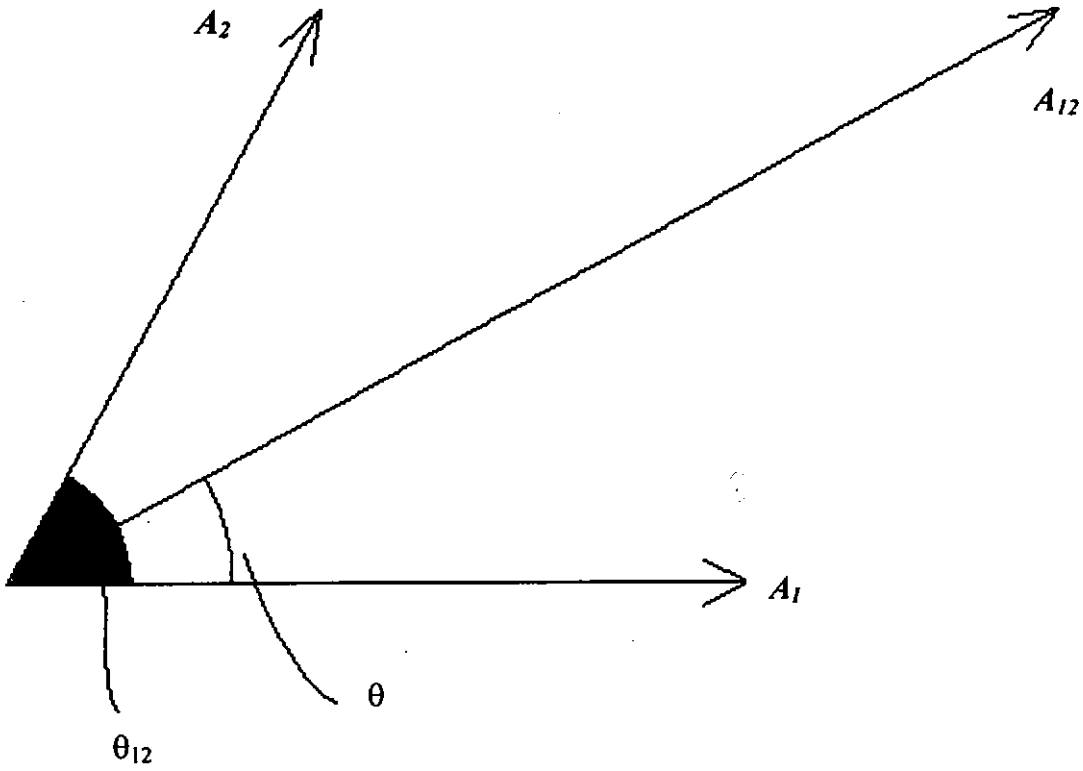

Figure 6-5. Facets with different orientations A_1 and A_2.

6.4 Maximum visibility direction

For any object, there exists a direction in which the maximum amount of boundary surfaces is visible. Using the EGI model, the maximum visibility direction for a jewel ring model can be easily found. Each element in the EGI model has direction $\mathbf{n}_i$ and magnitude $\Sigma_j A_{ji}$. The maximum visibility direction is the resultant vector. It can be expressed as: $\Sigma_i(\Sigma_j A_{ji})\mathbf{n}_i$

However, parallel projection area of arbitrary 2-manifold object along direction $\mathbf{v}$ is equal to those along $-\mathbf{v}$. Therefore, direct vector sum of all EGI elements of an object will result in zero vector, i.e. $\Sigma_i(\Sigma_j A_{ji})\mathbf{n}_i = \mathbf{0}$. As a result, the EGI elements are combined in absolute value of their Cartesian components, i.e.

$$\Sigma_i[|(\Sigma_j A_{ji})\mathbf{n}_i \cdot \mathbf{i}|\,\mathbf{i} + |(\Sigma_j A_{ji})\mathbf{n}_i \cdot \mathbf{j}|\,\mathbf{j} + |(\Sigma_j A_{ji})\mathbf{n}_i \cdot \mathbf{k}|\,\mathbf{k}]$$

or

$$\Sigma_i|(\Sigma_j A_{ji})\mathbf{n}_i \cdot \mathbf{i}|\,\mathbf{i} + \Sigma_i|(\Sigma_j A_{ji})\mathbf{n}_i \cdot \mathbf{j}|\,\mathbf{j} + \Sigma_i|(\Sigma_j A_{ji})\mathbf{n}_i \cdot \mathbf{k}|\,\mathbf{k}$$

The maximum visibility direction is obtained by normalizing to unit vector in the above combination.

In summary, the maximum visibility building orientation can be found in four major steps (Figure 6-6). First, a smooth CAD model of a jewel ring is created. Second, a STL model of the jewel ring is generated. This is the discretized model. Third, unit normals of the facets are multiplied by the area of the corresponding facets. These vectors are compared and summed if they have the same unit normal direction. The vectors become elements of the EGI model of the jewel ring. Finally, the elements of the EGI model are resolved into three hemispheres along **i**, **j** and **k**. The maximum visibility direction are the resultant vector found by summing the resolved vectors along directions **i**, **j** and **k**.

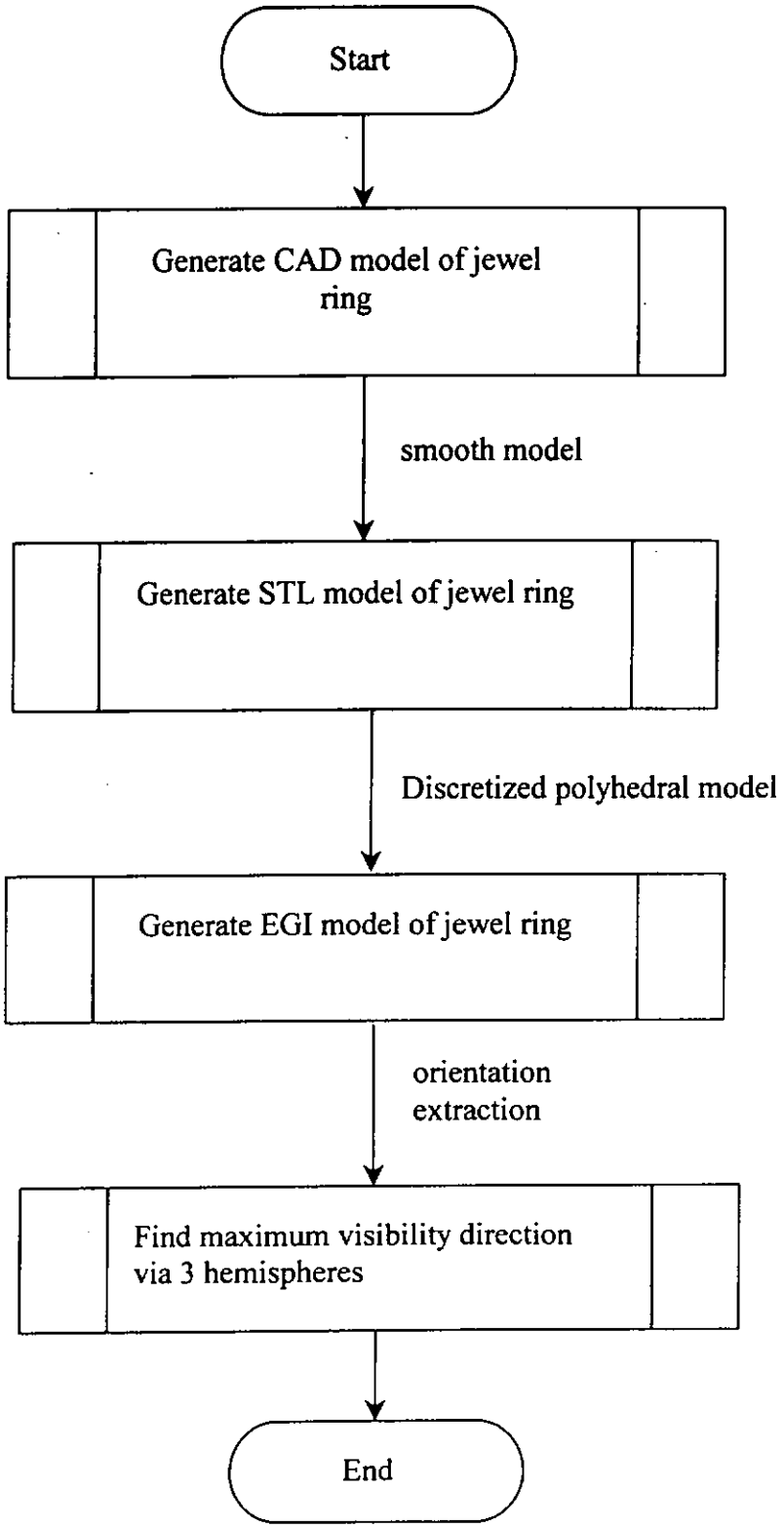

Figure 6-6. Processes of finding maximum visibility direction.

6.5 Best-building direction

The rapid prototype of a jewel ring model will have the best quality if it is built in the direction with minimum staircase error. The best building direction is, however, not the maximum visibility direction nor the minimum visibility direction. This will be discussed in the following sections.

6.6 Analysis of best-built direction

The rapid prototype of a jewel ring model will have the best quality (minimum staircase error) if the building direction is orthogonal to the maximum visibility direction. This will be explained as follows.

Figure 6-7 shows an ellipsoid with its maximum visibility direction. If the ellipsoid is built by the three building methods (Figure 6-8) with the maximum visibility direction orthogonal to the building direction, the slab models will be as shown in Figure 6-9. Figure 6-9a shows that the original model O encloses the slab model M. Figure 6-9b shows that the slab model encloses the original model. Figure 6-9c shows that the slab model intersects with the original model.

If the ellipsoid is built by the three methods with the maximum visibility direction aligns with the building direction, the slab model will be shown in Figure 6-10.

Table 6-1 shows the volumes of the slab models built. Table 6-2 summarizes the building errors corresponding to the six cases (Figure 6-9 and Figure 6-10). From the results in Table 6-1 and Table 6-2, the building error obtained when the ellipsoid is built with maximum visibility direction orthogonal to the building direction is smaller than if the maximum visibility direction is aligned to the building direction. Thus, the rapid prototype of a jewel ring model will have the best quality if the building direction is orthogonal to the maximum visibility direction.

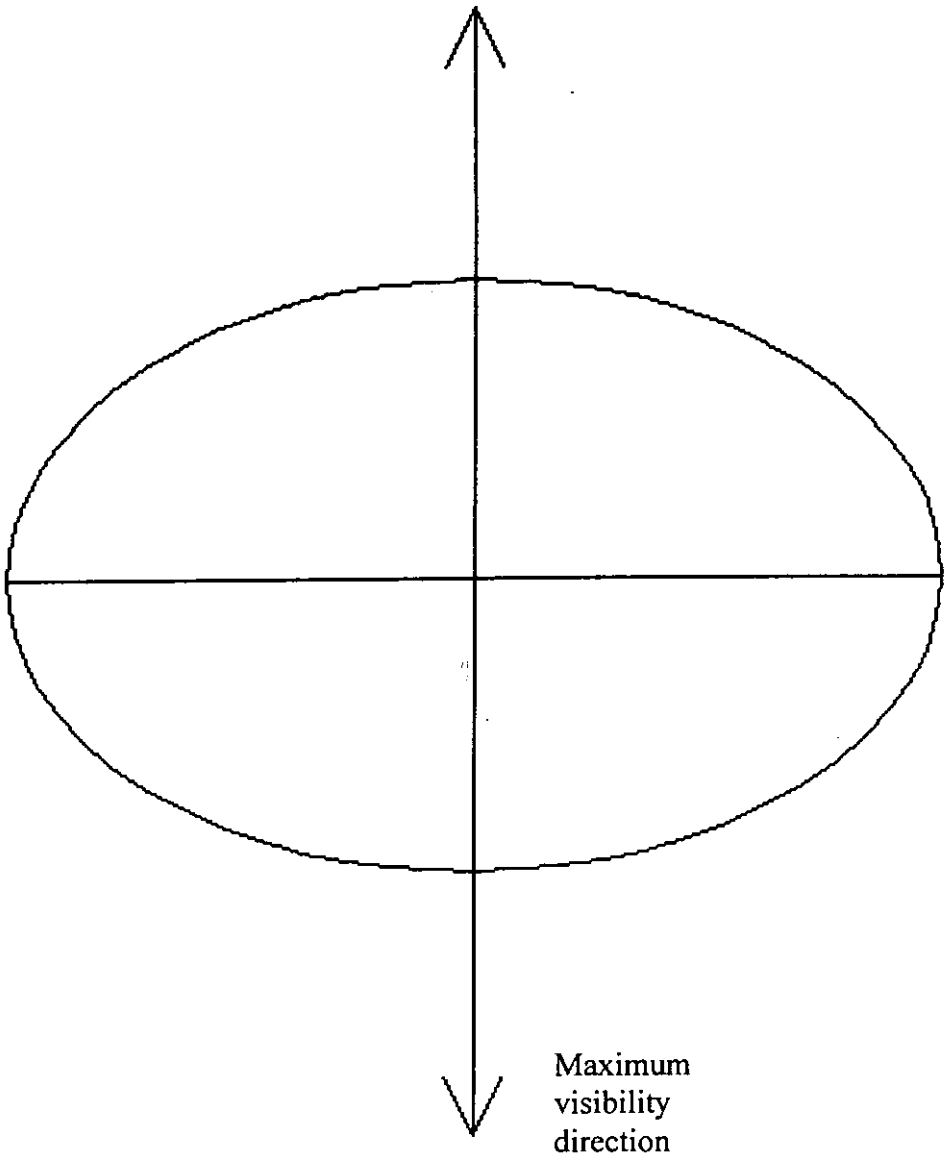

Figure 6-7. Ellipsoid with its maximum visibility direction.

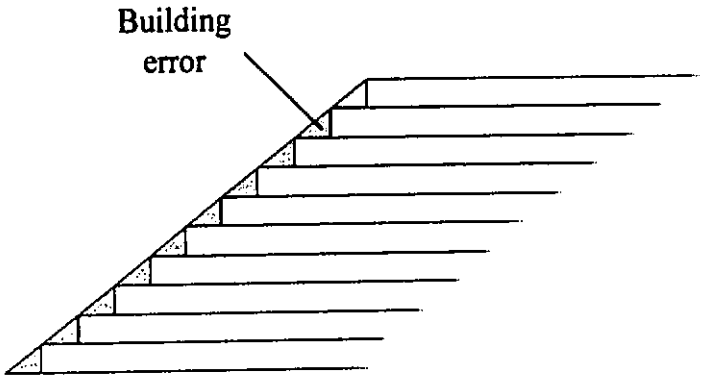

(a) Building error in which the original model encloses the model being built.

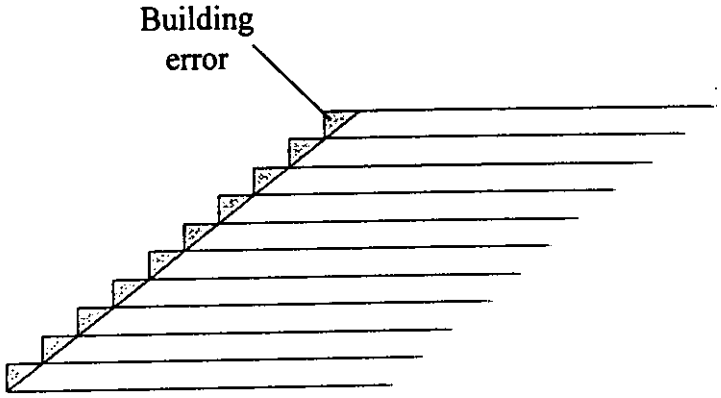

(b) Building error in which the model being built encloses the original model.

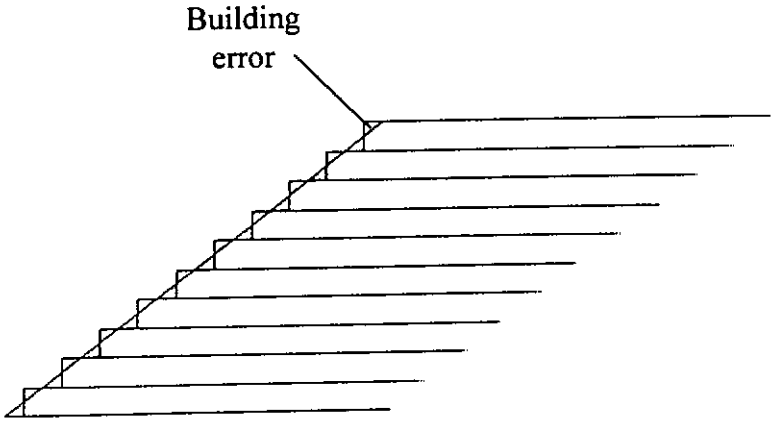

(c) Building error in which the original model intersects with the model being built.

Figure 6-8. Three building methods with different building error of the three building cases in layered manufacturing.

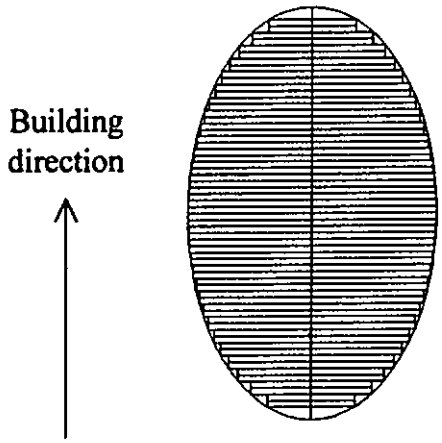

(a) Ellipsoid built with the original model O encloses the slab model M (maximum visibility direction perpendicular to the building direction).

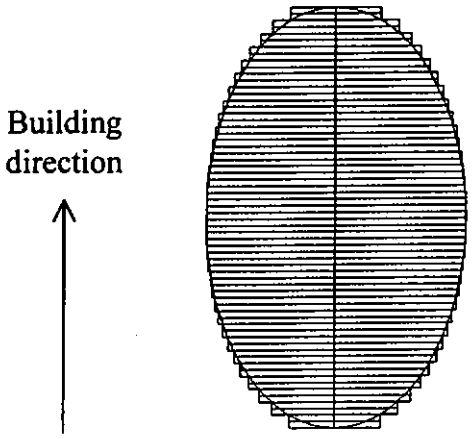

(b) Ellipsoid built with the slab model M intersects with the original model O (maximum visibility direction perpendicular to the building direction).

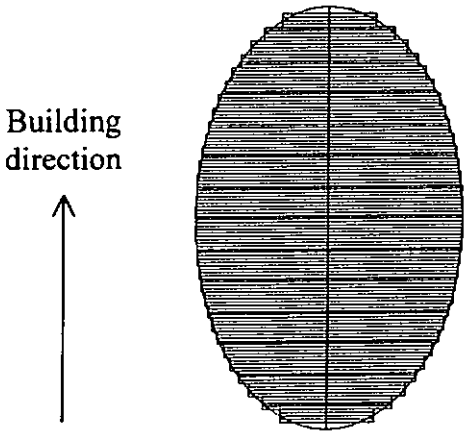

(c) Ellipsoid built with the slab model M encloses the original model O (maximum visibility direction perpendicular to the building direction).

Figure 6-9. Ellipsoid is built by using three types of building methods with maximum visibility direction orthogonal to the building direction.

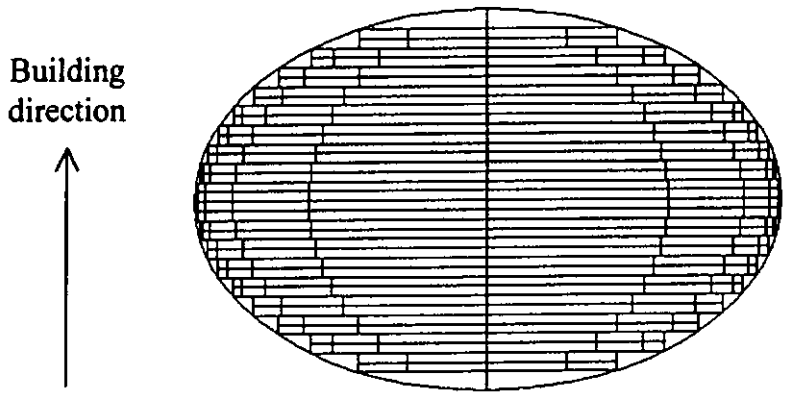

(a) Ellipsoid built with the original model O encloses the slab model M (maximum visibility direction aligns with the building direction).

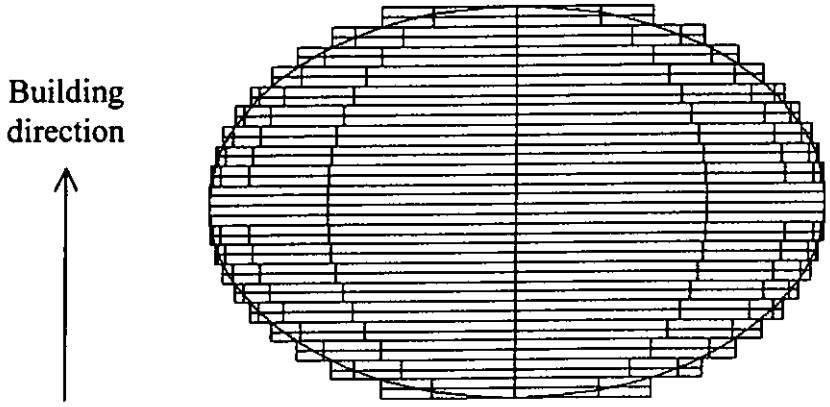

(b) Ellipsoid built with the slab model M encloses the original model O (maximum visibility direction aligns with the building direction).

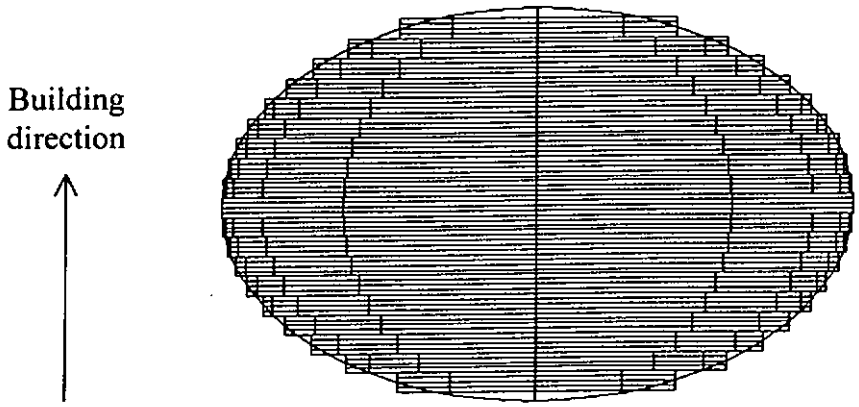

(c) Ellipsoid built with the original model intersects with the slab model M.

Figure 6-10. Ellipsoid is built by using three types of building methods with maximum visibility direction aligns to the building direction.

	Volume of slab model (V_{slab}), mm^3	
	Ellipsoid builds with maximum visibility direction orthogonal to building direction	Ellipsoid builds with maximum visibility direction aligns with building direction
Inscribing prototype	797.89 (Figure 6-9a)	772.84 (Figure 6-10a)
Circumscribing prototype	876.46 (Figure 6-9b)	898.52 (Figure 6-10b)
Intersecting prototype	837.17 (Figure 6-9c)	835.68 (Figure 6-10c)

Table 6-1. Volume of slab models in the six building methods.

	Percentage of building errors = $(V_{ellipsoid} - V_{slab})/ V_{ellipsoid}$	
	Ellipsoid builds with maximum visibility direction orthogonal to the building direction	Ellipsoid builds with maximum visibility direction aligns with the building direction
Inscribing prototype	0.047	0.077
Circumscribing prototype	0.046	0.07
Intersecting prototype	0.0007	0.0025

Table 6-2. Percentage of building errors.

Remark: volume of ellipsoid ($V_{ellipsoid}$) = 837.76 mm^3

6.7 Minimum visibility direction

In general, the minimum visibility direction is not perpendicular to the maximum visibility direction. For example, Figure 6-11 shows a cylinder in front view and isometric view. The minimum visibility direction of the cylinder is shown in Figure 6-12a and the maximum visibility direction is shown in Figure 6-12b. Obviously, the minimum visibility direction is not perpendicular to the maximum visibility direction.

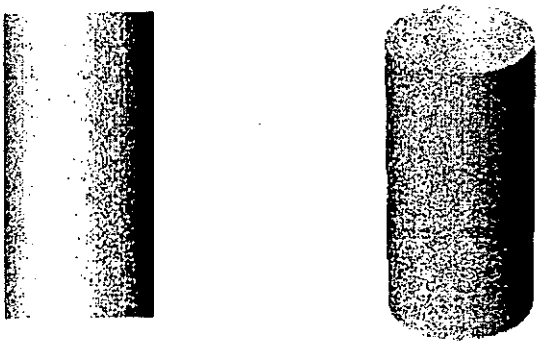

Figure 6-11. A cylinder shown in front view and isometric view.

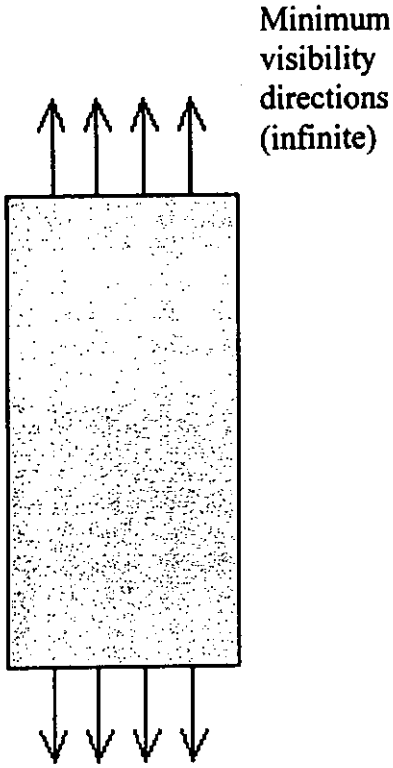

(a) Minimum visibility direction of a cylinder.

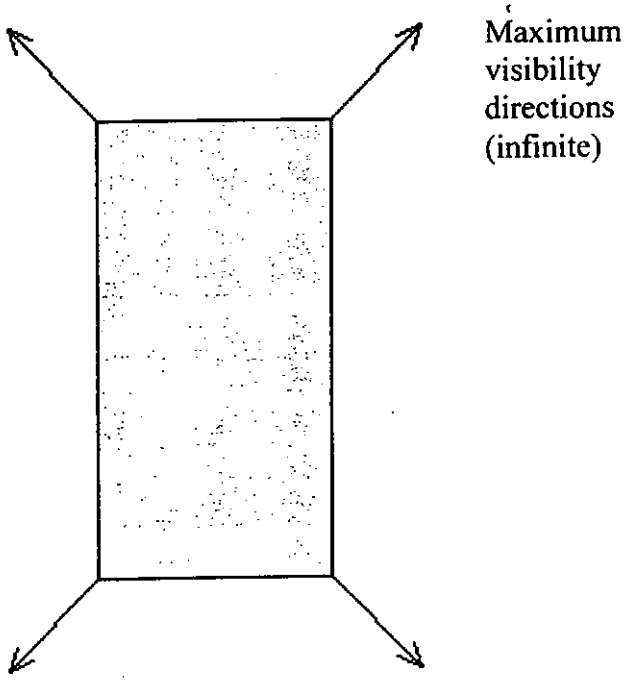

(b) Maximum visibility direction of a cylinder.

Figure 6-12. Minimum and maximum visibility directions of a cylinder.

CHAPTER 7

CASE STUDIES

7.1 Maximum inscribed slab slicing

7.1.1 Simple demonstration by using torus

A torus (Figure 7-1) acting as a simple representation of a jewel ring is used to demonstrate the bottom-up vertical slicing. The volume of the torus is 197.4 mm^3 by calculation in CAD software. Bottom-up vertical slicing is applied to the torus vertically (Figure 7-2) and horizontally (Figure 7-3).

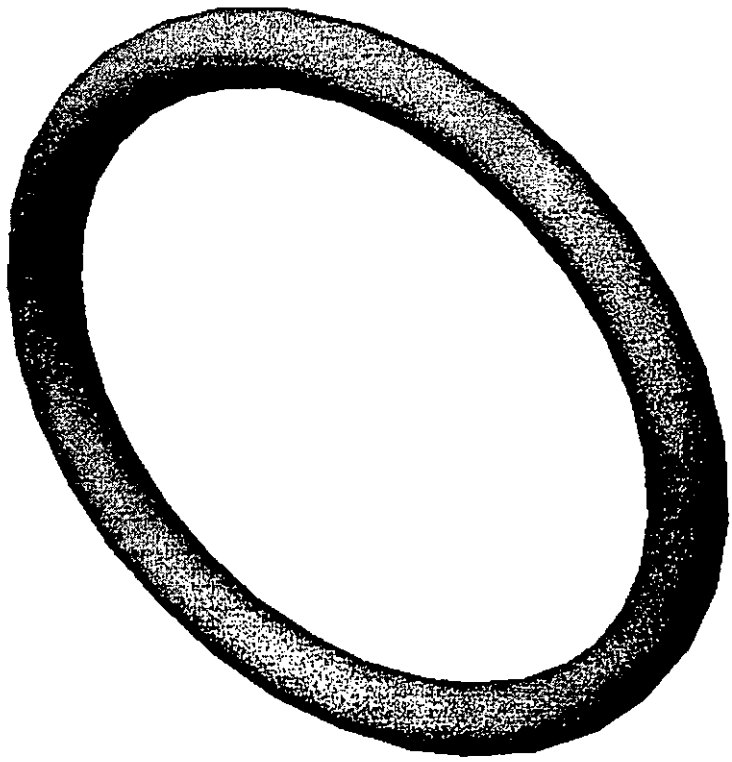

Figure 7-1. Solid torus used in bottom up vertical slicing.

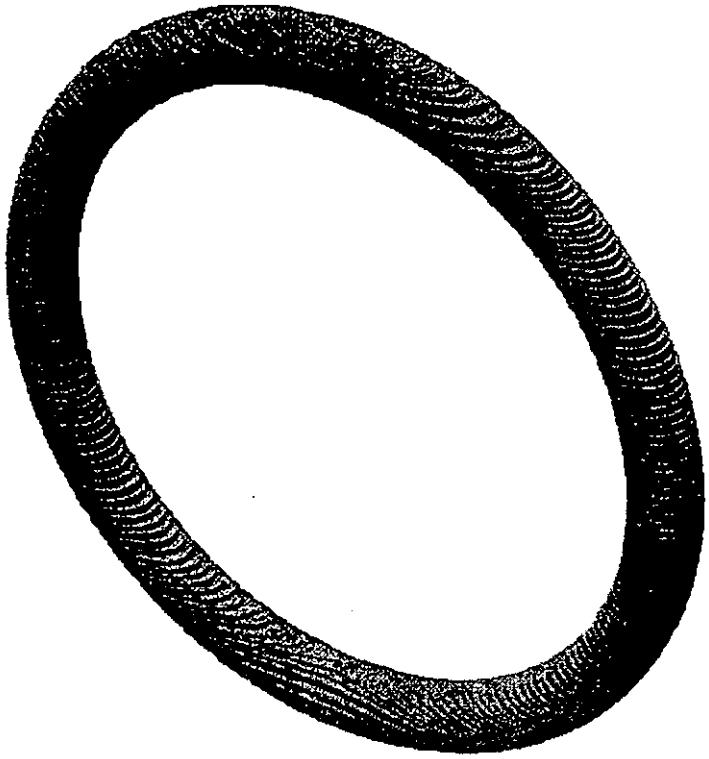

Figure 7-2. Maximum inscribed slab model of the torus placed vertically after bottom-up vertical slicing.

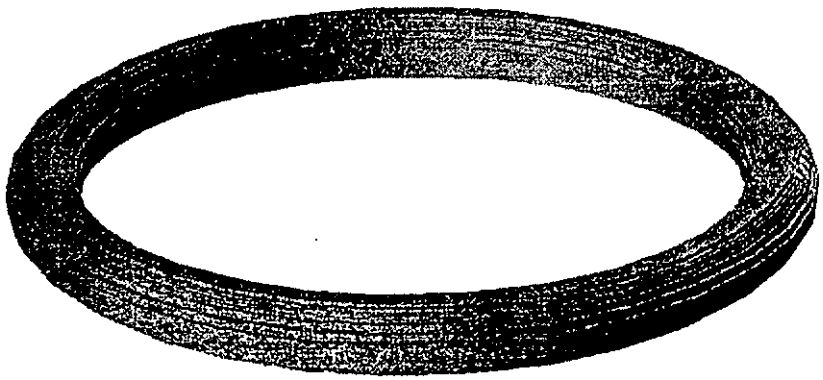

Figure 7-3. Maximum inscribed slab model of the torus placed horizontally after bottom-up vertical slicing.

The parameters of the slicing process in Figure 7-2 are:

Input volume efficiency $\eta = 0.9$

$\lambda = 5$

L_{min}: 0.05 mm

$L_{max} = 5 * L_{min} = 0.25$ mm

The results are:

Total number of slabs formed = 120

Volume of the maximum inscribed slab model = 187.2 mm^3

Volume of the 3D solid torus = 197.4 mm^3

Overall volume efficiency

= Volume of the maximum inscribed slab model / Volume of the 3D solid torus

= 0.948

The parameters of the slicing process in Figure 7-3 are:

Input volume efficiency $\eta = 0.9$

$\lambda = 5$

L_{min}: 0.05 mm

$L_{max} = 5 * L_{min} = 0.25$ mm

The results are:

Total number of slabs formed = 45

Volume of the maximum inscribed slab model = 183.43 mm^3

Volume of the 3D solid torus = 197.4 mm^3

Overall volume efficiency

= Volume of the maximum inscribed slab model / Volume of the 3D solid torus

= 0.93

7.1.2 Case studies of jewel ring

A jewel ring as shown in Figure 7-4 will be used in the case study of bottom-up vertical slicing. The ring is symmetrical about the principal plane YZ and is adapted from a sample in the part library of JewelCAD [JewelCAD]. After the bottom slab production (Appendix A, Algorithm A.1), middle slabs are produced by using Algorithms A.2, A.3 and A.4. Figure 7-5 shows the maximum inscribed slab model of the 3D jewel ring model sliced vertically by using the bottom-up vertical slicing. Figure 7-6 shows the maximum inscribed slab model of the 3D jewel ring model sliced horizontally by using the bottom up vertical slicing.

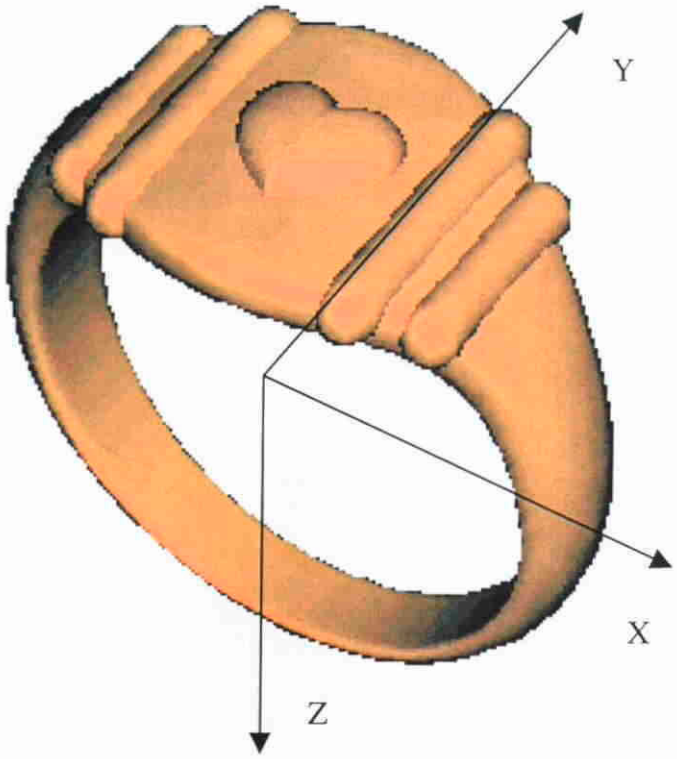

Figure 7-4. Shaded 3D model of a jewel ring.

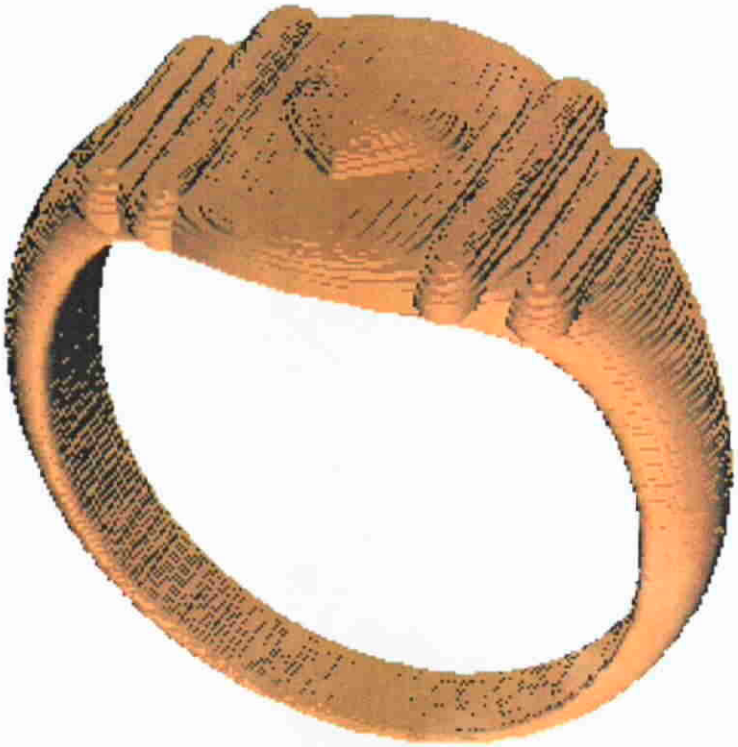

Figure 7-5. Vertical maximum inscribed slab model after bottom-up vertical slicing.

The parameters of the slicing process are:

Input volume efficiency $\eta = 0.9$

$\lambda = 5$

L_{min}: 0.05 mm

$L_{max} = 5 * L_{min} = 0.25$ mm

The results are:

Total number of slabs formed = 141

Volume of the maximum inscribed slab model = 570.3 mm^3

Volume of the 3D solid jewel ring = 597.9 mm^3

Overall volume efficiency

= Volume of the maximum inscribed slab model / Volume of the 3D solid jewel ring

= 0.95

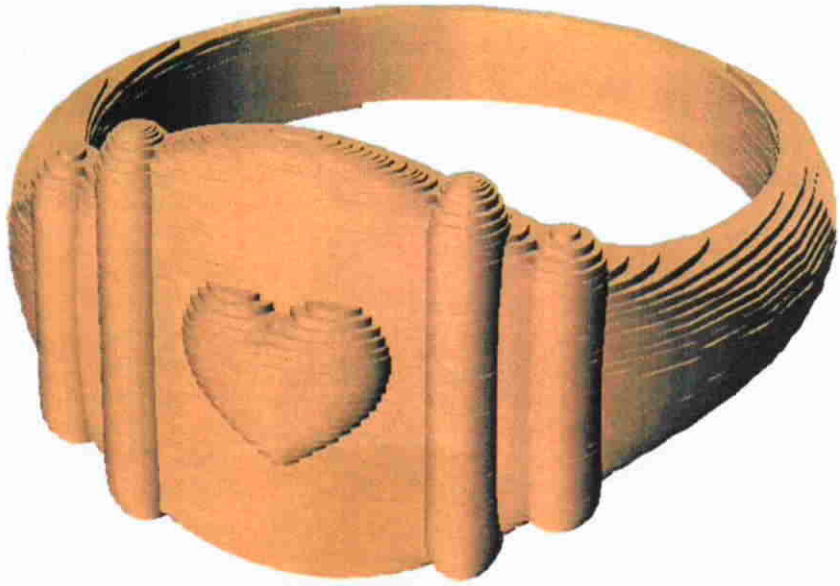

Figure 7-6. Horizontal maximum inscribed slab model after bottom-up vertical slicing.

The parameters of the slicing process are:

Input volume efficiency $\eta = 0.9$

$\lambda = 5$

L_{min}: 0.05 mm

$L_{max} = 5 * L_{min} = 0.25$ mm

The results are:

Total number of slabs formed = 68

Volume of the maximum inscribed slab model = 561.8 mm^3

Volume of the 3D solid jewel ring = 597.9 mm^3

Overall volume efficiency

= Volume of the maximum inscribed slab model / Volume of the 3D solid jewel ring

= 0.94

From the above two case studies, the volume efficiency of the torus and jewel ring built in vertical direction is higher than that in horizontal direction by using bottom-up vertical slicing. The reason is that the staircase effect in the cases of vertical direction is less than the cases of horizontal direction. Besides, the difference of the volume efficiency between these two cases is 0.01. This is significant as the method chose will affect the amount of precious metal added to the jewel ring model in the jewel ring production process.

Four slicing methodologies have been applied to the four types of symmetrical jewel rings. The results are shown in Table 7-1. The initial input of the volume efficiency η is 0.9, L_{min} is 0.05 mm and L_{max} is equal to 0.25 mm.

The volume efficiency of these four slicing methods is in the range of 0.93 to 0.95. Although the difference between these values is equal to or less than 0.02, it is significant. It is because jewel rings are made up of precious metal, the slab model with high volume efficiency is chosen for minimization of precious metal addition.

		Overall volume efficiency			
		Jewel rings symmetrical about principal planes XY, YZ and ZX	Jewel rings symmetrical about principal planes YZ and ZX	Jewel rings symmetrical about principal plane YZ	Jewel rings symmetrical about principal plane ZX
Types of maximum inscribed slab slicing	Bottom-up vertical slicing	0.929	0.93	0.94	0.942
	Top-down vertical slicing	0.92	0.923	0.928	0.93
	Middle-up vertical slicing	0.943	0.946	0.954	NA
	Middle-up horizontal slicing	0.948	0.95	NA	0.95

(Remark: NA = not applicable)

Table 7-1. Results of case studies.

From Table 7-1, the volume efficiency of the middle-up slicing methodology is found to have the highest overall volume efficiency.

In general, the overall volume efficiency of the middle up vertical slicing and the middle up horizontal slicing is higher than that in the bottom up vertical slicing and the top down vertical slicing. However, bottom up vertical slicing and top down vertical slicing are always used in the production of jewelry. The reason will be explained in the discussion section.

Figure 7-7 shows the slicing of the jewel ring model in QuiceSlice v6.0. Then, the jewel ring models are built in FDM for verification of algorithm.

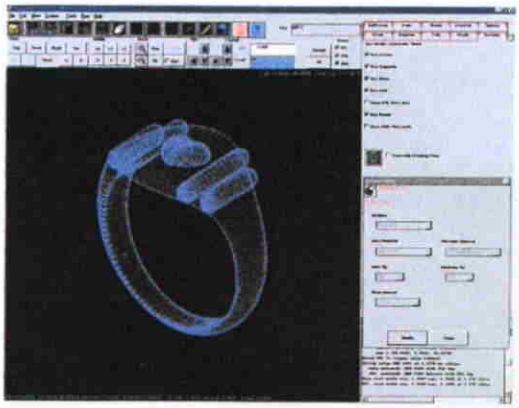

(a) Wireframe of jewel ring prototype is sliced in QuiceSlice v6.0.

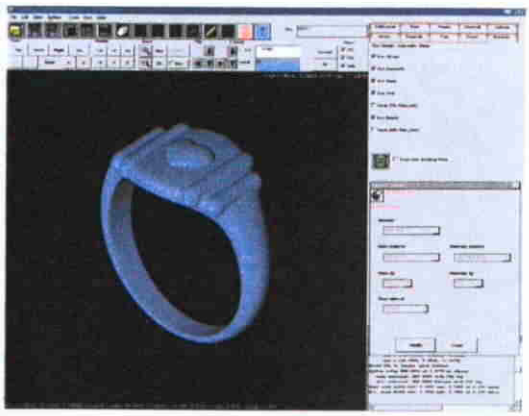

(b) Shaded model of jewel ring prototype is sliced in QuiceSlice v6.0.

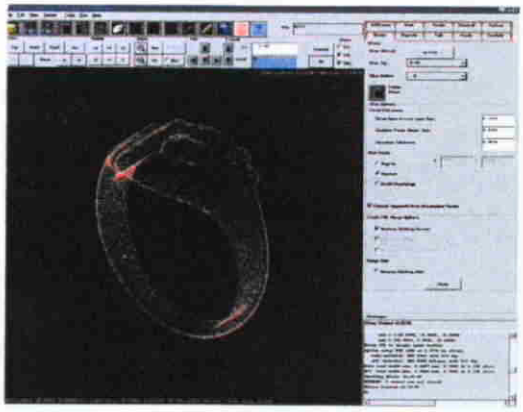

(c) The model is sliced.

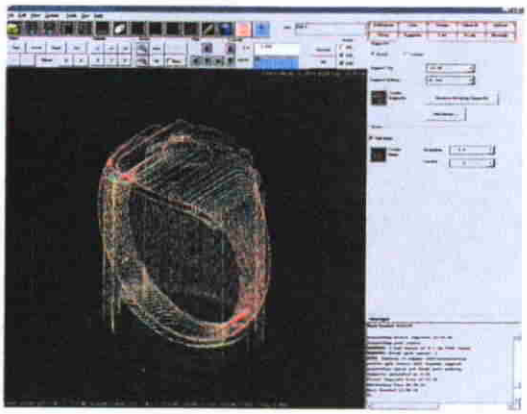

(d) Support is created.

Figure 7-7. Jewel ring model sliced in QuiceSlice v6.0 and built in FDM.

7.2 Maximum visibility building orientation

Figure 7-8 is a simple jewel ring for demonstration of the maximum visibility building orientation. Figure 7-9 shows the facet model of the jewel ring. Figure 7-10 is the EGI model of the jewel ring. Figure 7-11 is the maximum visibility direction obtained.

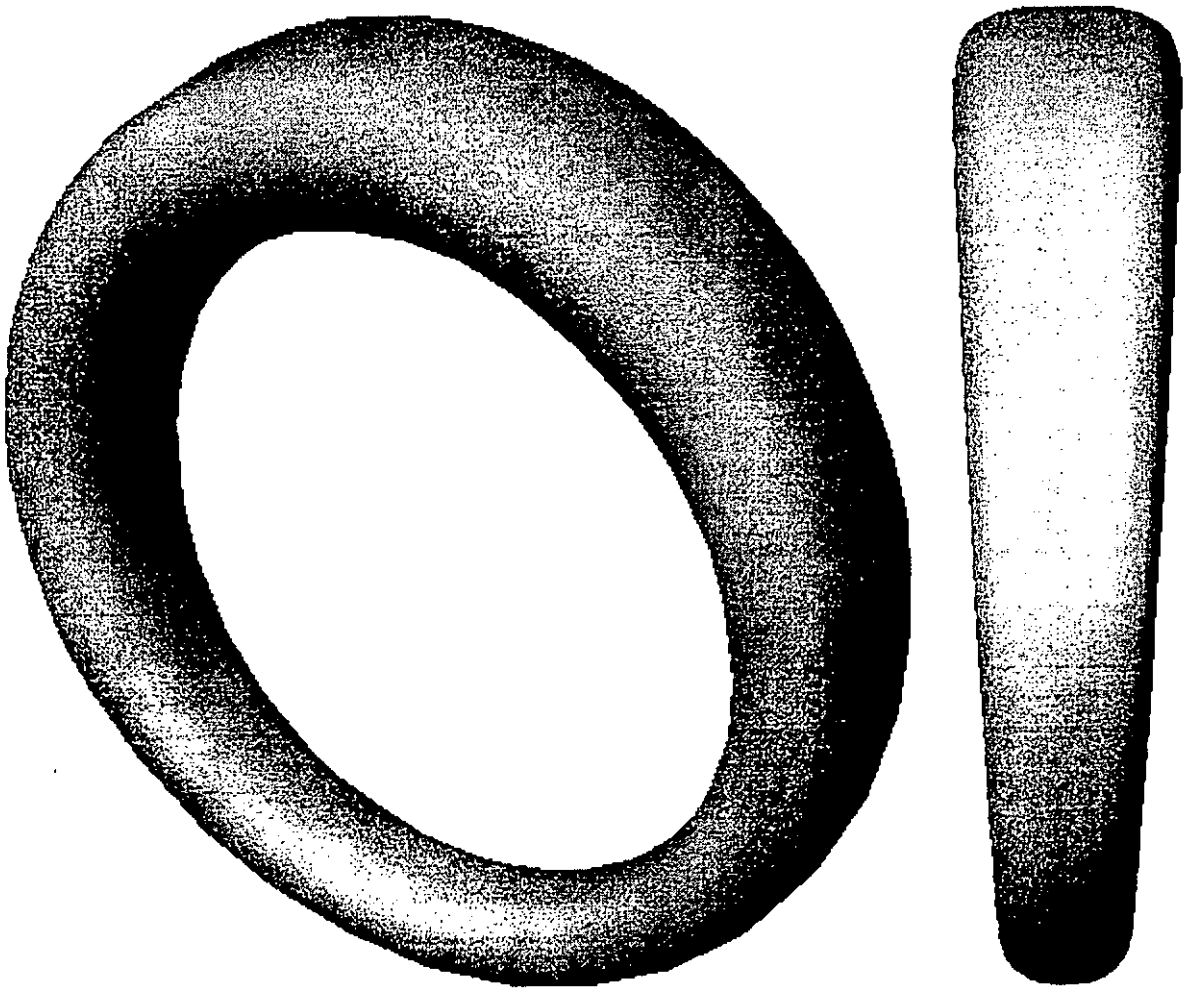

Figure 7-8. A simple jewel ring in isometric view and side view.

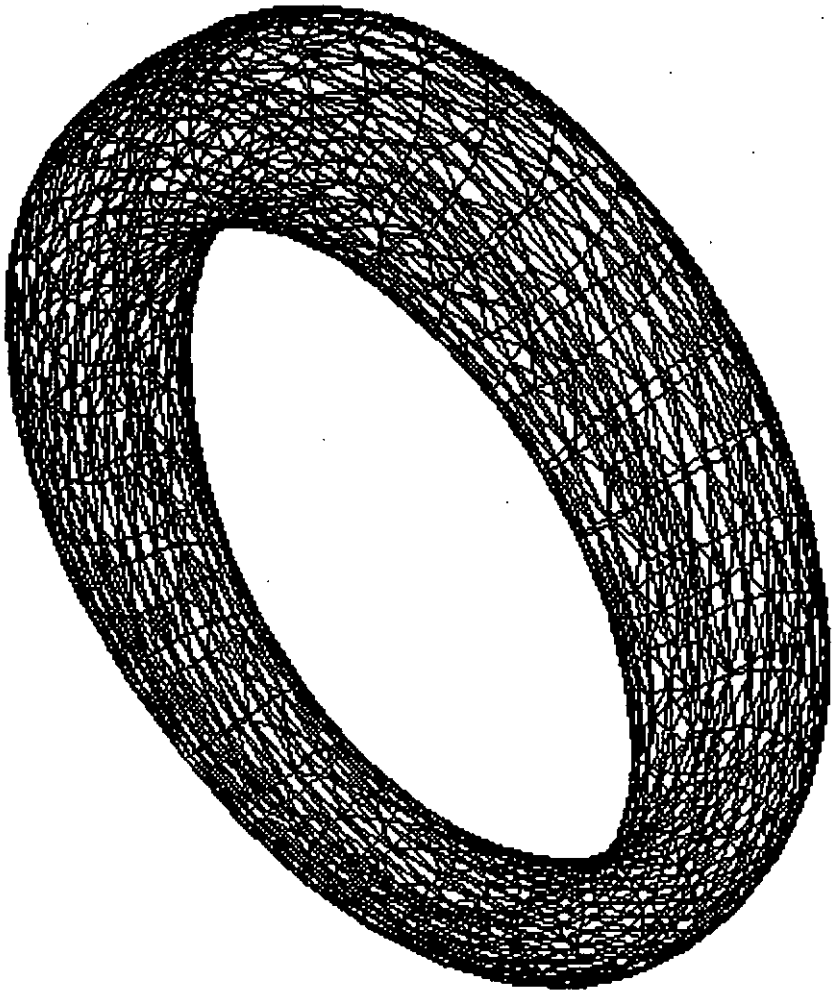

Figure 7-9. Facet model of jewel ring.

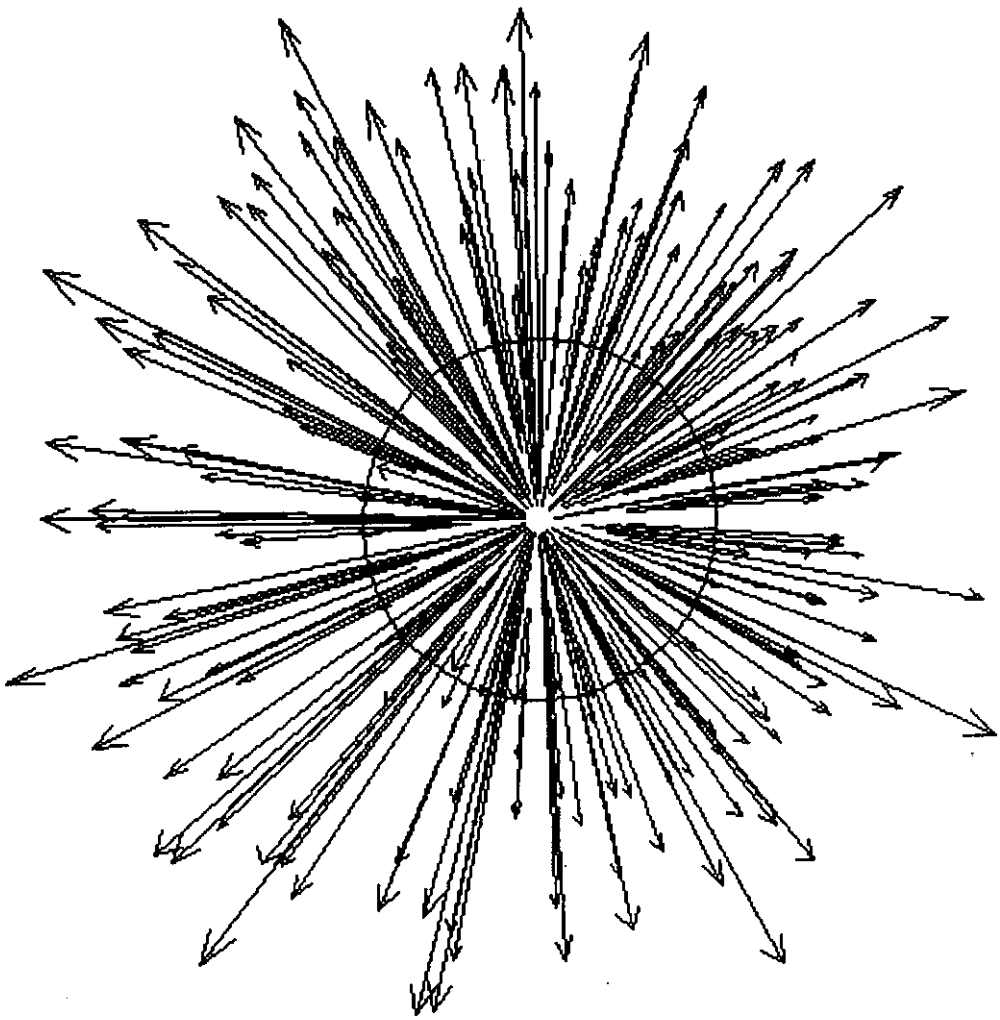

Figure 7-10. EGI of the jewel ring.

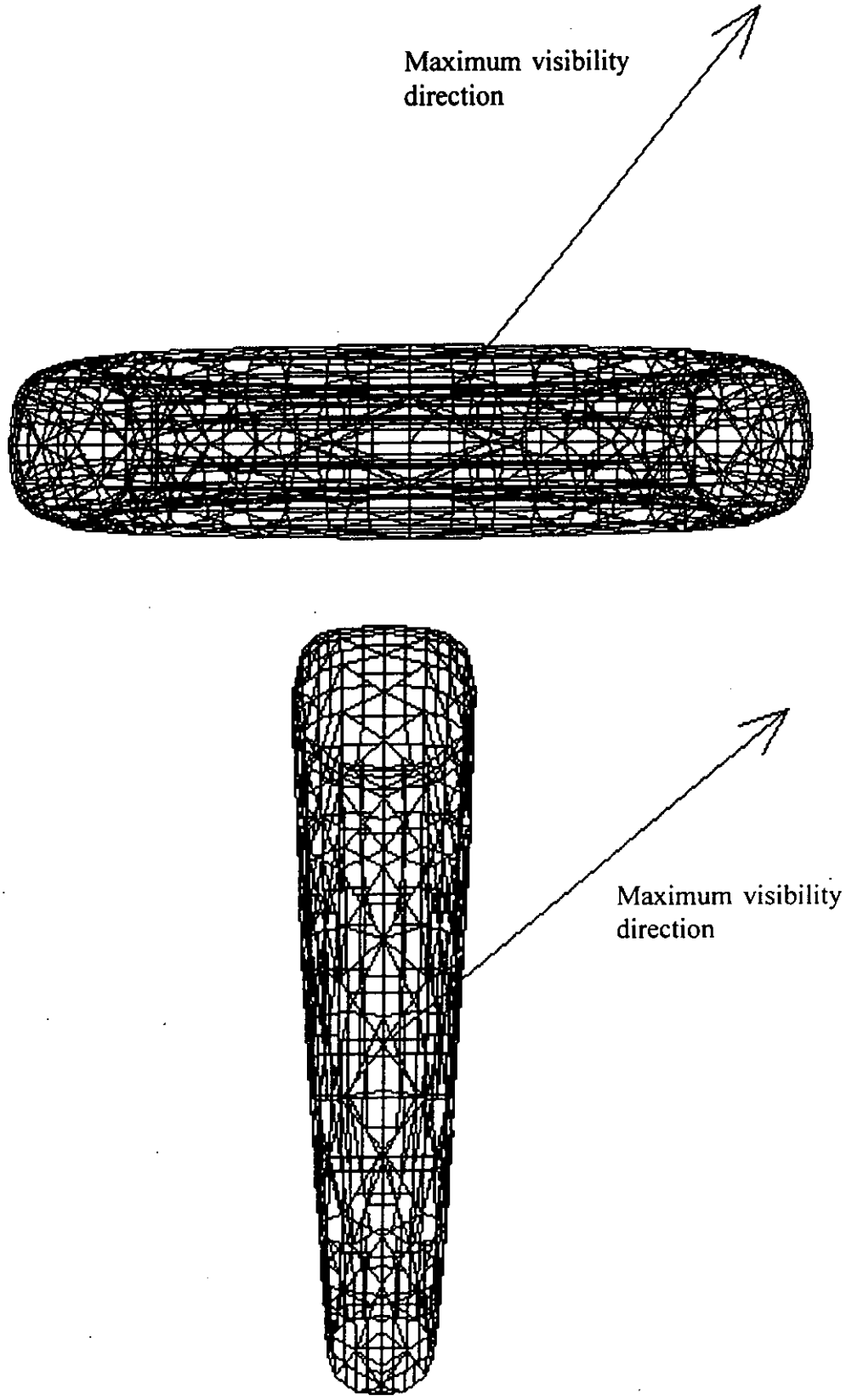

Figure 7-11. Maximum visibility direction in front view and side view.

A jewel ring as shown in Figure 7-12 and Figure 7-13 is used in the case study for the maximum visibility building orientation. The ring is adapted from a sample in the part library of JewelCAD [JewelCAD]. Figure 7-12 is the shaded model. Figure 7-13 is the wireframe model. Figure 7-14 shows the facet model of jewel ring. Figure 7-15 shows the EGI model obtained. Figure 7-16 shows the maximum visibility direction obtained.

Figure 7-12. Shaded 3D model of a jewel ring.

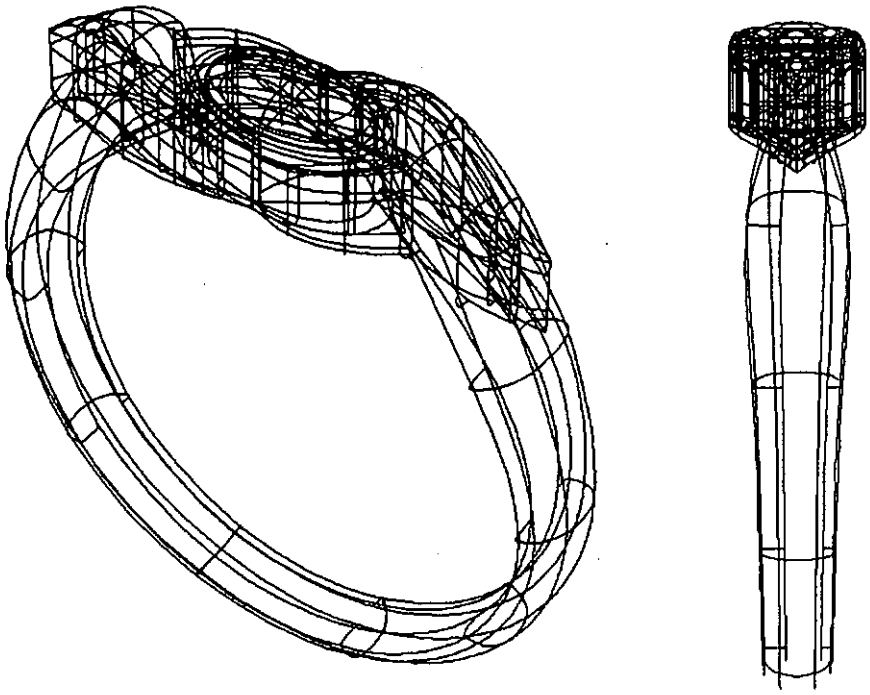

Figure 7-13. Wireframe model of jewel ring in isometric view and side view.

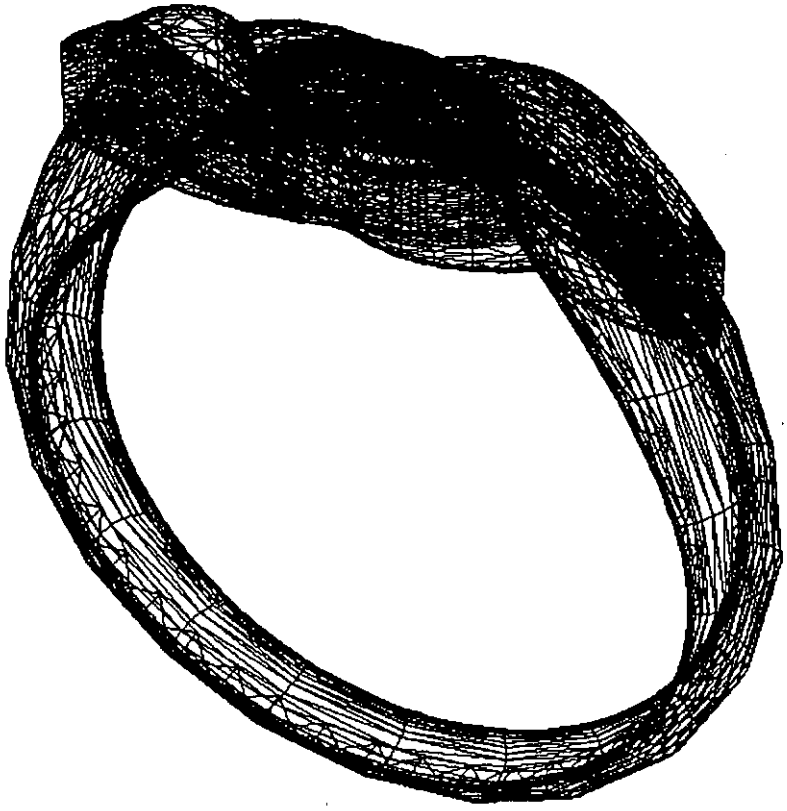

Figure 7-14. Facet model of jewel ring.

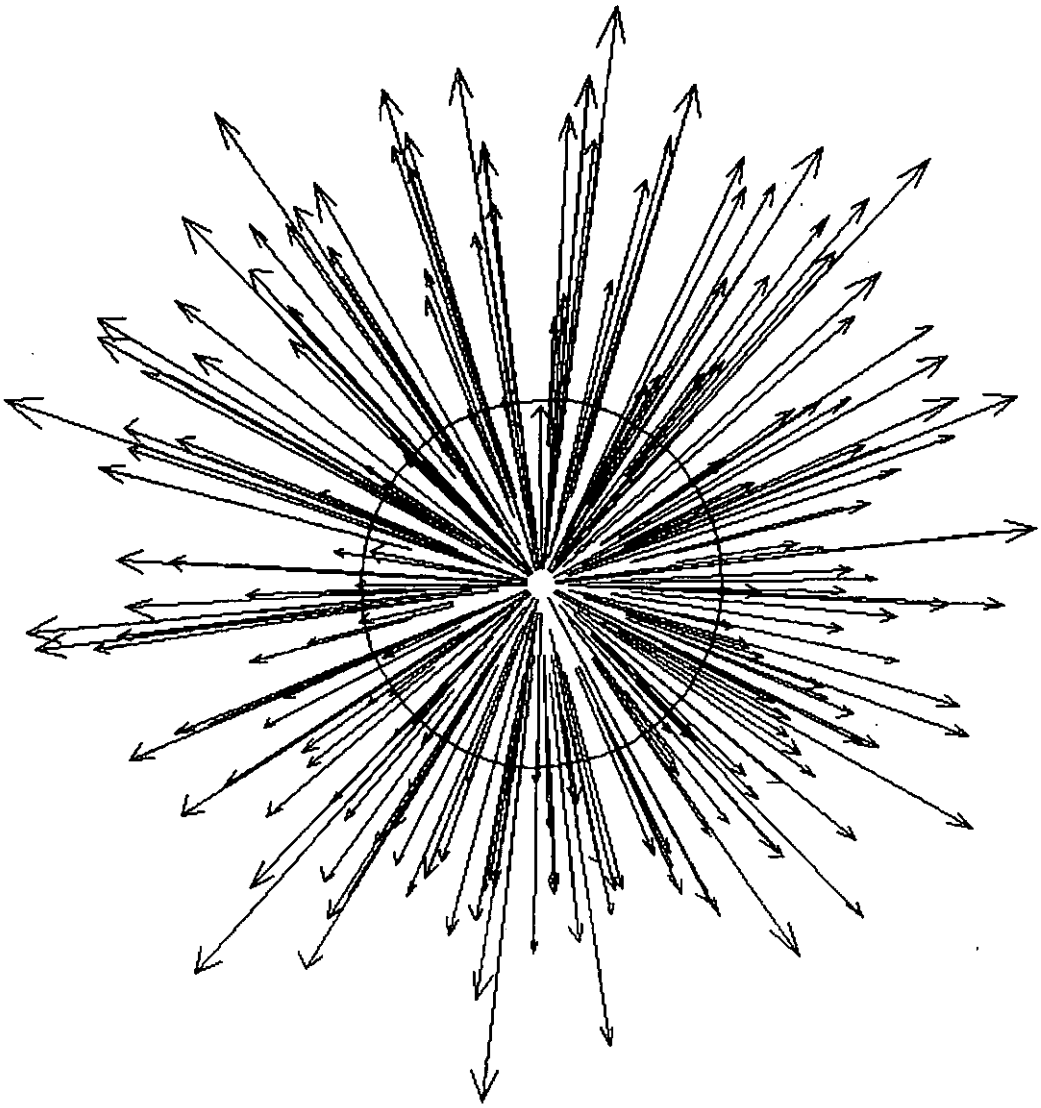

Figure 7-15. EGI of the jewel ring of Figure 7-12.

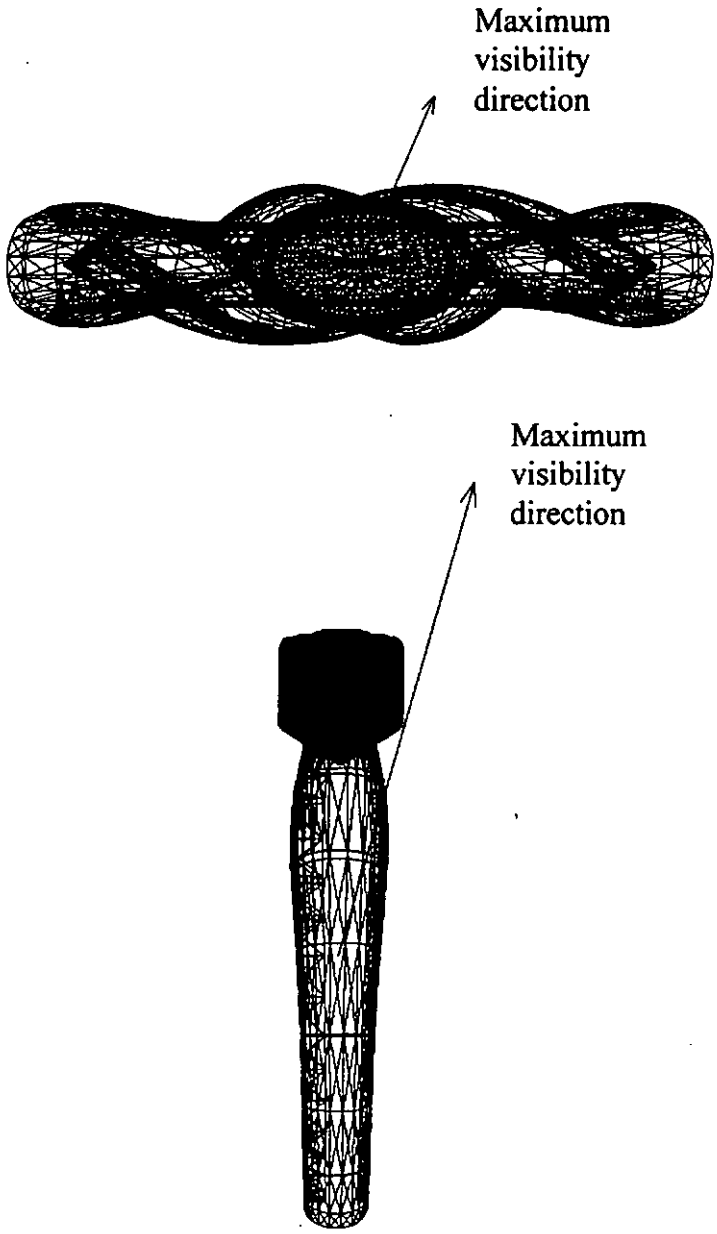

Figure 7-16. Maximum visibility direction obtained in top view and side view.

CHAPTER 8

DISCUSSION

8.1 Multi-shell building of rapid jewel ring prototypes.

In previous sections, it concerns that the jewel ring model is built in the rapid prototyping machine as a single body. However, different jewel rings have different styles. Some style consists of only one part, but some consists of more than one part (Figure 8-1).

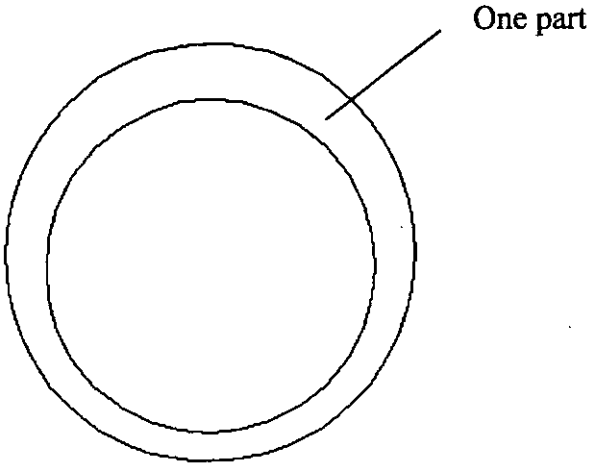

(a) Jewel ring consists of one part.

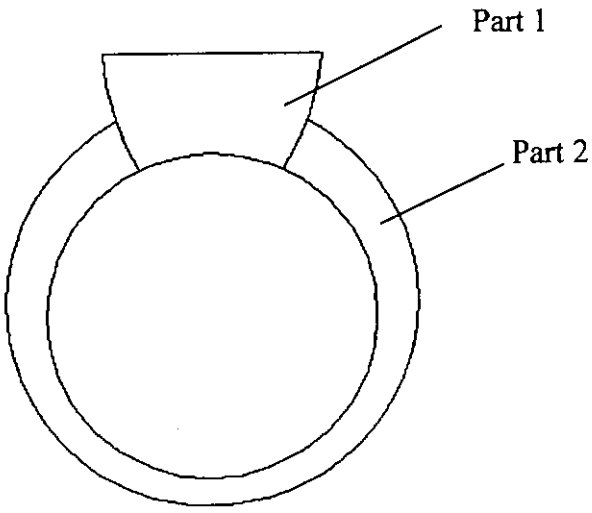

(b) Jewel ring consists of more than one part.

Figure 8-1. Partitions of jewelry.

In previous sections, jewel ring is also considered to be built as one single part by using discretized EGI concept and visibility concept. If the jewel ring consists of more than one part (Figure 8-1b), the parts have to be considered individually. The new process flow is shown in Figure 8-2.

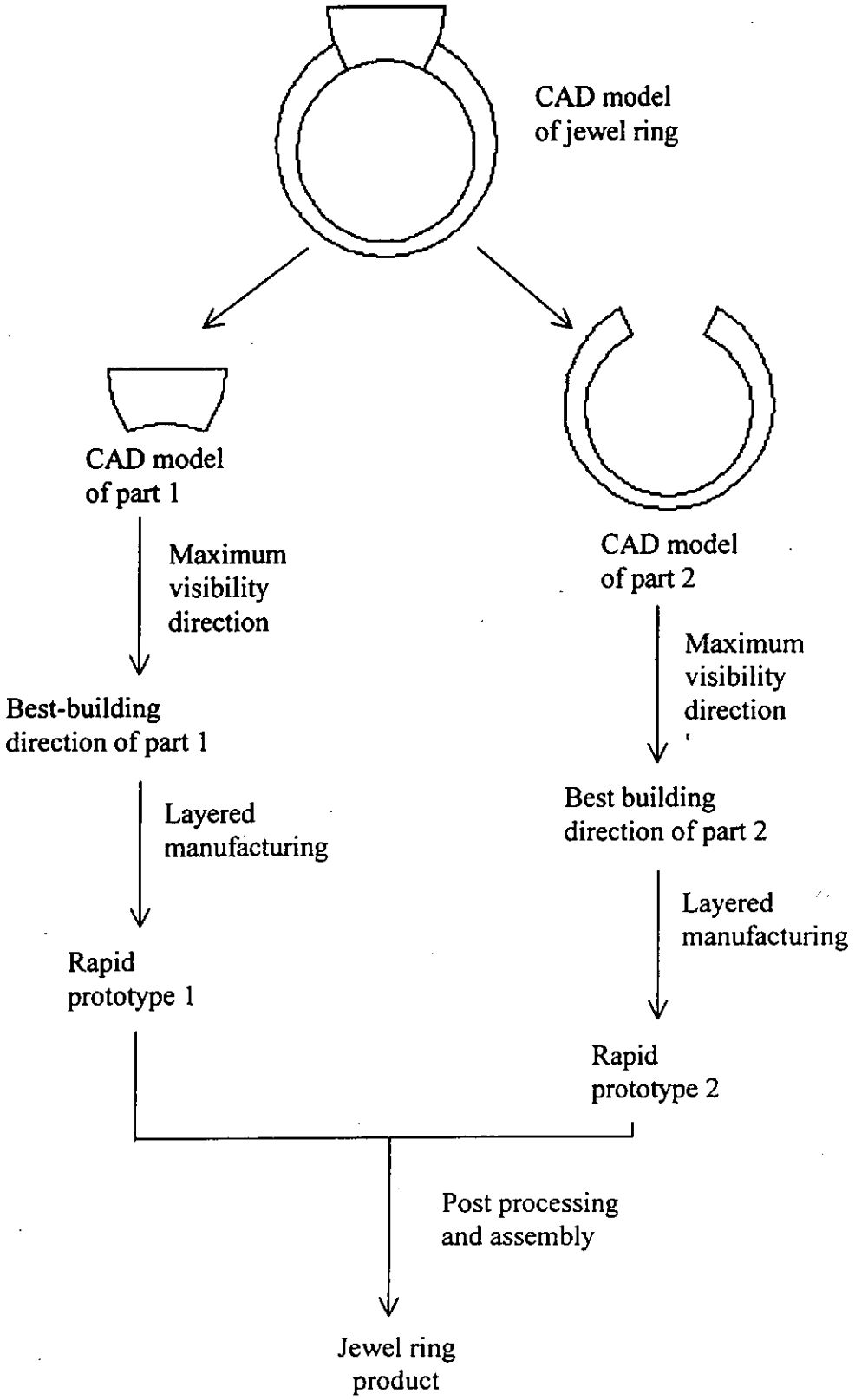

Figure 8-2. Process flow of building a jewel ring consists of more than one part.

8.2 EGI for finger wearing jewel ring

In previous sections, it mentions only the EGI of the jewel ring model is considered to find the best building direction of the jewel ring. However in real life, the jewel ring product is worn on the finger. Therefore, the EGI of the finger should also be taken into consideration. In Figure 8-3, the cylinder is used as an approximation of a human finger (ring finger). A jewel ring model is worn on the cylinder. If the EGI of the whole assembly is considered, the maximum visibility direction is shown in Figure 8-4. As cylinder has infinite maximum visibility directions, the maximum visibility direction in Figure 8-4 is one of the many possible maximum visibility direction.

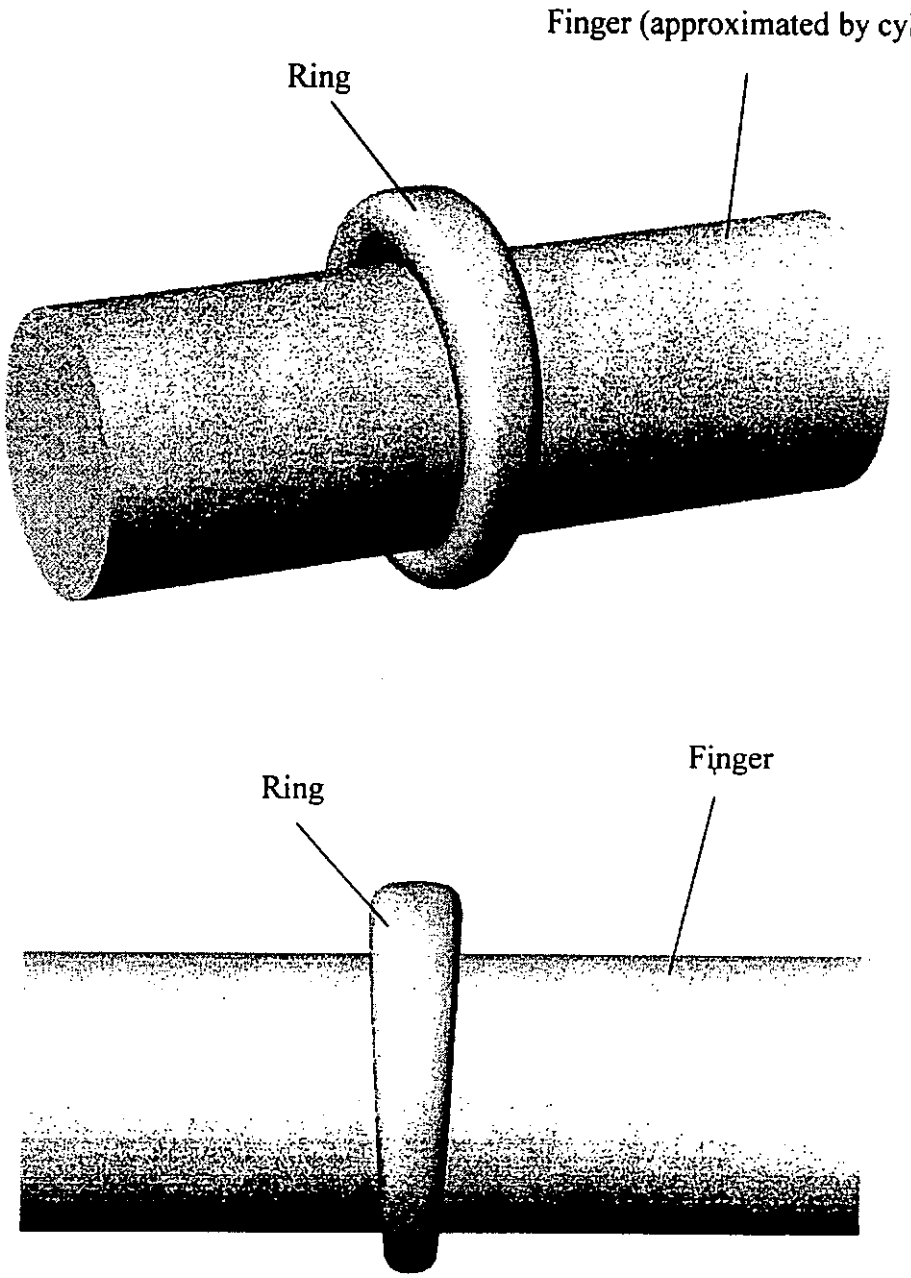

Figure 8-3. Human finger wearing a jewel ring in perspective view and side view.

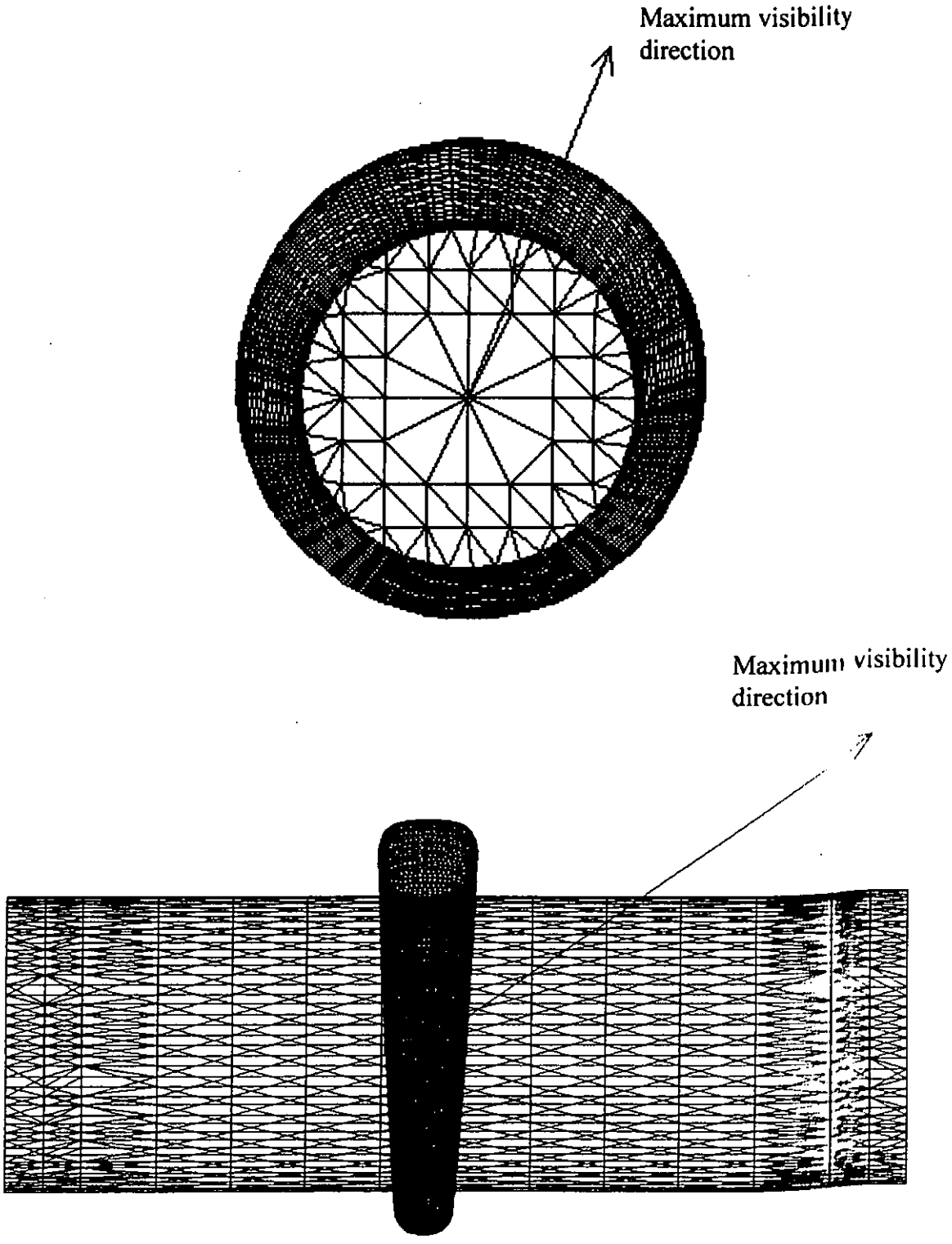

Figure 8-4. Maximum visibility direction of the jewel ring model and the cylinder (finger) in front view and side view.

In a jewel ring, the surfaces can be divided into three parts: visible aesthetic surface, inner surface and base surface (Figure 8-5). Visible aesthetic surface is on the top of the jewel ring and it contains diamonds, opals, etc. Base surface is in the bottom half of the jewel ring and it is also in the outer portion. The inner surface belongs to the inner part of the jewel ring and is not visible when people wearing the ring. It only contacts with the finger of the person who wears the ring. Obviously, the quality and surface finish of the visible aesthetic surface is the most important. The base surface is the second important part while the inner surface has the least significance. In real life, people mainly concentrate on the appearance of the visible aesthetic surface. Therefore, in layered manufacturing process, the visible aesthetic surface should not be penetrated by support material as this will affect the appearance of the rapid prototype and the post process time will also be increased.

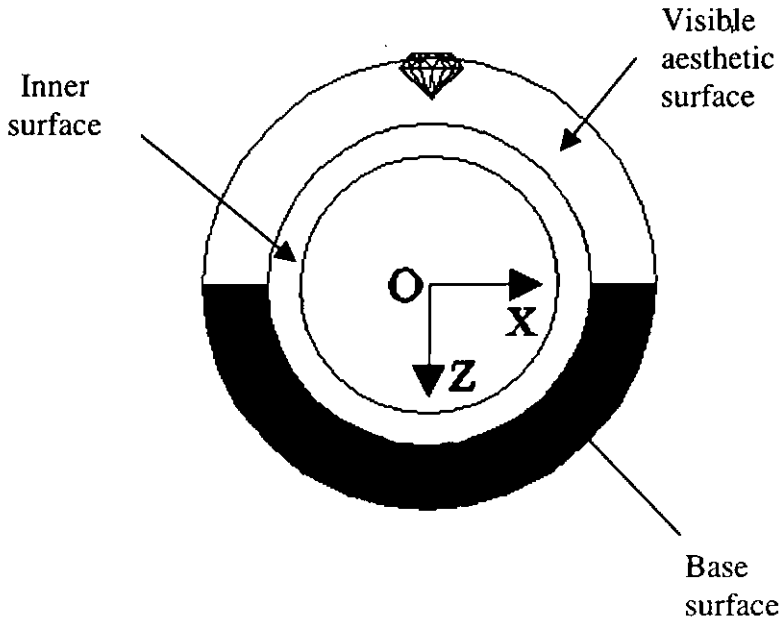

Figure 8-5. Three types of surface in a jewel ring.

8.3 Comparison with other methods

8.3.1 Optimization of slab in slicing

Previous research in slicing mainly used curvature to deduce the layer thickness of slab in layered manufacturing. However, this would be complicated and time consuming. The advantage of using maximum inscribed slab slicing is that it is simplier than that in previous research as it just uses volume comparison to adjust and optimize the slab thickness.

Volume ratio of volume of slab to the volume of part between two adjacent slices is used to optimize the slab thickness. For each slab, the thickness is set to be $\lambda * L_{min}$ first ($L_{max} = \lambda * L_{min}$). If the volume efficiency satisfies the pre-set value, the current slab is retained. Otherwise, the current slab is unused. The current slab is re-produced with slab thickness equal to $(\lambda-1) * L_{min}$. Volume efficiency checking proceeds then. The checking continues until $\lambda = 1$. If $\lambda = 1$, the checking will stop and the slab with maximum volume efficiency among λ , λ - 1, ..., 2 will be retained and set as the current slab. Through this method, the thickness of each slab can be optimized.

8.3.2 Building orientation

In previous research of building orientation, they only concerned the part accuracy, building time, support structure and part stability of the prototype. However, aesthetic quality of part have not been concerned. In jewelry production, aesthetic quality is an essential concern. Therefore, maximum visibility building orientation is introduced to find the best building orientation for improving the aesthetic quality of products particularly in jewelry industry.

8.3.3 Efficiency of algorithms

Computational efficiency is an important concern in layered manufacturing process in previous research. However, in jewelry industry, production cost minimization (including wastage minimization) and aesthetic quality of products are two highest priority concerns. Therefore, efficiency of algorithms is not a consideration in this research.

8.4 Extension of methods to other products

The maximum inscribed slab slicing and maximum visibility building orientation can be extended to other products other than symmetrical jewel ring models. These include non-symmetrical jewel ring, jewel rings with more complex shapes and other products. First the maximum visibility direction is found by using maximum visibility building orientation. Then the model is orient by its maximum visibility direction perpendicular to the building direction. Then, the model is sliced by using the maximum inscribed slab slicing to produce a maximum inscribed slab model for layered manufacturing.

8.5 Integration of slicing and orientation approach

In this research, maximum inscribed slab slicing and maximum visibility building orientation are introduced to rapid jewel ring prototype production. As slicing and foundation of building orientation are two essential processes in layered manufacturing, they should be considered in parallel. For jewel rings with symmetrical property, preservation of symmetrical property of prototypes is a must. Therefore, the maximum inscribed slab slicing should be used to slice and orient the models to preserve the symmetrical property. If maximum visibility building

orientation is used to orient the models, the symmetrical property may not be preserved as the best building orientation may not be the same as the building orientation found in the maximum inscribed slab slicing.

For jewel ring with no symmetrical property, maximum visibility building orientation is used to find the best building orientation as no symmetrical property needs to preserve. Therefore, there is no contradictory situation for the two approaches.

CHAPTER 9

FUTURE WORK AND CONCLUSION

9.1 Future work

In this research, maximum inscribed slab slicing is introduced. The advantage of using the maximum inscribed slab slicing is that the methodology is simple and efficient. It only considers the ratio of the volume of slab to the volume of part between two adjacent layers. However, in this research, only four types of symmetrical jewel rings are considered. If unsymmetrical jewel rings are considered, the algorithm may need further refinement. Besides, in the proposed slicing methodology, only jewel rings are considered. Other jewelry products such as pendants, earrings and bangles could also be considered in the future. In addition, slicing is only one factor affecting the slab model quality in rapid prototyping. Other factors such as shrinkage of prototypes, temperature of build and material properties are also important for further improvement.

A new orientation methodology, maximum visibility building orientation is introduced in this research. However, as jewel ring or other jewelry products have different types of surfaces: inner surface, visible aesthetic surface and base surface, these may be needed to take into consideration of building orientation in future work.

Computational efficiency improvement is another problem in the layered manufacturing of jewelry production. However, it is not the highest priority problem. Therefore, this can consider in the future work.

9.2 Conclusion

In this research, a new methodology, maximum inscribed slab slicing is introduced for layered manufacturing in jewelry production. There are four types of maximum inscribed slab slicing: bottom-up vertical slicing, top-down vertical slicing, middle-up vertical slicing and middle-up horizontal slicing. The stacked slab models obtained from the slicing process can maintain the symmetrical properties of original models. Besides, the maximum inscribed slab models can compensate post-treatment operations by optimizing the total material being added to or removed from the stacked slab models. As a result, wastage of precious metal like gold, platinum or silver can be minimized. This helps to reduce production cost (including labour cost), increases the efficiency of post-treatment operations, and ultimately benefits the whole production process.

In the orientation of part, a new methodology, maximum visibility building orientation is introduced. Maximum visibility direction is found to assist the foundation of best-building direction. EGI concept is applied in the theory. The methodology can build the jewelry products, not only jewel rings with high quality and this can reduce the post process applied in the jewel prototypes afterwards (e.g. polishing).

REFERENCES

[Allen 1994]

Allen, S., Dutta, D. and Arbor, A., "On the computation of part orientation using support structures in layered manufacturing", Proceedings of the Fifth Solid Freeform Fabrication Symposium, University of Texas at Austin, 1994, pp.259-269.

[Alexander 1998]

Alexander, P., Allen, S. and Dutta, D., "Part orientation and build cost determination in layered manufacturing", Computer-Aided Design, Volume 30, Number 5, 1998, pp.343-356.

[Campbell 1998]

Campbell, I., "Optimisation of build orientation for feature-based surface roughness requirements", Proceedings of the 1st International Conference on Rapid Prototyping & Manufacturing'98, Beijing, 1998, Shanxi Science and Technology Press, pp.632-638.

[Cheng 1995]

Cheng, W., Fuh, F.Y.H., Nee, A.Y.C., Wong, Y.S., Loh, H.T. and Miyazawa, T., "Multi-objective optimization of part-building orientation in stereolithography" Rapid Prototyping Journal, 1995, Volume 1, Number 4, pp.12-23.

[Chua 1989]

Chua, C. K.; Lim, B. S.; Chong, T. T., "Design and Manufacture of personal artifacts using CAD/CAM/CAE techniques", Computer Applications in production and Engineering, Proceedings of the Third International IFIP Conference, 1989, CAPE, pp171-178.

[Chua 1991a]

Chua, C.K., Lee, H. B., Ko, M. S., Gay, R. K. L. and Leong K. F., "Integrating SLA with Computer-Aided design and manufacturing", *Computer applications in Production and Engineering*, 1991, pp.149-156.

[Chua 1991b]

Chua, C. K. and Robert, G., "CAD/CAM/CAE for ring design and manufacture", *Computer-Aided Engineering Journal*, February, 1991, pp.13-24.

[Dolenc 1994]

Dolenc, A. and Makela, I., "Slicing procedures for layered manufacturing techniques", Computer-Aided Design, 1994, Volume 26, Number 2, pp.119-126.

[Frank 1994]

Frank, D. and Fadel, G., "Preferred direction of build for rapid prototyping processes", Proceedings of the Fifth International Conference on Rapid Prototyping, Dayton, OH, June 1994, pp.191-200.

[Guo 1998]

Guo, J., Guo, B. and Menon, J., "Region boundary approximations of sweeps and Minkowski operations", CSG' 98, Information Geometers, 1998, pp.169-185.

[Horn 1984]

Horn, B.K.P., "Extended Gaussian Images", Proceeding of the IEEE, December 1984, Volume 72, Number 12, pp.1671-1686.

[Hur 1998]

Hur, J.H. and Lee, K.W., "The development of a CAD environment to determine the preferred build-up direction for layered manufacturing", International Journal of Advanced Manufacturing Technology, 1998, Volume 14, pp.247-254.

[Jacobs 1996]

Jacobs, P.F., Stereolithography and other RP&M Technologies, American Society of Mechanical Engineers (ASME) Press, 1996, pp.4.

[Ippolite 1995]

Ippolite, R., Inliano, L.and Gatto, A., "Integrating reverse engineering, rapid prototyping and investment casting in the jeweller's craft", *11th International Conference on Computer-Aided Production Engineering (IMech E Conf. Transaction3)*, 1995, pp.85-90.

[JewelCAD]

JewelCAD standard samples, web site: http://www.jcadcam.com/index.html.

[Johnson 1994a]

Johnson, J.L., Principles of Computer Automated Fabrication, Palatino Press, 1994, pp.8-9.

[Johnson 1994b]

Johnson, J.L., Principles of Computer Automated Fabrication, 1994, Palatino Press, pp.16, Figure 1-7.

[Kallenberg 2000]

Kallenberg, L., Modeling in wax for jewelry and sculpture, Krause Publications, 2000, Second edition, pp.8-26.

[Kochan 1993]

Kochan, D., "Solid freeform manufacturing', 1993, Elsevier, pp.44, Figure 4.17.

[Kulkarni 1995]

Kulkarni, P. and Dutta, D., "Adaptive slicing of parametrizable algebraic surfaces for layered manufacturing", ASME Design Engineering Technical Conferences, 1995, DE series 82, Volume 1, pp. 211-217.

[Kulkarni 1996]

Kulkarni, P. and Dutta, D., "An accurate slicing procedure for layered manufacturing", Computer-Aided Design, 1996, Volume 28, Number 9, pp.683-697.

[Lee 1997]

Lee, K.H. and Yoo, L.S., "An extended slicing method for rapid prototyping", International Conference on Manufacturing Automation Proceedings, ICMA' 97, Hong Kong, April 28-30, 1997, Volume 1, pp.449-454 University of Hong Kong,.

[Lee 1998]

Lee, K.H. and Choi, K.I., "An adaptive slicing method using both contour and vertical character lines", Proceedings of 7th European Conference on Rapid Prototyping and Manufacturing, University of Nottingham, Aachen, Germany, July 7th-9th, 1998, pp.109-126.

[Leong 1998]

Leong, K. F., Chua, C. K. and Tam, C. H., "Microblasting characteristics of jewellery model built using stereolithography apparatus (SLA)", International Journal of Advanced Manufacturing Technology, 1998, 14, pp.450-458.

[Loh 1998]

Loh, H. T., Xu, F. and Wong, Y. S., "Optimal orientation selection in different rapid prototyping processes", Proceedings of the First International Conference on Rapid Prototyping & Manufacturing'98, Beijing, 1998, Shanxi Science and Technology Press, pp.140-148.

[Lu 1998]

Lu, C.J., Liu, J. and Zhang, Y.L., "An adaptive slicing procedure for rapid prototyping", Proceedings of the 1st International Conference on Rapid Prototyping & Manufacturing '98, Beijing, 1998, Shanxi Science and Technology Press, pp.693-698.

[Maswood 1998]

Maswood, S.H., Rattanwong, W. and Iovenitti, P., "Minimisation of volumetric error in part orientations in rapid prototyping", Proceedings of the 1st International Conference on Rapid Prototyping & Manufacturing'98, Beijing, 1998, Shanxi Science and Technology Press, pp.79-85.

[Mani 1999]

Mani, K., Kulkarni, P. and Dutta, D., "Region-based adaptive slicing", Computer-Aided Design, 1999, Volume 31, Number 2, pp.317-333.

[Meriam 1997]

Meriam, J.L. and Kraige, L.G., Engineering Mechanics: Dynamics, Fourth edition, Wiley, 1997, pp.560-561.

[Ng 1997]

Ng, W.M. Micky and Tan, S.T., "Feature based optimization of part orientation for rapid prototyping", International Conference on Manufacturing Automation Proceedings, ICMA' 97, Hong Kong, April 28-30, 1997, Volume 1, pp.434-442, University of Hong Kong.

[Pham 1999]

Pham, D. T., Dimov, S. S. and Gault, R. S., "Part orientation in stereolithography", International Journal of Advanced Manufacturing Technology, 1999, Volume 15, Number 9, pp.674-682.

[Sabourin 1996]

Sabourin, E., Houser, S.A. and Bohn, F.H., "Adaptive slicing using stepwise uniform refinement", Rapid Prototyping Journal, 1996, Volume 2, Number 4, pp.20-26.

[Siu 1997]

Siu, W. C., "Improvement of product quality and production process performance in jewellery manufacturing through "Integrated craftsmanship"", Proceedings of the 2nd International Conference on Quality and Reliability, 1997, 1, pp.219-225.

[Solidscape]

Solidscape, Inc., web site: http://www.sanders-prototype.com/.

[Suh 1994]

Suh, Y.S. and Wozny, M.J., "Adaptive slicing of solid freeform fabrication processes", Proceedings of the 5th Solid Freeform Fabrication Symposium, Austin, Texas, Aug 8-10, 1994, University of Texas at Austin, pp.404-411.

[Wong 1999]

Wong, T. N., Cheung, C. H. and Lau H., "Decision support system for a jewellery manufacture", International Journal of Production Economics, 1999, 60-61, pp.211-219.

[Xu 1997a]

Xu, F., Wong, Y.S., Loh, H.T., Fuh, F. Y. H., "Optimal orientation with adaptive slicing for part building in SLA", Proceedings of the seventh International Conference on Rapid Prototyping, 1997, pp.148-155.

[Xu 1997b]

Xu, F., Wong, Y.S., Loh, H.T., Fuh, F.Y.H. and Miyazawa, T., " Optimal orientation with variable slicing in stereolithography", Rapid Prototyping Journal, 1997, Volume 3, Number 3, pp.76-88.

[Xu 1999]

Xu, F., Loh, H. T. and Wong, Y. S., "Considerations and selection of optimal orientation for different rapid prototyping systems", Rapid Prototyping Journal, 1999, Volume 5, Number 2, pp.54-60.

[Zhao 1998]

Zhao, Z.W. and Laperriere, L., "Adaptive direct slicing of the solid model for rapid prototyping", Proceedings of the 1st International Conference on Rapid Prototyping & Manufacturing '98, Beijing, 1998, Shanxi Science and Technology Press, pp.272-278.

[3D Systems]

3D Systems, web site: http://www.3Dsystems.com.

APPENDIX A

ALGORITHM OF BOTTOM-UP VERTICAL SLICING

The general algorithm of the bottom up vertical slicing is shown in Algorithm A. The sub-routines of the algorithm are shown in Algorithms A.1, A.2, A.3, A.4 and A.5.

Algorithm A: Bottom_Up_Vertical_Slicing

Input: Solid torus ,T; volume efficiency, $\eta(0.85 \leq \eta \leq 1)$;

minimum layer thickness achieved by the rapid prototyping system, L_{min};

multiplied constant, λ, $\lambda \in N$(where $L_{max} = \lambda * L_{min}$ and L_{max} is the maximum layer thickness achieved by the rapid prototyping system).

Output: Slabs of the maximum inscribed slab model

BEGIN

Bottom_Slab_Production

Middle_Slabs_Production

Top_Slab_Production

maximum inscribed slab model ← Union of all slabs

END

Algorithm A.1: Bottom_Slab_Production

Planar region A_1 ← Slice at $Z = R - L_{min}$

$Slab_0$ ← Extrude A_1 downwards: direction: *k*, height: L_{min}

RETURN

Algorithm A.2: Middle_Slabs_Production

$i = 1$

FOR $1 \leq i \leq N - 1$ DO

IF $Z_i + R \leq L_{min}$ THEN

Top_Slab_Production

ELSE

$A_{i+1} \leftarrow$ Slice at $Z = Z_{i+1} = Z_i - n * L_{min}$

$A_{i+1}' \leftarrow$ Translate A_{i+1} downwards: direction: *k*, distance: $Z_i - Z_{i+1}$

$S_i \leftarrow$ Detection_Of_Critical_Point

$Slab_n \leftarrow$ Extrude S_i upwards: direction (*-k*, distance: $Z_i - Z_{i+1}$)

$Slab_i \leftarrow$ Optimization_Of_$Slab_n$

END IF

$i = i + 1$

RETURN

Algorithm A.3: Detection_Of_Critical_Point

IF $Z_{i+1} < 0$ and $Z_i > 0$ THEN

$A_0 \leftarrow$ Slice at $Z = 0$

$A_0' \leftarrow$ Translate A_0 downwards: direction *k*, distance: Z_i

$S_i \leftarrow A_i \cap A_{i+1}' \cap A_0'$

ELSE

$S_i \leftarrow A_i \cap A_{i+1}'$

END IF

RETURN

Algorithm A.4: Optimization_Of_Slab

Input η

$n = \lambda$

$Z_{i+1} \leftarrow Z_i - n * L_{min}$

WHILE $Z_{i+1} \leq -R$ DO

$n = n - 1$

IF $n < 1$ THEN

RETURN

Input λ /* Override default λ */

END IF

END WHILE

Find $Slab_n$, volume of $Part_n$, volume of $Slab_n$ and η_n.

Set $\eta_i = \eta_n$, $Slab_i = Slab_n$

WHILE $\eta_n < \eta$ DO

$n = n - 1$

IF $n \geq 1$ THEN

Find $Slab_n$, volume of $Part_n$, volume of $Slab_n$ and η_n

ELSE

RETURN

END IF

IF $\eta_n \geq \eta$ THEN

Set $Slab_i = Slab_n$

RETURN

ELSE

IF $\eta_n > \eta_i$

Set $\eta_i = \eta_n$, $Slab_i = Slab_n$

END IF

END WHILE

RETURN

Algorithm A.5: Top_Slab_Production

Planar region $A_N \leftarrow$ Slice at $Z = Z_i$ such that $Z_i + R \leq L_{min}$

$Slab_N \leftarrow$ Extrude A_N upwards: direction: $-k$, height: L_{min}

RETURN